

TRAPPING OF SEDIMENT IN TIDAL ESTUARIES

Alexander Chernetsky

TRAPPING OF SEDIMENT IN TIDAL ESTUARIES

PROEFSCHRIFT

ter verkrijging van de graad van doctor
aan de Technische Universiteit Delft,
op gezag van de Rector Magnificus Prof. ir. K.C.A.M. Luyben,
voorzitter van het College voor Promoties,
in het openbaar te verdedigen op dinsdag 10 april 2012 om 15.00 uur
door

Alexander Sergeevich CHERNETSKY

Master of Science in Mechanica en Toegepaste Wiskunde
Dnepropetrovsk Nationale Universiteit, Oekraïne,

geboren te Dnepropetrovsk, Sovjet-Unie (Oekraïne)

Dit proefschrift is goedgekeurd door de promotor:

Prof. dr. ir. A.W. Heemink

Copromotor:

Dr. ir. H.M. Schuttelaars

Samenstelling promotiecommissie:

Rector Magnificus,	voorzitter
Prof. dr. ir. A.W. Heemink,	Technische Universiteit Delft, promotor
Dr. ir. H.M. Schuttelaars,	Technische Universiteit Delft, copromotor
Prof. dr. V.N. de Jonge,	University of Hull
Prof. dr. H.E. de Swart,	Universiteit Utrecht
Prof. dr. ir. H. Ridderinkhof,	Universiteit Utrecht/NIOZ
Prof. dr. ir. J.C. Winterwerp,	Technische Universiteit Delft
Prof. dr. ir. M.J.F. Stive,	Technische Universiteit Delft

ISBN 978-90-5335-534-3

Copyright © Alexander Chernetsky 2012

This research was carried out in the section of Mathematical Physics at the Department of Applied Mathematics, Delft Institute of Applied Mathematics, Faculty of Electrical Engineering, Mathematics and Computer Science, Delft University of Technology, The Netherlands.

All rights reserved. No part of this publication may be reproduced, stored in a retrieval system or transmitted in any form or by any means, electronic, mechanical, photocopying, recording or otherwise, without the prior written permission of the author.

All models are wrong, but some are useful
George Box

To my parents

Contents

1	Introduction	1
1.1	Estuarine Systems	2
1.2	Importance of Estuaries	3
1.3	The Ems/Dollart System	5
1.4	Modeling estuarine flow and transport of suspended sediment	9
1.4.1	Water motion	10
1.4.2	Sediment transport and trapping	10
1.4.3	Condition of morphodynamic equilibrium	13
1.5	Outline of the thesis	13
2	The effect of tidal asymmetry and temporal settling lag on sediment trapping	17
2.1	Introduction	18
2.2	Model Formulation	20
2.3	Perturbation analysis and solutions	25
2.3.1	Leading order system of equations	26
2.3.2	Higher order system of equations	27
2.3.2.1	Water motion	27
2.3.2.2	Sediment dynamics	30
2.3.3	Morphodynamic equilibrium condition	31
2.4	Results	32
2.4.1	Characteristics of the Ems estuary	32
2.4.2	Model setup	35
2.4.3	Water motion	37
2.4.4	Sediment Dynamics	39
2.5	Discussion	40
2.5.1	Hydrodynamics	41
2.5.2	Analysis of the residual sediment transports	44
2.5.2.1	Changes between 1980 and 2005	48

2.5.2.2	Grain size sensitivity	52
2.5.3	Parameter sensitivity	52
2.6	Conclusions	54
3	Influence of high concentration and geometrical characteristics on the estuarine turbidity maxima	57
3.1	Introduction	58
3.2	Model	60
3.3	Solution Method	63
3.3.1	First Order Hydrodynamics	64
3.3.2	First Order Sediment Dynamics	68
3.3.3	Morphodynamic equilibrium condition	69
3.4	Results	71
3.4.1	Turbidity currents	72
3.4.2	Sensitivity to bathymetry	78
3.4.3	Sensitivity to the external forcing	84
3.5	Conclusions	87
4	Influence of viscosity parametrization and strain-induced periodic stratification on the ETM	91
4.1	Introduction	92
4.2	Modeling Approach	93
4.3	Solution Method	97
4.4	Results	99
4.5	Conclusions	105
5	Conclusions	109
5.1	Main conclusions	109
5.2	Recommendations	111
A	Appendix	113
A1	Derivation of Width-Averaged Shallow Water Equations	113
A1.1	Continuity equation	113
A1.2	Momentum equation	115
A2	The Width-Averaged Sediment Concentration Equation	116
A3	Morphodynamic Equilibrium Condition	118
A4	Perturbation Analysis and Solutions	120
A4.1	Leading order system of equations	124

A4.2	First order system of equations	127
A4.2.1	Water motion	127
A4.2.2	Sediment dynamics	130
A4.3	Morphodynamic equilibrium condition	131
A5	Confidence Intervals for the Best Fit	132
A6	Parameter Sensitivity	134
A7	Water Motion Components	138
A8	Transport components	139
Summary		157
Samenvatting		159
Acknowledgements		161
Curriculum vitae		163

Introduction

The main objective of this thesis is to investigate physical mechanisms in the along-estuary direction that result in the trapping of suspended sediment in partially and well mixed tidal estuaries and to analyze the influence of individual mechanisms on the trapping location. The investigation is conducted using an idealized model approach. A width-averaged analytical model of a tidal estuary is developed, which allows to model the velocity distribution, the suspended sediment dynamics and analyze the occurrence of suspended sediment trapping in morphodynamic equilibrium. The model allows to reproduce hydro- and sediment dynamic conditions in tidal estuaries via a calibration of model parameters using field observations. Once the model is calibrated properly and results are validated, the importance of various trapping mechanisms and their sensitivity can be studied.

The aim of this chapter is to introduce the reader to estuarine systems and known physical mechanisms that influence the hydrodynamics, suspended sediment distribution and trapping in estuaries. In Section 1.1, a general definition of estuaries and an estuarine classification are introduced. In Section 1.3, the Ems/Dollard estuary is discussed as a prototype example of a partially mixed estuary. In Section 1.4, the modeling techniques and known physical mechanisms that result in sediment trapping in estuaries are presented. Followed by Section 1.5, where the main research questions and research approach are discussed, and the outline of this thesis is given.

1.1 Estuarine Systems

According to [Perillo \(1995\)](#), there are over 40 different definitions of estuaries. The most commonly used definition is the definition of [Cameron and Pritchard \(1963\)](#): 'An estuary is a semi-enclosed coastal body of water which has free connection to the open sea and within which sea water is measurably diluted with freshwater derived from land drainage'. However, this definition does not include the effect of tides, which can be significant in many estuaries. [Dyer \(1997\)](#) has extended this definition by including the influence of tides: 'An estuary is a semi-enclosed coastal body of water which has free connection to the open sea, *extending into the river as far as the limit of tidal influence*, and within which sea water is measurable diluted with freshwater derived from land drainage'. In other words, estuaries are basins where freshwater from rivers interacts with salt water from the open sea. Estuaries are found in all parts of the world, for example the Humber estuary (UK), the Amazon estuary (Brazil), the Hudson estuary (USA), the Ems estuary (the Netherlands/Germany), etc.

Each estuary is unique and is characterized by a number of parameters, such as tidal range, river discharge, topographical features, etc. To compare different estuaries and to formulate unified principles of how to understand and predict the behavior of these complex systems, estuaries have to be classified. Many different classification schemes are possible, depending on which criteria are considered. For example, in [Valle-Levinson \(2010\)](#) an estuarine classification is provided on the basis of **water balance in estuaries**, **geomorphology**, **hydrodynamics** and **vertical structure of salinity**.

In this thesis, the research focus is on shallow estuaries, where tides have a significant influence on mixing processes. Different tidal ranges result in different circulation patterns, density stratification and mixing processes in shallow estuaries. In such estuaries, a good basis for classification would be the salinity distribution within an estuary and the water stratification. In [Pritchard \(1955\)](#); [Cameron and Pritchard \(1963\)](#), the following estuarine types are distinguished based on the vertical salinity structure (see sketches in Fig. 1.1).

- **Salt wedge estuaries.** These are estuaries with a relatively weak or no tidal influence and strong river discharge. Under these conditions, the less dense riverine freshwater flows seawards over the surface of the saline water with virtually no mixing between the layers. During flood, the sea water enters into these estuaries in a wedge shape and the system becomes highly stratified. A typical salinity profile is shown in Fig. 1.1(a).

Examples: Mississippi (USA) and Rio de la Plate (Argentina);

- **Strongly stratified estuaries.** These estuaries are characterized by a significant river discharge and low or moderate tidal influence. The river influence is dominant over the tidal influence. This type is similar to the salt wedge type. The main difference between them is that in strongly stratified estuaries the stratification stays strong throughout the whole tidal cycle, see Fig. 1.1(b). *Example: Silver Bay (Alaska);*
- **Partially mixed estuaries.** This type of estuaries is significantly influenced by tides with low or moderate river discharge. The entire volume of the estuary is mixed during ebb and flood, with the saline water being mixed upwards and freshwater mixed downwards (Fig. 1.1(c)).
Examples: James River and San Francisco Bay (USA);
- **Well mixed estuaries** are usually shallow estuaries with strong tidal mixing and low river discharge. Such combination allows to mix the saline water from the sea throughout the entire estuary, see Fig. 1.1(d).
Examples: the Delaware Bay (USA) and the Raritan Estuary (USA)

From this classification, it is evident that the estuarine type is substantially determined by the tidal and riverine influence. Estuarine systems may change from one type to another on a monthly or seasonal basis, due to variations in the freshwater discharge (MacCready, 1999) or by spring-neap variations (Jay and Smith, 1990; Peters, 1997; Ralston and Stacey, 2005). For example, the Columbia river (USA) changes from a strongly to a weakly stratified estuary within a tidal month (Jay and Smith, 1990). **In this thesis, the main research interest is in the partially and well mixed estuaries.**

1.2 Importance of Estuaries

An estuary is an ideal habitat for various aquatic species due to its fertile waters. Constant import of nutrients and minerals from the river creates ideal conditions for algae and phytoplankton primary production, which serves as a food base for many inhabitants. At the same time, estuaries and adjacent rivers are used as fast navigation routes between the coastal and inland territories. For these reasons, estuaries have always been of great interest to people. The area around estuaries is usually densely populated and the land is extensively used.

The fast industrial development and the subsequent growth of trade have led to large-scale anthropogenic alterations of estuarine systems. Estuaries are streamlined and deepened to ensure a safe navigation for larger ships. Dams are con-

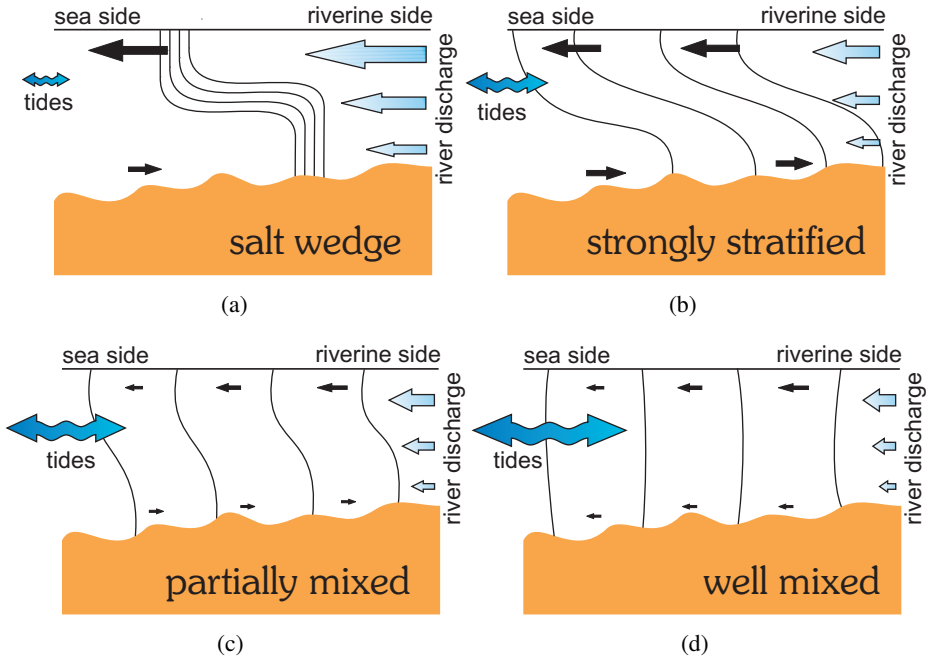


Figure 1.1: Sketch of a tidally-averaged longitudinal salinity profile in a salt wedge (a), strongly stratified (b), weakly stratified (c) and well-mixed estuary (d)

structured to protect the farmland, households and industrial buildings from floods. Moreover, land reclamation, deforestation and various agricultural activities result in higher sediment and freshwater input into estuaries. All these activities lead to fundamental alterations of the hydro- and sediment dynamics, mixing and circulation processes within estuarine systems.

An estuarine system, taken out of its natural balance, is always trying to restore the equilibrium or reach a new steady state. This can result in, for example, an increased siltation and the estuarine depth has to be constantly maintained via annual dredging activities. Engineering interventions are expensive and they create a substantial load on the local inhabitants, because a biological system cannot readjust to new conditions within a short period of time. Hence, these activities pose many problems from both the ecological and economic point of view. A proper understanding of estuarine processes is essential to minimize the negative consequences of human influence and to develop a long-term restoration and development plan for many problematic estuaries.

To understand estuarine physical processes, many tools can be used, such as raw field data, conceptual models or widely used large scale numerical models. However, 3D numerical models are computationally expensive and include the sum of many processes (e.g., baroclinic circulation, tidal straining, tidal pumping, flocculation, settling and scour lag, non-linear interactions, etc.), it becomes difficult to isolate the magnitude and importance of particular processes or investigate parameter sensitivity. These limitations motivate the development of idealized models in which specific physical mechanisms can be studied in isolation. The advantage of an idealized model is that it is complex enough to reproduce the physical behavior of the system well, yet it is relatively simple to construct analytical solutions using standard mathematical techniques, avoiding high computational costs. Idealized models based on first principles are an important tool to gain insight into estuarine physical processes and to mitigate the anthropogenic influence. Idealized models allows us to identify and analyze the importance of each forcing mechanism separately. In Section 1.3, the Ems/Dollart estuary is discussed as an example of a heavily engineered system.

1.3 The Ems/Dollart System

The Ems/Dollart estuary belongs to the larger Wadden Sea system, shown in Fig. 1.2 with a zoomed image of the Ems/Dollart estuary. The Wadden Sea is a shallow sea and the largest mudflat area in the world of approximately 600 km long, which consists of a series of tidal basins protected from direct North Sea influence by a system of barrier islands. These islands are separated by tidal inlets. A number of rivers drain into the Wadden Sea, such as the Elbe, Weser and Ems river. The river Ems has a length of approximately 330 km and its drainage basin covers approximately 12,650 km². A long-term average discharge is approximately 120 m³ s⁻¹, measured near Pogum (Hinrich, 1974).

The part of the Ems river which is affected by the tidal influence is called the Ems/Dollart estuary, a detailed map is presented in Fig. 1.3 (De Jonge, 2000). The estuary is located at the border between the Netherlands and Germany and it is an important navigation route for sea and river vessels from the Netherlands and Germany. There are three important harbors located along the estuary: Eemshaven, Delfzijl and Emden, and a shipyard located in Papenburg.

The estuary runs for approximately 100 km from the tidal weir, located near the city of Herbrum, to the system of barrier islands. The tidal weir in Herbrum was constructed in 1900, thus, splitting the river into the tidally influenced



Figure 1.2: *Satellite image of the Wadden Sea at low tide with a zoom on the Ems/Dollart estuary. Landsat images from different years combined. Sources: www.waddensea-secretariat.org and maps.google.com*

Ems/Dollart estuary and the river itself. The estuary comprises of three characteristic regions, outlined by dashed red lines in Fig. 1.3. The **upper part of the estuary** consists of the Ems river from the city of Herbrum to Pogum and the shallow Dollart bay. The Dollart bay is separated from the main estuary by a semiporous dam, called the Geisedamm. This dam goes from the city of Pogum to Knock. A limited water exchange is possible via numerous perforations in the dam. The mean natural depth of the Ems estuary was 4 – 5 m at the beginning of the 20th century. Since the late 1950's, the shipping channel has been streamlined, canalized and maintenance dredging of the navigation channel has started. The current depth of the estuary is maintained by annual dredging activities at approximately 7 – 8 m. Nowadays, the mean water depth of the Dollart bay is

approximately 1.2 m and approximately 85% of the bay is covered by tidal flats.

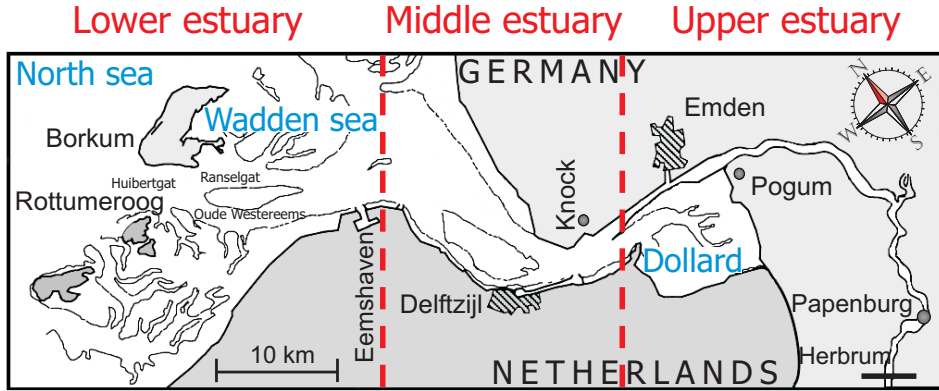


Figure 1.3: Map of the Ems/Dollart estuary

The **middle estuary** stretches from the Dollard bay to the Emshaven port, where it meets the Wadden sea. This section of the estuary has a classic funnel-shape cross-section and up to 45% of the middle estuary is covered by intertidal flats. One of these flats divides the estuary into two channels. One of the channel is a navigation channel and the other one is closing up quickly due to increased siltation processes. The water depth in the navigation channel increases in the seaward direction from 7 m to 12 m and the average water depth is 3.5 m.

The **lower estuary** is located between the Emshaven port and the barrier islands Borkum and Rottumeroog. The North sea influences the Ems estuary via the tidal inlet Huibertgat, located between these islands. The lower estuary has two deep channels, called Oude Westereems and Ranselgat, separated by a number of shoals. The Ranselgat channel is used as a navigation channel and its depth is approximately 14 m (Van Leussen and Cornelisse, 1996). Approximately 44% of this section of the Ems estuary consists of tidal flats.

The morphology of the Ems has been changing gradually over the centuries due to natural and anthropogenic processes. However, the active human intervention into the Ems system, started at the beginning of the 20th century, has significantly changed the natural course of morphological evolution. The current length of the estuary was fixed in 1900, when a tidal weir had been constructed near the city of Herbrum. At a later stage, the Ems estuary and some of its tributaries were canalized sequentially in 1900, 1911, 1925, 1928 and 1959. The fast industrial development and growth in the region required the transportation of a large-size cargo by sea and river vessels. Furthermore, the Meyer shipyard (Papenburg, lo-

cated ~ 90 km inland from the North Sea), which produced medium-size wooden ships in the 19th century, switched to the construction of larger gas tankers, cargo ships and passenger cruise liners with a draft up to 7 – 8 m. To ensure the passage of bigger ships with a larger draft, a significant deepening of the navigation channels started in the 1960's. Furthermore, a storm surge barrier was built near the village of Pogum.

In 1965, 1972 and 1978 a series of extensive dredging campaigns took place between the village of Pogum and the city of Papenburg. A subsequent dredging of the navigation channel took place in the following order (V. de Jonge, personal communication):

- In **1984-1985**, the 'Homeric-deepening' campaign increased the depth to 5.7 m;
- In **1991**, the 'Zenith-deepening' activities increased the depth up to 6.3 m;
- In **1993**, the navigation channel has been deepened to 6.8 m;
- In **1994-1995**, the 'Oriana-deepening' campaign increased the depth up to 7.3 m.

Such extreme anthropogenic interventions, enhanced by activities as land reclamation, development of ports and sand mining, have significantly changed the hydrodynamics and sediment distribution patterns in the estuary (De Jonge, 1983, 1992; Talke et al, 2009a). Since the construction of the weir at Herbrum and the other anthropogenic interventions, the tidal range has changed significantly in the entire Ems estuary. The largest increase of the tidal range by 1.5 m was observed in the upstream reaches near the city of Papenburg. For example in 1980, the measured tidal range near Knock and Papenburg was 3.1 and 2.3 m, respectively. Similar observations of 2005 showed a tidal range of 3.2 and 3.8 m at the same locations (more details can be found in Section 2.4.1).

At the same time, the surface suspended sediment concentration (SSC) in the Ems estuary has increased by a factor of five between the 1950's and 2000's. Measurements of 1954 indicate an average surface SSC of approximately 130 mg/l with a distinct region of maximum sediment concentration (ETM) of 200 mg/l near the city of Emden. In 1975, the mean SSC increased to 200 mg/l and the concentration in the turbidity region, which had advanced upstream by 10 km, increased to 400 mg/l. Observations of 1992 indicate an increase of the average SSC up to 600 mg/l and the concentration in the turbidity region has risen to 900 mg/l

(De Jonge, 1983, 1992). Moreover, measurements of 2005-2006 show the average surface SSC of approximately 1 g/l with no distinct turbidity region between Papenburg and Emden anymore (Talke et al, 2009a). These levels of suspended sediment concentration in the water column tremendously affect both the local ecosystem and the hydrodynamics of the estuary itself.

Another example of rapid morphodynamic changes in the estuary is the intensified closure of channels. In 1976, due to an increased sedimentation, the navigation channel Oude Westereems in the lower estuary could not be used anymore and the Ranselgat channel was chosen for navigation purposes. An increased sedimentation is also observed in other channels.

Such significant examples of changes in the Ems estuary are a good motivation for an in-depth analysis and understanding of estuarine physical processes and how they change due to both natural evolution and anthropogenic influence. The latter can lead to an increase of the suspended sediment concentration and occurrence of turbidity regions in estuaries. In the following section, the modeling approach and known physical mechanisms that result in the suspended sediment trapping are discussed.

1.4 Modeling estuarine flow and transport of suspended sediment

To understand and predict geomorphological evolution in estuaries, a model is required which is able to describe the dynamics of the water motion, sediment movement and the evolution of the erodible bottom.

In Fig. 1.4, a schematization of this modeling process is shown. At the initial step, the hydrodynamic equations are solved to obtain the velocity distribution and water level in the estuary. At the next step, the obtained hydrodynamic variables are used as input parameters to get the suspended sediment dynamics in the water column. This is a branching point. If the suspended sediment concentration is relatively low and does not influence the hydrodynamics the so-called condition of morphodynamic equilibrium is used to obtain the locations of suspended sediment trapping within the estuary. Otherwise, the suspended sediment concentration affects the water motion by altering the density of the water and the turbulence characteristics, and a feedback loop is required to recalculate the hydrodynamic parameters under these new conditions. At the final step, the locations of suspended sediment trapping are calculated. In the subsequent subsections, the modeling approach is briefly described for these three aspects.

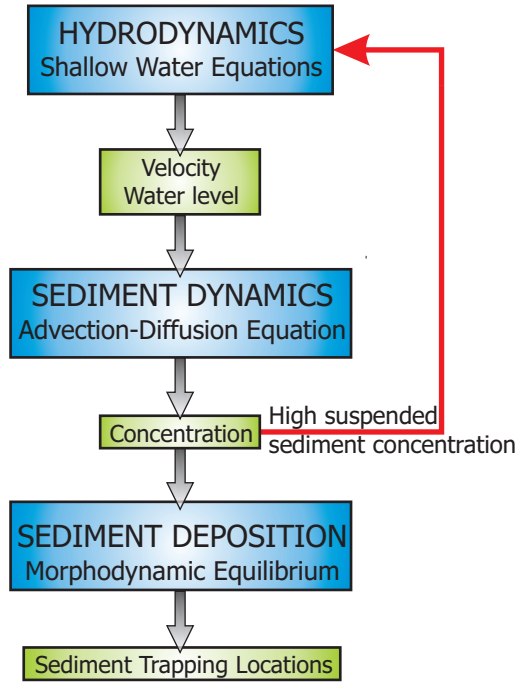


Figure 1.4: Interaction between different modeling stages

1.4.1 Water motion

The water motion in tidal estuaries is driven by a complex interaction of different physical processes forced by the influence of the sea, the river and the wind. These include tides, density gradient due to the presence of saline and freshwater, riverine freshwater discharge, turbidity currents, tidal return flow and various nonlinear interactions. In this study, we consider estuaries where the typical horizontal length scale is much larger than the typical vertical length scale. The hydrodynamics in such estuaries can be described using the shallow water equations (Csanady, 1982). From the shallow water equations, we can obtain the spatial distribution and temporal variations of the velocity fields and sea surface elevations in an estuary.

1.4.2 Sediment transport and trapping

In estuaries, two types of sediment movement are distinguished (Sleath, 1984; Dyer, 1986; Van Rijn, 1993). A sediment particle can be transported as **bed load**

and as **suspended load**. In the first case, the particle stays in contact with the bed at all times and its motion is conducted by rolling, sliding, hopping or saltating over the bed within a thin boundary layer. Suspended sediment transport means that a sediment particle is picked up from the boundary layer and becomes suspended in the water column. Due to advective and diffusive processes, the particle is transported away from the initial location, where it settles to the bottom due to gravity. The latter form of transport accounts for most sediment transport in estuaries, and in this thesis, we assume that sediment is transported as suspended load.

Sediment particles only start their movement when the bed shear-stress, which is related to the so-called frictional velocity, exceeds a certain critical threshold. Therefore, the sediment transport starts to act when the flow velocity in an estuary is equal to a certain critical frictional velocity and the lift force is able to compensate the gravitational force. This process is called **erosion**. In general, the stronger the currents are, the more sediment is eroded. Once an eroded particle is in suspension, the horizontal motion of the sediment particle is governed by the advective and diffusive processes. The suspended particles settle down to the bottom under the influence of the gravitational force. This process is called **deposition**. However, the deposition location of an individual suspended particle can be and is usually different from the erosion location due to a horizontal transport by advection and diffusion. This results in a net sediment transport in estuaries. If sediment particles are eroded at various locations in an estuary, but are transported to and deposited mainly at one specific region, this region is called the estuarine turbidity maxima (ETM) or the trapping region.

Trapping of suspended sediment can occur under various conditions and a number of different physical processes and their interaction are responsible for this. Mechanisms, that result in ETM, cover almost the entire spectrum of estuarine hydrodynamic processes. One of the most significant physical mechanisms that results in a net sediment transport is **the tidal velocity asymmetry** (Festa and Hansen, 1978). If there is tidal asymmetry, the velocity and duration of flood and ebb tides are different. Therefore, the amount of suspended sediment during flood and ebb is not the same, resulting in a net sediment transport, i.e., there is either an import or export of sediment in the estuarine system. This mechanism and its influence is explained and analyzed in detail in Chapters 2 and 3 (see also Allen et al (1980)).

Another relevant mechanism that results in a net sediment transport is **settling lag**. Two types of the settling lag are distinguished: the temporal and spatial settling lag. In general, the settling lag results from the fact that a finite period

of time is needed for a sediment particle in suspension to settle down through a water column after the cessation of its transportation (Postma, 1954; Groen, 1967; De Swart and Zimmerman, 2009). The effect of the temporal settling lag is investigated in Chapter 2.

Other processes resulting in particle trapping are related to the presence of residual **gravitational circulation** and so-called **tidal mixing asymmetry**. The first mechanism puts emphasis on the convergence of sediment near the bed of the residual landward-directed gravitational circulation and seaward-directed river outflow (Hansen and Rattray, 1965). The effect of tidal mixing asymmetry on ETM dynamics was first described in Jay and Musiak (1996) and later in many other papers, i.e., (Scully and Friedrichs, 2003; Winterwerp, 2011). In moderately and highly stratified estuaries the reduction in turbulent mixing due to stratification reduces the sediment transport capacity of the flow causing sediment to be trapped near the landward limit of the salt intrusion. In periodically stratified estuaries, this mechanism is called **the strain-induced periodic stratification (SIPS)** (Simpson et al (1990)) and it is investigated in Chapter 4. Moreover, other relevant physical processes are **tide-topography interaction** (Ianniello, 1979) and **wind forcing** (Weir and McManus, 1987).

Apart from these mechanisms, Lang et al (1989) included the influence of sediment availability by prescribing a longitudinally varying erosion coefficient. Transversal circulations are reported to influence the transport of sediment and character of ETM (Dyer, 1977; Cáceres et al, 2002; Kim and Voulgaris, 2008; Scully et al, 2009). In some systems particle aggregation results in an enhanced trapping of sediment (Van Leussen, 1988).

Recently, it has become increasingly clear that there is a strong interaction between physical and biological processes in ETM. In the highly turbid water, the penetration of light into the water is limited. At the same time, due to hydrodynamic processes high concentrations of nutrients are usually found in the region of the ETM. Therefore, the turbidity regions are favorable for river organisms if their growth is nutrient limited, but unfavorable if it is light limited. The occurrence of ETM depends on the bed erodibility and other sediment characteristics (Burchard and Baumert, 1998). The erodibility of cohesive sediment is influenced by biological and physical processes. Sediment stabilization (an increase of the erosion critical threshold) is influenced by biota, ranging from benthic algal films (Sutherland et al, 1998) to mussel beds (Widdows et al, 1998a), as well as sediment dehydration during a prolonged air exposure. Sediment destabilization (an increase of the erosion rate) can result from bioturbation, caused by benthos (Widdows et al, 1998b), combined with physical disturbance by tidal currents, storm

events, river flow and wave action. Furthermore, benthos may directly affect sediment characteristics (Meadows and Tait, 1989).

1.4.3 Condition of morphodynamic equilibrium

In this thesis, the sediment is assumed to be transported as suspended load transport only. Therefore, the evolution of the erodible bed is governed by the erosion and deposition fluxes. Following Friedrichs et al (1998); Huijts et al (2006), it is assumed that the estuarine system under investigation is in morphodynamic equilibrium. This means that there is no evolution of the bed over a tidal period. This approach is valid when the easily erodible sediment is redistributed on a much shorter timescale than the typical timescale at which the external forcing changes significantly. Hence there is a balance between the tidally averaged erosion and deposition at the bottom. Using this condition, the locations of suspended sediment trapping can be calculated.

1.5 Outline of the thesis

In this thesis, the following research questions are addressed (all questions apply to partially and well mixed estuaries)

- *Q1*: Is it possible to reproduce the hydro- and sediment dynamics, observed in partially mixed tidal estuaries, using an idealized analytical width-averaged model?
- *Q2*: What are the dominant physical mechanisms resulting in suspended sediment trapping? And what physical mechanisms can result in multiple estuarine turbidity maxima? Is it possible to quantify the influence of natural and anthropogenic processes on the hydrodynamics and suspended sediment deposition locations.
- *Q3*: What is the influence of the high turbidity in the water column on the location of the estuarine turbidity maximum?
- *Q4*: What is the effect of geometrical characteristics of the estuary and external forcing on the position of the ETM?
- *Q5*: How do different vertical eddy viscosity parametrizations affect the turbidity zone? What is the influence of the SIPS mechanism on the turbidity zone.

To answer these research questions, an idealized analytical modeling approach is chosen. This model is aimed to reflect the physical behavior of the velocity fields distribution, the dynamics of suspended sediment and suspended sediment trapping locations in tidal estuaries. A similar modeling tactic, with a focus on the cross-section processes presented by Huijts et al (2006), proved the feasibility of such an approach. In this thesis, the main emphasis is on the investigation of the influence of longitudinal processes on the occurrence and behavior of the turbidity zone. Therefore, a width-averaged model is developed. The hydrodynamic conditions in the tidal basin are modeled by the width-averaged shallow water equations (derivation is provided in Appendix A1) and the dynamics of suspended sediment in the water column is governed by the width-averaged advection-diffusion equation (see Appendix A2). The along-channel distribution of sediment available for resuspension at the bottom is modeled using the condition of morphodynamic equilibrium (derivation is provided in Appendix A3).

The estuary is assumed to be partially or well-mixed with a prescribed along-channel salinity distribution. The bathymetry varies in the longitudinal direction. The sediment is assumed to be mainly transported as suspended load and consists of noncohesive particles.

A solution to this problem is constructed by means of a perturbation approach. As a first step, the importance of different terms in the governing equations is identified by performing a scaling analysis, i.e., variables in the model equations are nondimensionalized by their characteristic scales. As a reference estuary, the Ems-Dollart estuary is considered. Characteristic scales for the Ems estuary can be found in Table A.1. One of the dimensionless parameters, that appears in the scaled equations, turns out to be small (its magnitude is much smaller than 1). Using this information, all physical variables in the governing equations are expanded in power series of this small parameter. By collecting terms of equal order in this small parameter, a system of hydrodynamic and concentration equations is constructed at each order. The resulting partial differential equations can be solved semi-analytically. The systems of equations are given in Chapters 2–4, and details of the scaling analysis and solution methods are presented in Appendix A4.

The research questions $\mathcal{Q}1$ – $\mathcal{Q}5$ are answered in different chapters of this thesis. In **Chapter 2**, the analytical width-averaged hydro- and sediment dynamic model is introduced to investigate the hydrodynamic processes and determine main importing/exporting mechanisms that results in (multiple) trapping of suspended sediment in an estuary. The model is calibrated to the Ems estuary, and the model results are compared to historical observations conducted in 1980 and 2005. This chapter addresses research question $\mathcal{Q}1$ and $\mathcal{Q}2$.

In **Chapter 3**, the model of Chapter 2 is developed further to include the influence of high suspended sediment concentration on the water density. This component is responsible for the formation of turbidity currents in an estuary that affect the turbidity region. This study answers research questions 21 and 23. Moreover, we conduct a sensitivity analysis of the suspended sediment trapping locations to geometrical characteristics and external forcing to answer research question 24.

The aim of **Chapter 4** is to investigate how different vertical eddy viscosity parametrization affects the turbidity zone and to answer the final research question 25. This is done by changing the parametrization of vertical mixing using different vertical eddy viscosity profiles.

Chapter 5 concludes the thesis by summarizing answers to the stated research questions and giving recommendations for further research.

The effect of tidal asymmetry and temporal settling lag on sediment trapping

Over decades and centuries, the mean depth of estuaries changes due to sea-level rise, land subsidence, infilling and dredging projects. These processes produce changes in relative roughness (friction) and mixing, resulting in fundamental changes in the characteristics of the horizontal (velocity) and vertical tides (sea surface elevation) and the dynamics of sediment trapping.

To investigate such changes, a 2DV model is developed. The model equations consist of the width-averaged shallow water equations and a sediment balance equation. Together with the condition of morphodynamic equilibrium, these equations are solved analytically by making a regular expansion of the various physical variables in a small parameter. Using these analytic solutions we are able to gain insight into the fundamental physical processes resulting in sediment trapping in an estuary by studying various forcings separately.

As a case study we consider the Ems estuary. Between 1980 and 2005 successive deepening of the Ems estuary has significantly altered the tidal and sediment dynamics. The tidal range and the surface sediment concentration has increased and the position of the turbidity zone has shifted into the freshwater zone. The model is used to determine the causes of these historical changes. It is found that the increase of the tidal amplitude towards the end of the embayment is the combined effect of the deepening of the estuary and a 37% and 50% reduction in the vertical eddy viscosity and stress parameter, respectively.

This chapter is based on Chernetsky AS, Schuttelaars HM, Talke SA (2010) *The effect of tidal asymmetry and temporal settling lag on sediment trapping in tidal estuaries*, Ocean Dynamics, Vol. 60, No. 5, pp. 1219 - 1241

The physical mechanism resulting in the trapping of sediment, the number of trapping regions and their sensitivity to grain size are explained by careful analysis of the various contributions of the residual sediment transport. It is found that sediment is trapped in the estuary by a delicate balance between the M_2 transport and the residual transport for fine sediment ($w_s = 0.2 \text{ mm s}^{-1}$) and the residual, M_2 and M_4 transports for coarser sediment ($w_s = 2 \text{ mm s}^{-1}$). The upstream movement of the estuarine turbidity maximum into the freshwater zone in 2005 is mainly the result of changes in tidal asymmetry. Moreover, the difference between the sediment distribution for different grain sizes in the same year can be attributed to changes in the temporal settling lag.

2.1 Introduction

In many estuaries, regions are found with sediment concentrations exceeding those directly upstream or downstream. The region where the highest sediment concentration is found is called the estuarine turbidity maximum (ETM). Quite often multiple peaks of high concentration are found in estuaries (see e.g. [Lin and Kuo \(2001\)](#) and references therein). This trapping of sediment is the result of the complex interaction of the water motion (forced by tides, river discharge, density gradients) and sediment dynamics (availability of sediment, sediment size, flocculation). At the locations with high sediment concentrations, depleted levels of oxygen (and hence degraded environmental conditions) are often observed ([De Jonge, 1983](#); [Talke et al, 2009a](#)). Since anthropogenic and natural changes (e.g., sea-level rise, land subsidence, etc.) in estuaries can influence the locations where sediment is trapped and/or the amount of sediment being trapped, it is important to understand the physical mechanisms resulting in the trapping of sediment and how these mechanisms are influenced by changes to the system.

An example of an estuary where major changes took place over the past 25 years is the Ems estuary, located on the border between the Netherlands and Germany. Recent observations on the river Ems document an increase in tidal range and suspended sediment concentration (SSC) and the development of hypoxic conditions between 1980 and the present as a response to maintenance dredging and deepening ([Krebs and Weilbeer, 2008](#); [Talke et al, 2009a,b](#)). The tidal river has also shifted from a sandy bed to a silty bed ([Krebs and Weilbeer, 2008](#)). Further details about the estuary and changes are provided in Section 2.4.1 and Table 2.1. The ETM has moved upstream, but the physical mechanism producing this change is still debated. [Talke et al \(2009a\)](#) show that observed changes can be reproduced with a simple model of gravitational circulation and river dis-

charge; however, other studies speculate that tidal pumping and tidal asymmetry are important (Wurpts and Torn, 2005).

To understand this kind of changes in estuarine dynamics, large scale numerical models are often applied (see e.g. Weilbeer (2008) for the Ems estuary). Because 3D numerical models are computationally expensive and include the sum of many processes (e.g., baroclinic circulation, tidal straining, tidal pumping, flocculation, settling and scour lag, non-linear interactions, etc.), it becomes difficult to isolate the magnitude and importance of particular processes or investigate parameter sensitivity. These limitations motivate the development of idealized models in which specific physical mechanisms can be studied in isolation. The advantage of an idealized model is that it is complex enough to reproduce the physical behavior of the system well, yet it is relatively simple to construct analytical solutions using standard mathematical techniques, avoiding high computational costs. This allows us to identify and analyze the importance of each forcing mechanism separately.

Various mechanisms have been identified that can result in the trapping of sediment. For example, using a tidally averaged numerical model, Festa and Hansen (1978) investigated the convergence zone of sediment due to the balance between gravitational circulation (Hansen and Rattray, 1965; Officer, 1976) and freshwater discharge. Recently, the Festa and Hansen approach was extended to include the influence of longitudinal suspended sediment concentration gradients on the tidally averaged flows and the trapping of sediment (Talke et al, 2009b). The importance of tidally varying processes on the formation of residual (tidally averaged) flows and sediment transports is discussed in many publications (Simpson et al, 1990; Geyer, 1993; Jay and Musiak, 1994; Burchard and Baumert, 1998). Recently, an idealized model was developed to study the depth-dependent water motion on the tidal time-scale in an estuarine cross-section (Huijts et al, 2009) and its interaction with the entrainment of sediment in the lateral direction (Huijts et al, 2006). However, no such model has been developed that describes these processes in the longitudinal direction.

The main aim of the present chapter is to develop an analytical model that simulates the along-channel flows resulting from various forcings such as the semi-diurnal and first overtide external forcing, the horizontal density gradient and river discharge (our first longitudinal analytical model for residual hydrodynamic model was presented in Chernetsky et al (2008)). From the water motion we calculate the sediment concentration in morphodynamic equilibrium in the estuary. Using the model we are able to investigate the relative importance of various forcing mechanisms and parameters (e.g. tidal dynamics, sediment grain

size, residual flows, etc.) on the changes that occurred between 1980 and 2005. In this chapter we address the following research questions. Why did the tidal range increase by 1.5 m in the upstream reaches between 1980 and 2005? Which mechanisms result in the trapping of sediment and in the variation of the trapping location for sediment with a different grain size under the same hydrodynamic conditions? Why is there an upstream shift of the turbidity zone in 2005 compared to 1980?

In Section 2.2, we discuss the model equations we use to model the water motion and sediment dynamics: the width-averaged shallow water and advection-diffusion equations, respectively. We make a perturbation analysis and provide analytic solutions of the problem in Section 2.3. Comparison with observations and results are provided in Section 2.4, followed by a discussion in Section 2.5 and conclusions in Section 2.6.

2.2 Model Formulation

To focus on the water motion and sediment dynamics in the longitudinal direction, we develop a width-averaged model for an estuary that is constrained by a weir at the landward side. The seaward boundary of the estuary is located at $x = 0$, the weir is found at $x = L$ (see Fig. 2.1). The estuary is assumed to be exponentially converging, i.e., the width $B(x)$ of the estuary is given by

$$B(x) = B_0 e^{-x/L_b}, \quad (2.1)$$

with B_0 the width of the estuary at the seaward side and L_b the exponential convergence length. We assume there are no tidal flats. The bed profile is described by $z = -H(x)$, $z = 0$ denotes the undisturbed water level and $z = \zeta(t, x)$ denotes the water surface.

The flow in the longitudinal direction is modeled by the width-averaged shallow water equations:

$$u_x + w_z - \frac{u}{L_b} = 0, \quad (2.2a)$$

$$u_t + uu_x + wu_z + g\zeta_x - \frac{g\rho_x}{\rho_0}(z - \zeta) - (A_v u_z)_z = 0. \quad (2.2b)$$

Here, $x(u)$ and $z(w)$ denote the along-channel and vertical coordinate (velocity), respectively. Time is denoted by t , $g \sim 10 \text{ m}^2/\text{s}$ is the gravitational acceleration, $\rho_0 \sim 1020 \text{ kg m}^{-3}$ is the reference density and A_v is the vertical eddy viscosity function.

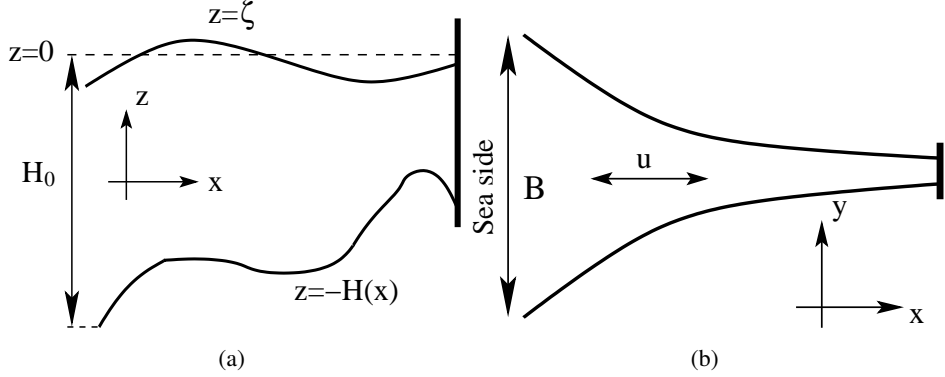


Figure 2.1: Sketch of the model geometry. The left panel depicts the side view of the estuary and the right one presents the top view. A Cartesian coordinate system is used, with x the along-channel coordinate directed landwards, y the transverse coordinate and z the vertical coordinate pointing upwards. Other variables are introduced in the text.

The along-channel density of the estuarine water is denoted by $\rho(x)$ and varies in general due to the salinity s , suspended sediment concentration c , temperature and pressure. To simplify, we neglect the density gradients caused by suspended sediment concentration (SSC), temperature and pressure, and assume that the temporal variations of the salinity field are small compared to the time-averaged salinity field. Furthermore, we assume that the salinity is vertically well-mixed. Hence, the along-channel density ρ is modeled as

$$\rho(s) = \rho_0(1 + \beta \langle s(x) \rangle), \quad (2.3)$$

where $\beta \sim 7.6 \times 10^{-4} \text{ psu}^{-1}$ converts salt to density and the angular brackets $\langle \cdot \rangle$ denote a tidal average. Here, $\langle s(x) \rangle$ is the observed along-channel time- and depth-averaged salinity profile which describes the gradual decrease of the salinity from the sea to the river (i.e. the model is diagnostic in salinity). The salinity profile is prescribed as a hyperbolic tangent profile along the estuary that depends on the freshwater discharge (see [Talke et al \(2009a\)](#)).

Following [Friedrichs and Hamrick \(1996\)](#), the vertical eddy viscosity function A_v is parameterized as

$$A_v(x) = A_{v0} \frac{H(x)}{H_0}, \quad (2.4)$$

with A_{v0} the eddy viscosity coefficient and H_0 the water depth at the entrance of the estuary.

At the free surface, $z = \zeta$, the boundary conditions are the no stress condition and the kinematic boundary condition:

$$A_v u_z = 0 \quad \text{and} \quad w = \zeta_t + u \zeta_x. \quad (2.5)$$

As boundary condition at the bottom, $z = -H(x)$, we assume the bed to be impermeable, i.e.,

$$w = -u H_x \quad (2.6)$$

and prescribe a partial slip condition:

$$\tau_b \equiv \rho_0 A_v u_z = \rho_0 s u \quad \text{at} \quad z = -H(x). \quad (2.7)$$

Note that this condition must be evaluated at the top of the constant stress layer instead of at the true bed. The bottom stress τ_b is proportional to friction velocity squared. By linearizing the quadratic friction law (Zimmerman, 1992) τ_b can be related the velocity at the bed and reads $\tau_b = \rho_0 s u$. Hence, the partial slip condition can be rewritten as $A_v u_z = s u$ (Schramkowski et al, 2002). Here, the parameter s is the so-called stress or slip parameter that can still depend on the longitudinal coordinate. Following Friedrichs and Hamrick (1996) and Schramkowski et al (2002), this dependency is taken to be linear in the local water depth, i.e.,

$$s = s_0 \frac{H(x)}{H_0}.$$

The water motion is forced by a prescribed tidal elevation at the seaward side of the estuary, $x = 0$, that consists of a semi-diurnal (M_2) constituent and its first overtide (M_4)

$$\zeta(t, 0) = A_{M_2} \cos \sigma t + A_{M_4} \cos(2\sigma t - \phi),$$

where $\sigma = 1.4 \cdot 10^{-4} \text{ s}^{-1}$ is the tidal frequency of the M_2 semi-diurnal tidal constituent, and A_{M_2} and A_{M_4} are the amplitude of the M_2 and M_4 (externally forced) tidal constituent, respectively. The relative phase ϕ is the phase difference between the M_4 and M_2 tidal components, defined by $\phi = \phi_{\zeta_{M_4}} - 2\phi_{\zeta_{M_2}}$, where $\phi_{\zeta_{M_2}}$ ($\phi_{\zeta_{M_4}}$) denotes the phase of the M_2 (M_4) tidal constituent. Apart from the externally prescribed M_4 overtide, overtidal components are generated internally by nonlinear interactions. The combination of the M_2 and M_4 constituents results in so-called tidal asymmetry: an estuary is called flood (ebb) dominant if flood currents are stronger (weaker) than ebb currents.

At the riverine side, $x = L$, a constant river discharge Q is prescribed and the tidal discharge is required to vanish

$$B(L) \int_{-H}^{\zeta} u(L, z) dz = Q. \quad (2.8)$$

Sediment is assumed to consist of noncohesive fine particles that have a uniform grain size (constant settling velocity) and are transported primarily as suspended load. The governing equation for the sediment dynamics is the width-averaged sediment mass balance equation (for a derivation, see Appendix A2)

$$c_t + uc_x + wc_z = w_s c_z + (K_h c_x)_x + (K_v c_z)_z - \frac{1}{L_b} K_h c_x, \quad (2.9)$$

where c denotes the width-averaged suspended sediment concentration and $w_s \sim 0.2 - 5 \text{ mm s}^{-1}$ the settling velocity. The turbulent vertical eddy diffusivity function K_v is assumed to be equal to A_v . The horizontal diffusivity coefficient is denoted by K_h . Suspended sediment is transported due to diffusive contributions, temporal (or local) settling lag effects (related to tidal asymmetry and local inertia, see Groen (1967)), and spatial settling lag effects (which are related to the finite time for sediment particles to settle, see Postma (1954); De Swart and Zimmerman (2009)).

At the surface, we require that no sediment particles enter or leave the domain, i.e., the normal component of the settling and diffusive flux balance

$$w_s c + K_v c_z - K_h c_x \zeta_x = 0 \quad \text{at} \quad z = \zeta. \quad (2.10)$$

The normal component of the sediment flux at the bottom due to erosion is given by

$$E_s \equiv -K_v c_z n_z - K_h c_x n_x = w_s c_* \quad \text{at} \quad z = -H(x). \quad (2.11)$$

Here, $\vec{n} = (n_x, n_z)$ is the upward unit normal vector at the bottom with n_x and n_z being components along the x and z axes and c_* is a reference concentration. It is defined as

$$c_*(t, x) = \rho_s \frac{|\tau_b(t, x)|}{\rho_0 g' d_s} a(x), \quad (2.12)$$

where the density of sediment is denoted by ρ_s , the dimensionless bed shear stress by $\tau_b/(\rho_0 g' d_s)$ with τ_b defined in Eq. (2.7) and the erosion coefficient by $a(x)$.

Furthermore, d_s is the grain size of the sediment and $g' = g(\rho_s - \rho_0)/\rho_0$ is the reduced gravity. The erosion coefficient $a(x) \sim 10^{-5}$ models the along-channel distribution of easily erodible sediment, available in mud reaches.

Following [Friedrichs et al \(1998\)](#) and [Huijts et al \(2006\)](#), we will consider our system to be in morphodynamic equilibrium, which means that there is no evolution of the bed over a tidal period. This approach is valid when the easily erodible sediment is redistributed on a much shorter timescale than the typical timescale at which the external forcing changes significantly. Hence there is a balance between the tidally averaged erosion and deposition at the bottom $z = -H(x)$. The erosion flux is defined in Eq. (2.11), the depositional sediment flux D is defined by

$$D = w_s c n_z \quad \text{at} \quad z = -H(x).$$

Assuming that $\langle E \rangle - \langle D \rangle = 0$, a condition for morphodynamic equilibrium is obtained by integrating the sediment mass balance equation (Eq. (2.9)) over depth. Using boundary conditions (2.5), (2.6), (2.10) and averaging the result over a tidal period, the morphodynamic equilibrium condition reads (for details, see Appendix A3)

$$\left\langle \int_{-H}^{\xi} (uc - K_h c_x) dz \right\rangle = 0, \quad (2.13)$$

where we assumed that there is no residual sediment flux at the weir. Here, angular brackets $\langle \cdot \rangle$ indicate an average over the tidal period.

The sediment concentration in the morphodynamic equilibrium still depends on the unknown erosion coefficient $a(x)$. Since the sediment concentration depends linearly on the erosion coefficient and the water motion is assumed to be independent of c , the morphodynamic equilibrium condition (2.13) can be rewritten as a first order linear differential equation for the erosion coefficient $a(x)$

$$F \frac{da}{dx} + Ta = 0, \quad (2.14)$$

where $F = \left\langle \int_{-H}^{\xi} -K_h \frac{c}{a} dz \right\rangle$ and $T = \left\langle \int_{-H}^{\xi} \left(u \frac{c}{a} - K_h \left(\frac{c}{a} \right)_x \right) dz \right\rangle$.

By prescribing the total amount of sediment available at the bottom for resus-

pension, the integration constant can be determined by requiring

$$\frac{\int_0^L B(x)a(x)dx}{\int_0^L B(x)dx} = a_*, \quad (2.15)$$

where a_* is the average amount of sediment available for resuspension. Note that a_* is an input parameter and the model yields the suspended sediment concentration up to a specified concentration.

2.3 Perturbation analysis and solutions

In this section we will approximate the system of equations discussed in Section 2.2 to obtain a (semi-) analytic solution. Here, we will only give a short outline of the procedure used to construct the reduced system of equations, for a detailed description of this procedure and the solution method used to solve the resulting reduced system of equations (see Appendix A4).

First, the relative importance of the various terms in the model equations is established by performing a scaling analysis, using parameter values representative for the Ems estuary (see Table 2.1, which is discussed in detail in Section 2.4). One of the dimensionless parameters that appears in the scaled equations is the ratio of the M_2 tidal amplitude A_{M_2} and the undisturbed water depth H_0 . This ratio, denoted by ε , is much smaller than one, i.e. $\varepsilon = A_{M_2}/H_0 \ll 1$. The other dimensionless parameters are compared to this small parameter ε .

Next, we approximate the solution of the dimensionless equations and the boundary conditions by expanding the physical variables in power series of the small parameter ε . This expansion is substituted in the scaled equations and terms of the zeroth (first) order of ε are collected, resulting in a leading (first order) system of equations. The leading order system is presented in Section 2.3.1, the first order system in Section 2.3.2 and the morphodynamic equilibrium condition is discussed in Section 2.3.3.

2.3.1 Leading order system of equations

In leading order, i.e. $\mathcal{O}(\varepsilon^0)$, the dimensional system of equations describing the water motion reads

$$u_x^{02} + w_z^{02} - \frac{u^{02}}{L_b} = 0, \quad (2.16a)$$

$$u_t^{02} + g\zeta_x^{02} - (A_v u_z^{02})_z = 0. \quad (2.16b)$$

The first superscript denotes the order of ε , the second superscript is the index of the lunar constituent under consideration, i.e. in leading order only an M_2 signal is present in the water motion.

The boundary condition at the riverine side requires the depth-averaged velocity to vanish at the weir. At the entrance the system is forced by an externally prescribed semi-diurnal tide. These conditions read

$$\zeta^{02} = A_{M_2} \cos(\sigma t) \quad \text{at} \quad x = 0, \quad (2.17a)$$

$$\int_{-H}^0 u^{02} dz = 0 \quad \text{at} \quad x = L. \quad (2.17b)$$

At the free surface $z = 0$, the boundary conditions are given by

$$w^{02} = \zeta_t^{02} \quad \text{and} \quad A_v u_z^{02} = 0. \quad (2.18)$$

At the bottom $z = -H(x)$, the boundary conditions read

$$w^{02} = -u^{02} H_x \quad \text{and} \quad A_v u_z^{02} = s u^{02}. \quad (2.19)$$

The solution of Eqs. (2.16)-(2.19) describes the propagation of tidal waves in a medium with effectively a homogeneous density and a varying depth. It is solved by reducing the system to a homogeneous ordinary boundary-value problem for the sea surface elevation ζ^0 (see Ianniello (1977) and Appendix A4.1 for details).

The dynamics of the sediment concentration in leading order is given by

$$c_t^0 - w_s c_z^0 = (K_v c_z^0)_z. \quad (2.20)$$

Hence, in leading order, the evolution of the sediment concentration is governed by local inertia, settling and vertical mixing of sediments.

Boundary conditions at the free surface $z = 0$, require no flux through the boundary,

$$w_s c^0 + K_v c_z^0 = 0. \quad (2.21)$$

At the bottom, $z = -H(x)$, the boundary condition reads

$$-K_v c_z^0 = w_s \rho_s \frac{s|u^0(t,x)|}{g'd_s} a(x). \quad (2.22)$$

Since the water motion only consists of an M_2 tidal signal in leading order, it follows that the concentration has a residual (tidally averaged) component and all constituents with frequencies that are an even multiple of the M_2 tidal frequency, hence

$$c^0 = c^{00} + c^{04} + \dots \quad (2.23)$$

The sediment concentration c^0 still depends on the unknown erosion coefficient $a(x)$.

The solution method and analytical expressions of the semi-diurnal tidal velocity and sediment concentration components are given in Appendix A4.1.

2.3.2 Higher order system of equations

In this section, the first order system of equations is given. The water motion is discussed in subsection 2.3.2.1 and sediment dynamics in 2.3.2.2.

2.3.2.1 Water motion

The dimensional hydrodynamic equations in first order, i.e. $\mathcal{O}(\varepsilon^1)$, are given by

$$u_x^1 + w_z^1 - \frac{u^1}{L_b} = 0, \quad (2.24a)$$

$$u_t^1 + \underline{u_x^{02} u_x^{02}} + \underline{w_z^{02} u_z^{02}} + g \zeta_x^1 - g \beta \langle s \rangle_x z = (A_v u_z^1)_z, \quad (2.24b)$$

where the underlines $\underline{\quad}$ denote individual forcing terms, which are discussed later.

At the free surface $z = 0$, the boundary conditions read

$$w^1 = \zeta_t^1 - \underline{\zeta^{02} w_z^{02}} + \underline{u^{02} \zeta_x^{02}} \quad \text{and} \quad A_v u_z^1 + \underline{A_v \zeta^{02} u_{zz}^{02}} = 0, \quad (2.25)$$

and at the bottom $z = -H(x)$

$$w^1 = -u^1 H_x \quad \text{and} \quad A_v u_z^1 = s u^1. \quad (2.26)$$

The boundary conditions at the riverine side and entrance are given by

$$\int_{-H}^0 u^1 dz = \underline{Q/B} \quad \text{at} \quad x = L, \quad (2.27)$$

$$\zeta^1 = \underline{A_{M_4} \cos(2\sigma t - \phi)} \quad \text{at} \quad x = 0. \quad (2.28)$$

Careful inspection of Eqs. (2.24)-(2.28) shows that the order ε velocity fields u^1, w^1 and the sea surface elevation ζ^1 consist of the residual contributions ($u^{10}, w^{10}, \zeta^{10}$) and contributions ($u^{14}, w^{14}, \zeta^{14}$) which oscillate with twice the frequency of the semi-diurnal tide. These contributions are discussed separately in the following paragraphs. The solution method is presented in Appendix A4.2.

Residual flow. By averaging over a tidal period, a forced linear system that describe the residual flow is obtained:

$$u_x^{10} + w_z^{10} - \frac{u^{10}}{L_b} = 0, \quad (2.29a)$$

$$\underbrace{\langle u_x^{02} u_x^{02} + w_z^{02} u_z^{02} \rangle}_{\text{TS}} + g \zeta_x^{10} - \underbrace{g \beta \langle s \rangle_x}_z = (A_v u_z^{10})_z. \quad (2.29b)$$

where the underbraces $\underbrace{\cdot}$ denote the individual residual forcing terms. The semi-diurnal tidal components $u^{02}, w^{02}, \zeta^{02}$ were obtained in Section 2.3.1.

At the free surface $z = 0$, the boundary conditions are given by

$$w^{10} = - \underbrace{\langle \zeta^{02} w_z^{02} - u^{02} \zeta_x^{02} \rangle}_{\text{SD}} \quad \text{and} \quad A_v u_z^{10} + \underbrace{\langle A_v \zeta^{02} u_{zz}^{02} \rangle}_{\text{SC}} = 0. \quad (2.30)$$

At the bottom $z = -H(x)$, the boundary conditions read

$$w^{10} = -u^{10} H_x \quad \text{and} \quad A_v u_z^{10} = s u^{10}. \quad (2.31)$$

The boundary condition at the riverine side is that the depth and tidally averaged velocity equals the river discharge at the weir and at the entrance, the tidally averaged sea surface elevation in first order is zero. Those conditions read

$$\int_{-H}^0 u^{10} dz = \underbrace{\frac{Q}{B}}_{\text{RI}} \quad \text{at} \quad x = L, \quad (2.32a)$$

$$\zeta^{10} = 0 \quad \text{at} \quad x = 0. \quad (2.32b)$$

Equations (2.29) together with boundary conditions (2.30)-(2.32) describe the residual water motion in the estuary which is driven by the residual forcing terms. First, the water motion is forced by the residual constituent of nonlinear interactions of the leading order M_2 tide due to advective contribution (TS). Second, there is a time-independent forcing (GC) due to the presence of a salinity gradient $\langle s \rangle_x$ (gravitational circulation). Third, there is the tidal return transport (SD), which is the residual transport that compensates for the correlation between horizontal and vertical water motion (Stokes transport). Fourth, there is the residual constituent due to the no-stress condition at the surface (SC). Finally, there is a river discharge prescribed at the weir, resulting in a residual water motion in the estuary (RI).

Since this system of equations is linear, we can study the importance of each forcing mechanism separately, i.e. the resulting solution for the residual velocity fields u^{10} and w^{10} and the sea surface elevation ζ^{10} reads

$$\chi^{10} = \chi_{\text{TS}}^{10} + \chi_{\text{GC}}^{10} + \chi_{\text{SD}}^{10} + \chi_{\text{SC}}^{10} + \chi_{\text{RI}}^{10}, \quad (2.33)$$

where $\chi^{10} = (u^{10}, w^{10}, \zeta^{10})$.

First overtide (M_4) flow. The M_4 constituent of the water motion is described by the following system of forced equations

$$u_x^{14} + w_z^{14} - \frac{u^{14}}{L_b} = 0, \quad (2.34a)$$

$$u_t^{14} + \underbrace{[u_x^{02} u_x^{02} + w_z^{02} u_z^{02}]}_{\text{AC}} + g \zeta_x^{14} = (A_v u_z^{14})_z, \quad (2.34b)$$

where braces $[\cdot]$ denote the M_4 contribution and the underbraces $\underbrace{\cdot}$ are the individual M_4 forcing terms.

At the free surface $z = 0$, the boundary conditions are given by

$$w^{14} = \zeta^{14} + \underbrace{[u_x^{02} \zeta_x^{02} - \zeta_x^{02} w_z^{02}]}_{\text{FS}} \quad \text{and} \quad A_v u_z^{14} + \underbrace{A_v [\zeta_x^{02} u_{zz}^{02}]}_{\text{NS}} = 0. \quad (2.35)$$

At the bottom $z = -H(x)$, the boundary conditions read

$$w^{14} = -u^{14} H_x \quad \text{and} \quad A_v u_z^{14} = s u^{14}. \quad (2.36)$$

The boundary conditions at the entrance and riverine side are identical to those of the leading order conditions, but at the entrance the system is forced by the

externally prescribed M_4 tide. These conditions are

$$\zeta^{14} = \underbrace{A_{M_4} \cos(2\sigma t - \phi)}_{\text{EF}} \quad \text{at} \quad x = 0, \quad (2.37a)$$

$$\int_{-H}^0 u^{14} dz = 0 \quad \text{at} \quad x = L. \quad (2.37b)$$

System (2.34) and boundary conditions (2.35)-(2.37) describe the M_4 water motion in the estuary driven by: the M_4 constituent of nonlinear interactions of the leading order M_2 tide due to advective contribution (AC); the M_4 transport (FS) that compensates for the correlation between horizontal and vertical water motion; and the M_4 constituent of no-stress condition at the surface (NS). The AC, FS and NS constituents are produced within the estuary and are referred to as the internally generated overtide. Moreover, the water motion is forced by an externally prescribed overtide (forcing term EF). These four components result in a M_4 tidal motion in the estuary.

As with the residual flow, the solution to Eqs. (2.34) can be decomposed into different contributions, each induced by an individual forcing mechanism:

$$\chi^{14} = \chi_{\text{AC}}^{14} + \chi_{\text{FS}}^{14} + \chi_{\text{NS}}^{14} + \chi_{\text{EF}}^{14}, \quad (2.38)$$

where $\chi = (u^{14}, w^{14}, \zeta^{14})$. Thus, we can investigate the influence of each forcing separately.

2.3.2.2 Sediment dynamics

The sediment mass balance equation (Eq. 2.9) and its boundary conditions at first order are equivalent to those in leading order, with the first order component of the bed shear stress given by

$$|\tau_b^1| = \rho_0 s u^1 \frac{u^{02}}{|u^{02}|} \quad \text{at} \quad z = -H. \quad (2.39)$$

Based on Eq. (2.39), it can be concluded that the first-order sediment concentration is a result of the leading order and the first order tidal flow interaction.

Applying a Fourier analysis to the bottom boundary condition (2.11) for the sediment concentration equation, it can be deduced that the higher-order concentration consists of all tidal components

$$c^1 = c^{10} + c^{12} + \dots \quad (2.40)$$

Note that, we assume the nonlinear terms $uc_x + wc_z$ are of $\mathcal{O}(\varepsilon^2)$ and, therefore, they do not enter into the first order concentration equation (see Appendix A4). These terms result in the spatial settling lag effect. Treating these nonlinear terms as order ε^1 quantities will result in additional mean and overtide components of the first order. Solving these components will be straightforward, but will significantly complicate the analysis. Since our goal is to gain understanding of sediment transport, these nonlinear terms are neglected at a first step.

2.3.3 Morphodynamic equilibrium condition

The leading order morphodynamic equilibrium condition reads (for details, see Appendix A4.3)

$$\int_{-H}^0 (u^{10}c^{00} + \langle u^{02}c^{12} \rangle + \langle u^{14}c^{04} \rangle - K_h \langle c_x^{00} \rangle) dz + \langle \zeta^0 [u^{02}c^0]_{z=0} \rangle = 0. \quad (2.41)$$

Here, the first contribution models the residual transport of sediment due to interactions of the residual velocity and the time-averaged sediment concentration. Note that we can decompose this transport even further as we have separate expressions for the residual flow components due to different forcing agents (see Eq. (2.33)). The second term describes the semi-diurnal sediment transport which occurs due to the interactions of the semi-diurnal velocity and the M_2 concentration. The third component represents the first overtide transport of sediment and is a result of the interactions of the first overtide velocity and the M_4 concentration. The horizontal diffusive transport and a transport due to the correlation between the tidal return flow and concentration are represented by the fourth and fifth terms, respectively. Note that, as in the case with the residual sediment transport, we can perform further decomposition of the aforementioned fluxes.

The sediment concentration in the morphodynamic equilibrium condition still depends linearly on the unknown erosion coefficient $a(x)$, i.e., $c^{00} = a(x)c^{00a}$, $c^{04} = a(x)c^{04a}$ and $c^{12} = a(x)c^{12a}$, where c^{00a} , c^{04a} , and c^{12a} are independent of $a(x)$. This results in a linear first order ordinary differential equation for the erosion coefficient $a(x)$

$$Fa_x + Ta = 0, \quad (2.42)$$

with

$$F = \left\langle \int_{-H}^0 -K_h c^{00a} dz \right\rangle,$$

$$\begin{aligned}
T = & \underbrace{\int_{-H}^0 u^{10} c^{00a} dz + \left\langle \zeta^0 [u^{02} c^{0a}]_{z=0} \right\rangle}_{T_{\text{res}}} + \underbrace{\int_{-H}^0 \langle u^{02} c^{12a} \rangle dz}_{T_{M_2}} + \\
& \underbrace{\int_{-H}^0 \langle u^{14} c^{04a} \rangle dz}_{T_{M_4}} - \underbrace{\int_{-H}^0 K_h \langle c_x^{00a} \rangle dz}_{T_{\text{diff}}}.
\end{aligned}$$

Here, the underbraces $\underbrace{\quad}$ denote different contributions of the residual sediment transport T , induced by various interactions between the velocity and concentration: T_{res} is the transport, which results from the interaction of the residual velocity with the residual concentration, T_{M_2} is the transport due to the M_2 velocity and M_2 concentration interaction, T_{M_4} is the transport due to the M_4 velocity and M_4 concentration interaction and T_{diff} is the diffusive transport. These contributions are discussed in detail in Section 2.5.2.1.

2.4 Results

In this section the model developed in Sections 2.2 and 2.3 is used to gain insight into both the hydrodynamics and sediment dynamics in the Ems estuary. There has been a distinct change in both the water motion and sediment dynamics over the past 30 years in this estuary. These changes and the general characteristics of the Ems estuary are briefly discussed in Section 2.4.1. Using the observations carried out in 1980 and 2005 on the Ems estuary we will investigate the ability of the model to reproduce the main characteristics of the hydro- and sediment dynamics (Section 2.4.2), resulting in a physical explanation for why the dynamics changed so drastically. The water motion results are discussed in Section 2.4.3, followed by Section 2.4.4 in which the sediment dynamics and the trapping of sediment in the estuary are discussed.

2.4.1 Characteristics of the Ems estuary

The Ems estuary is situated on the border between the Netherlands and Germany and runs from the island of Borkum to the tidal weir in Herbrum. Its length from the geographical entrance (the barrier islands) to the tidal weir is approximately 100 km. In this chapter, the zero of the along-channel coordinate axis x is located at Knock, with x increasing towards the weir at Herbrum (see Fig. 2.2).

Moreover, in the remainder of the chapter the term entrance denotes the model entrance, which is km 0 in our coordinate system (Knock), and not the geographical entrance of the Ems estuary.

The Ems estuary is exponentially converging with a convergence length L_b of 30 km. The system is partially mixed and the landward limit of the salt intrusion varies with the river discharge and is usually found between 20 and 30 km (Talke et al, 2009a).

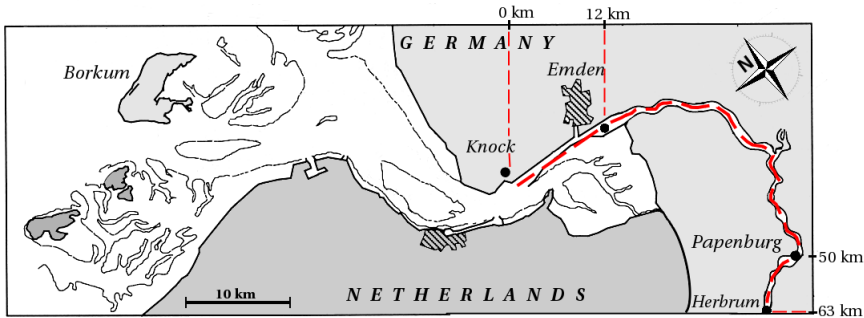


Figure 2.2: Map of the Ems estuary from the barrier island of Borkum in the North sea up to the tidal weir in Herbrum.

Approximately 90% of the fresh water input comes from the Ems river, the remaining 10% from other tributaries. The river discharge exhibits seasonal variations. The discharge is approximately $30 \text{ m}^3/\text{s}$ during low flow conditions (June–October) while $150 \text{ m}^3/\text{s}$ is observed during high flow conditions (November–April). The yearly average freshwater discharge is $70 \text{ m}^3/\text{s}$.

The solid red line in Fig. 2.3 shows the bathymetry of 1980. The depth of the navigation channel, i.e. the region between Emden and Papenburg, was approximately 4–5 m. At the entrance the tidal range was 3.1 m and the main tidal constituent was the M_2 tide with an amplitude of 1.43 m. The first overtide had an amplitude of approximately 0.25 m and a relative phase of -171.9° . The tidal range decreased upstream (near Papenburg it was approximately 2.3 m). Surface measurements registered that average SSC steeply increased from an average of 70 mg/l in Knock (km 0) to a maximum of 400 mg/l in Terborg (approximately km 25), and decreased sharply further upstream (De Jonge, 1983).

Between 1980 and 2005, shipping channels of the Ems river were deepened from 4–5 to 7 m. The solid blue line in Fig. 2.3 depicts the 2005 water depth (WSA Emden). At the entrance, the mean tidal range is now 3.2 m (the spring-

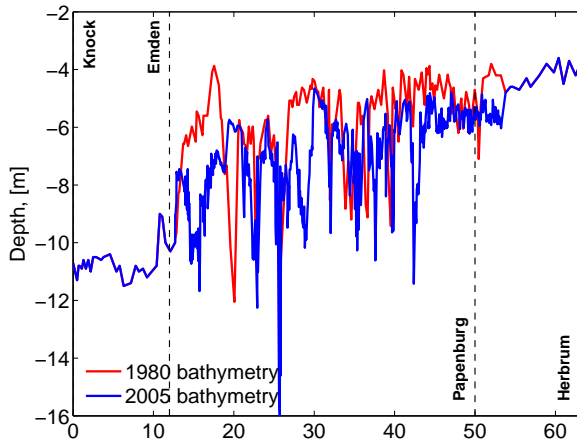


Figure 2.3: Bathymetry of the Ems estuary in 1980 and 2005.

neap tidal range is 3.5 and 2.7 m, respectively) and the main tidal constituent is the M_2 tide with an amplitude of 1.35 m. The first overtide has an amplitude of approximately 0.19 m and a relative phase of -174.6° . The tidal range increases upstream (near Papenburg it is approximately 3.8 m). Measurements between Pogum (km 15) and Rhede (km 59) in 2005-2006 found an average SSC of 950 mg/l with no distinct peak (V. de Jonge, personal communication).

A variety of measurements were used to calibrate the model to present conditions (labeled the '2005' case for convenience), and historical conditions (labeled '1980' for convenience). The variation of M_2 and M_4 water level at 8 locations (between kms 0, 13, 19.6, 27.4, 37.1, 44.4, 48, 63.5 in our coordinate system) along the estuary were obtained from measurements over 24 hours by the Wasser and Schifffartsamt (WSA), Emden on February 29th, 1980, during median tidal conditions. Concurrent measurements of water level and velocity from a nearly 14 hour period on April 25th, 1984 are used to estimate the historical phasing of flow and pressure. Velocity was estimated using hand held instruments every 15 minutes at 0.3 – 0.5 m increments in the water column at three locations on two cross sections located on Ems km 38.5 and 41.1. The phase difference between water level and flow used in the model is obtained from the average harmonic fit of near-surface measurements from the four available digitized data sets, and is approximately 65° .

Considerably more data was available to calibrate the '2005' model condition, which is subsequently better constrained. Continuous water level measurements

(5 - 30 minute increments) from 2005 and 2006 were obtained from the Niedersaechsischer Landesbetrieb fuer Wasserwirtschaft, Kuesten- und Naturschutz (NL-WKN) at the same locations as the 1980 data (between the towns of Knock and Herbrum). Additionally, velocity measurements from surface-moored Aandera RCM-9 probes deployed by WSA Emden were used to define the phase angle between surface tidal flows and water level at a total of six along-channel locations between January-April 2006. Because instruments were serviced occasionally or moved to different along-channel locations, some data gaps exist and the total data set spans approximately 2-2.5 months at each site. Bathymetry for the '2005' and '1980' case were obtained from surveys by WSA Emden in December 2004 and 1984, respectively.

Over most of the modeled estuary, bottom sediment consists primarily of silt (70 – 80%), with approximately 20 – 25% fine sand and $\sim 5\%$ clay (M. Krebs, personal communication). The channel bed before deepening was primary sandy (Krebs and Weilbeer, 2008). Observed flocculation settling velocities in the Ems-Dollart vary from < 0.0001 to 0.008 m s^{-1} (Van Leussen and Cornelisse, 1993, 1996; Van der Lee, 2000).

2.4.2 Model setup

Historical bathymetry, digitized from old charts, was only available between Emden and Herbrum. To be able to simulate the water motion and sediment dynamics for 1980, we have extended the available bathymetry of 1980 from Emden downstream to Knock and from Papenburg up to Herbrum by using the 2005 bathymetry. This is a fair assumption, since channel deepening was mainly carried out between Emden and Papenburg. Moreover, because we focus on flow and sediment pattern on the basin-scale, the bathymetries were smoothed using a lowpass filter.

Most other model parameters are directly obtained from the observations outlined in Section 2.4.1 and are summarized in Table 2.1.

The vertical eddy viscosity coefficient $A_{v,0}$ and the stress coefficient s_0 , which are unknown, are obtained by calibrating the model to the measured data. We minimize the difference between the observed and modeled semi-diurnal tidal amplitude (ζ_{M_2}), and the phase difference between the semi-diurnal free surface elevation and velocity ($\phi_{\zeta_{M_2}} - \phi_{u_{M_2}}$) in a least square sense. The other observations, such as the residual and M_4 tidal amplitude and velocity at the surface, are then used to validate the model. The resulting vertical eddy viscosity coefficient $A_{v,0}$ has decreased from $0.019 \text{ m}^2 \text{ s}^{-1}$ in 1980 to $0.012 \text{ m}^2 \text{ s}^{-1}$ in 2005. Apart from

Table 2.1: Model input parameters representing 1980 and 2005 measurements carried out along the Ems/Dollard estuary, respectively

Parameter	Symbol	Dimension	1980	2005
Semi-diurnal angular tidal frequency	σ	s^{-1}	1.4×10^{-4}	
Gravitational acceleration	g	$m s^{-2}$	9.8	
β	β	psu^{-1}	7.6×10^{-4}	
Ref. density	ρ_0	$kg m^{-3}$	1020	
Sediment density	ρ_s	$kg m^{-3}$	2650	
Length of the estuary	L	km	63.7	
Convergence length	L_b	km	30	
Water depth at the entrance	H_0	m	12.2	
M_2 tidal amplitude at the entrance	A_{M_2}	m	1.43	1.35
M_4 tidal amplitude at the entrance	A_{M_4}	m	0.25	0.19
Relative phase at the entrance	ϕ	degrees	-170.9	-174.6
Vertical eddy viscosity coefficient*	A_{v0}	$m^2 s^{-1}$	0.019	0.012
Stress coefficient*	s_0	$m s^{-1}$	0.098	0.049
River discharge	Q	m^3/s	65	
Settling velocity	w_s	$m s^{-1}$	0.0002 - 0.002	
Horizontal eddy diffusivity	K_h	$m^2 s^{-1}$	100	

Parameters marked with the asterisk * are obtained in Section 2.4.3.

this decrease of A_{v0} , $A_v(x)$ (see Eq. 2.4) decreased everywhere as well compared to the 1980 case. For the stress coefficient, we found $0.098 m s^{-1}$ in 1980 and $0.049 m s^{-1}$ in 2005 as best fit.

The river discharge that we use is $65 m^3 s^{-1}$. It is assumed that the turbulent vertical eddy diffusivity K_v is equal to the vertical mixing A_v . The horizontal diffusivity coefficient K_h is taken to be $100 m^2 s^{-1}$.

2.4.3 Water motion

Figs. 2.4(a) and 2.4(c) show the comparison of observations and model predictions of the semi-diurnal tidal amplitude, and Figs. 2.4(b) and 2.4(d) represent the phase difference between the semi-diurnal horizontal and vertical tide in 1980 and 2005, respectively (additional figures with comparison between observations and model predictions are given in Appendix A7). Unless explicitly stated otherwise, all velocities are taken at the sea surface. Here, the solid blue line represents the model results using parameter values given in Table 2.1, the red square marks the observed values. In dashed lines, we plotted the locations where the measurements were made in 2005. Comparison of these figures and additional model computations (see Appendix A6) shows that the tidal motion is closer to resonance in 2005 than 1980, as the M_2 amplitude increases and the phase difference between the horizontal velocity and water level is closer to 90° .

Fig. 2.5(a) shows the ratio of the M_4 over M_2 horizontal velocity at the surface. The solid blue (black) line represents the model results for the 2005 (1980) case, using parameter values given in Table 2.1 and the red square (cross) marks the observed values for 2005 (1980). The ratio of the M_4 over M_2 velocity amplitude has decreased from 1980 to 2005 in the first 20 km from the entrance and has increased everywhere else. Fig. 2.5(b) depicts the relative phase of the sea surface elevation, which is defined as $\phi_{\zeta M_4} - 2\phi_{\zeta M_2}$, where $\phi_{\zeta M_2}$ ($\phi_{\zeta M_4}$) is the phase of the M_2 (M_4) tidal elevation. The relative phase defines the duration of the rise and fall of the tide. Both observations and the model suggest that the duration of the falling tide is greater than the rising tide everywhere in the estuary, with no striking quantitative differences observed between 1980 and 2005. In Fig. 2.5(c), the relative phase of the horizontal velocity ($\phi_{u M_4} - 2\phi_{u M_2}$) is shown. The relative phase between the semi-diurnal tidal velocity, and its first overtide, i.e. the M_4 velocity, determines whether there is flood or ebb dominance (Aubrey and Speer, 1985; Van de Kreeke and Dunsbergen, 2000). If the relative phase is between -90° and 90° , the estuary is flood dominant; otherwise the estuary is ebb dominant. Model results presented in Fig. 2.5(c) suggest that the ebb/flood dominance changed between the two years. In 1980 there was only a pronounced flood dominance in the last 30 km of the estuary with a small ebb dominated region at the entrance. In 2005, however, the estuary was flood dominated everywhere.

In Fig. 2.6 the horizontal component of the residual velocity along the estuary is shown for 1980 (Fig. 2.6(a)) and 2005 (Fig. 2.6(b)). The maximum velocity magnitude of 0.4 m s^{-1} in both cases is located at the weir and results primarily from river discharge. From the weir towards the entrance the velocity gradu-

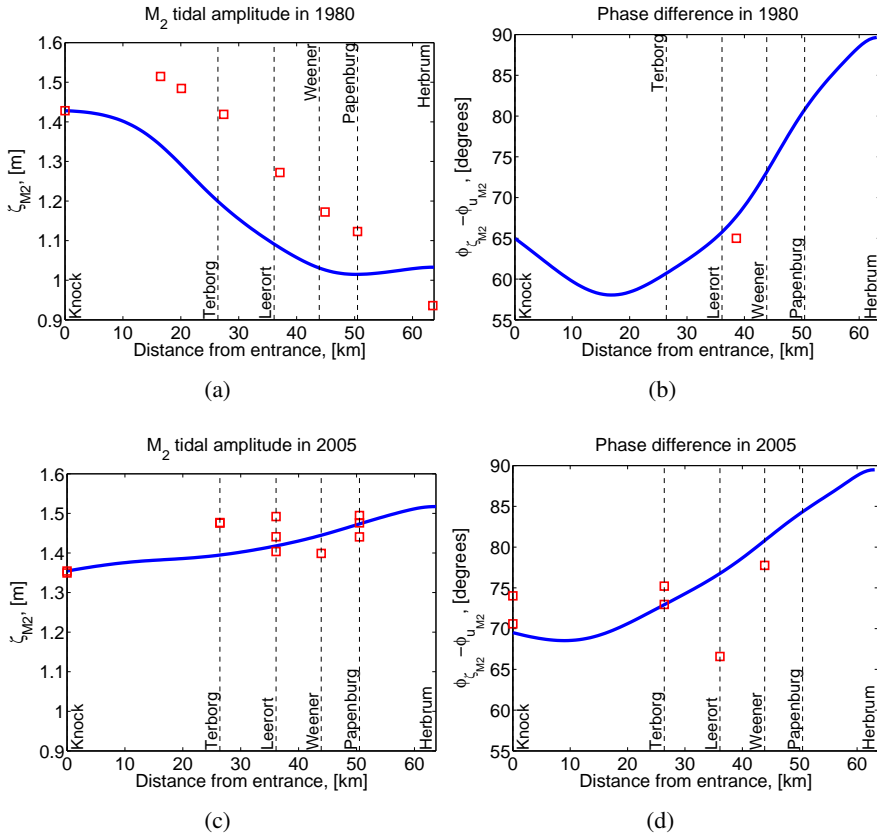


Figure 2.4: Comparison between observations and model predictions of the semi-diurnal tidal amplitude and phase difference between the semi-diurnal horizontal and vertical tide. The blue curves represent model predictions; the red squares show measured data at various measuring locations. The dashed lines depict locations at which the measurements were made in 2005. The left panels represent tidal amplitude along the estuary and the right ones depict relative phase shift between the free surface elevation and along-channel velocity component. The upper panels show 1980 case; the lower panels mimic the 2005 case.

ally decreases. At the entrance there is a region near the bed where the residual velocity changes direction from down-stream to up-stream (the zero contour is indicated by the black solid line). The model suggests that between 1980 and 2005, the region with up-stream directed velocity has advanced into the estuary by as much as 5 km.

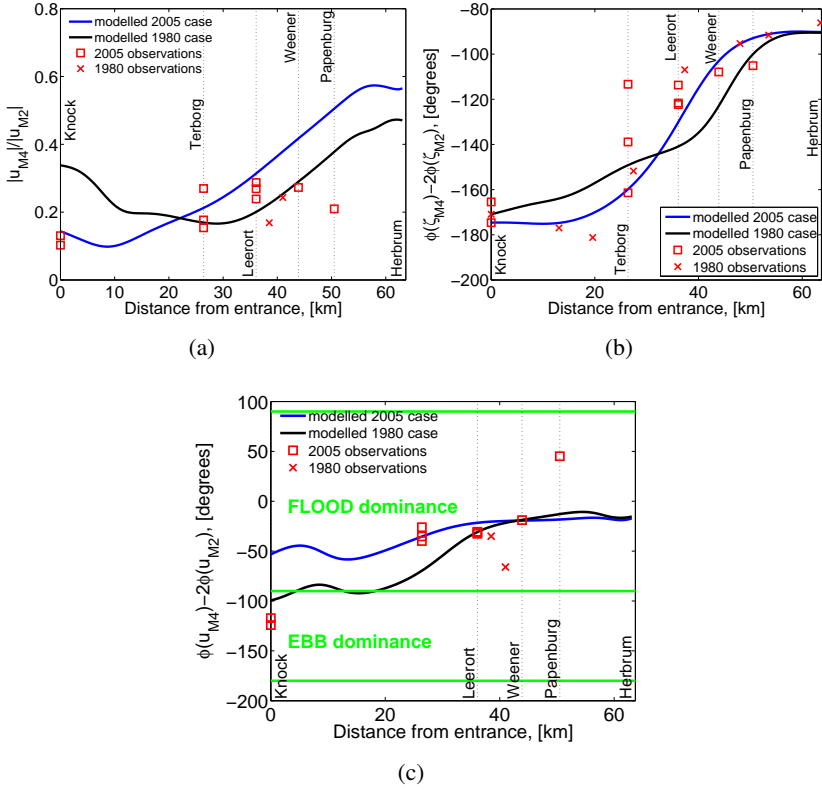


Figure 2.5: The water motion model results. The blue curves represent model predictions; the red marks show measured data at various locations. Scattered data at the same location means that measurements were done at various times. The dotted lines show locations at which the measurements were made in 2005. The upper left panel depicts the ratio of the M_4 over M_2 horizontal velocity at the surface and the upper right one represents the relative phase of the sea surface elevation. The lower panel shows the relative phase of the horizontal velocity at the surface. Changes from parameter regions with ebb and flood dominance are indicated by the green solid lines.

2.4.4 Sediment Dynamics

To reflect the observed variation in the grain size distribution, we modeled fine silt with a settling velocity w_s of approximately 0.0005 m s^{-1} and a coarser silt with a settling velocity of 0.002 m s^{-1} . All other parameters have their default values (see Table 2.1).

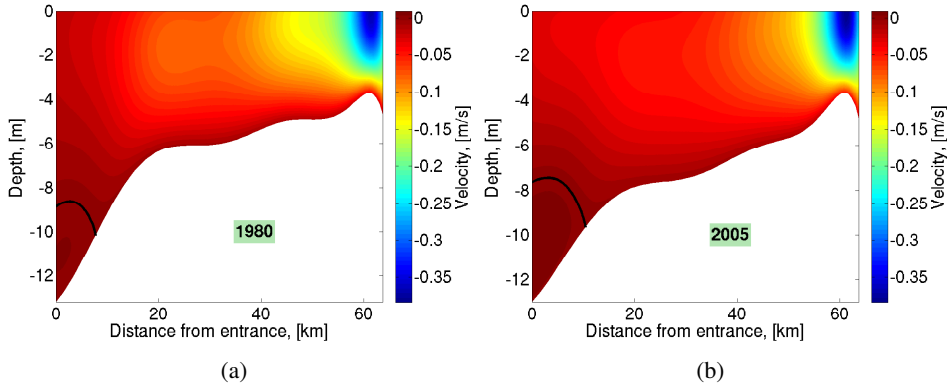


Figure 2.6: *The residual velocity model result. The black solid line depicts the zero contour. The left panel shows the 1980 case and the right one depicts 2005.*

Figs. 2.7(a) and 2.7(b) show the tidally averaged SSC for fine silt in morphodynamic equilibrium and Figs. 2.7(c) and 2.7(d) represent coarse silt in 1980 and 2005, respectively. In 1980 for both fine and coarse silt, Figs. 2.7(a) and 2.7(c) indicate that the trapping region is located near the upward limit of salt intrusion (from here on we define trapping of sediment at this location as the ETM at the classical location). For fine silt, this region is shifted upstream by approximately 7 km compared to coarse silt. In 2005 for fine silt, the trapping region has shifted upstream into the freshwater zone by approximately 19 km compared to the 1980 case. For coarse silt, we observe two ETMs: one near the upward limit of salt intrusion and the other one further upstream at km 42.5.

Note that the erosion coefficient $a(x)$ in the morphodynamic equilibrium condition is determined up to a constant a_* (see Eq. (2.15)). Here, we used $a_* = 10^{-5}$ to get the SSC at the surface of approximately 300 mg/l for fine sediment in 1980. An increase (decrease) of the constant a_* results in higher (lower) SSC. For both 1980 and 2005 we used the same a_* for consistency.

2.5 Discussion

In this section we will use the analytical model to explain the model results presented in the previous section. Section 2.5.1 provides an analysis of the hydrodynamic conditions in the estuary. In Section 2.5.2, we will study changes of trapping locations between 1980 and 2005 for fixed settling velocity w_s and river

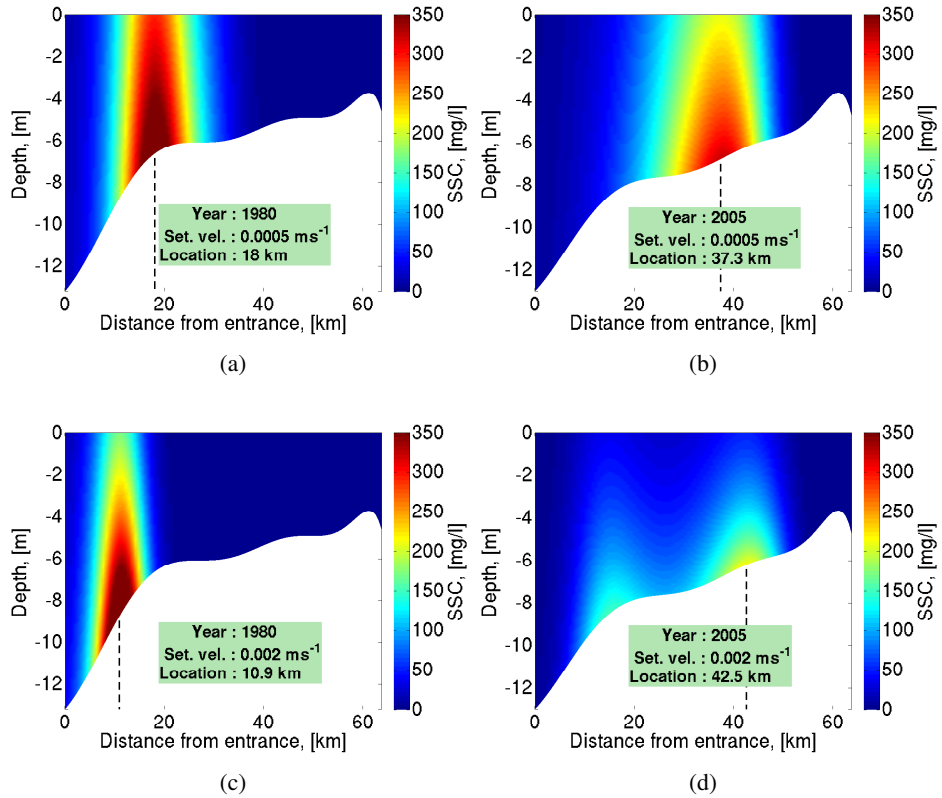


Figure 2.7: Tidally averaged suspended sediment concentration (SSC) in morphodynamic equilibrium. The upper panels show the SSC for fine silt and the lower ones depict coarse silt.

discharge Q and compare the difference in grain sizes for the same year. In Section 2.5.3, we will discuss the sensitivity of trapping locations to the settling velocity and river discharge.

2.5.1 Hydrodynamics

We start the analysis of the hydrodynamic conditions in the estuary by investigating the difference of the M_2 and M_4 tidal characteristics between 1980 and 2005. As shown in Fig. 2.4, the dimensionless M_2 tidal amplitude (the ratio of the M_2 tidal amplitude over its value at the entrance) at the landward side increased from

approximately 0.74 to 1.12 between 1980 and 2005. Furthermore, the relative phase between the horizontal velocity and water level is closer to 90° in 2005 compared to 1980, i.e. the character of wave has become more that of a standing wave and the estuary is closer to resonance. Spatial variation in phase have decreased. A similar amplification for the M_4 tide is observed.

We investigate the amplification of the M_2 tide by considering at two different scenarios (details are given in Appendix A6). Deepening the estuary to the 2005 depth, but keeping the 1980 A_v and s parameter values, results in an increase of the dimensionless M_2 tidal amplitude at the landward boundary to 0.89. Keeping the 1980 depth but using the 2005 parameter values for A_v and s results in the dimensionless M_2 tidal amplitude of approximately 0.99 at the landward side. Hence, we can conclude that, although the reduction of the vertical eddy diffusivity and stress parameter has more effect on the tidal resonance in the case of the Ems estuary, the observed amplification of the dimensionless M_2 tidal amplitude to approximately 1.12 in 2005 is a result of both factors acting simultaneously.

Next, we study the observed and modeled ebb and flood dominance in the estuary. The estuary is everywhere flood dominant in 2005, while in 1980 a small region at the entrance of the estuary was ebb dominated. The M_2 velocity phase curves have a similar trend, and they do not change the flood dominance between years (see Fig. 2.8(a)). The two contributions to the M_4 phase of the horizontal velocity at the surface are shown in Fig. 2.8(b). The blue line denotes the internally generated contribution which is caused by nonlinear interactions and the black line shows the externally forced contribution. Dashed lines depict the 1980 case and solid lines the 2005 case. The externally generated M_4 velocity phase shows qualitatively similar behavior for both years. The character of the internal M_4 velocity phase has changed significantly: in the region where we observe ebb dominance in 1980, the phase rapidly increases from approximately -250° to -100° , while in 2005 the phase is always about -100° , resulting in a stronger flood dominance in 2005 compared to 1980. So we can conclude that the main changes in ebb/flood dominance, as observed in the Ems, are a result of changes in the phase of the internally generated overtide.

Next, we focus on changes in the ratio of the modeled M_4 over M_2 horizontal velocity at the surface, plotted in Fig. 2.5(a). The M_2 and M_4 horizontal velocity at the surface are shown in Fig. 2.9. Fig. 2.9(a) indicates that the behavior of the M_2 velocity component did not change between 1980 and 2005. The only change is an average 12% amplification of the M_2 velocity in 2005 compared to 1980. In Fig. 2.9(b), we plotted both the externally forced and internally generated M_4 velocity amplitude at the surface for both years. In Section 2.4.3 we discriminated

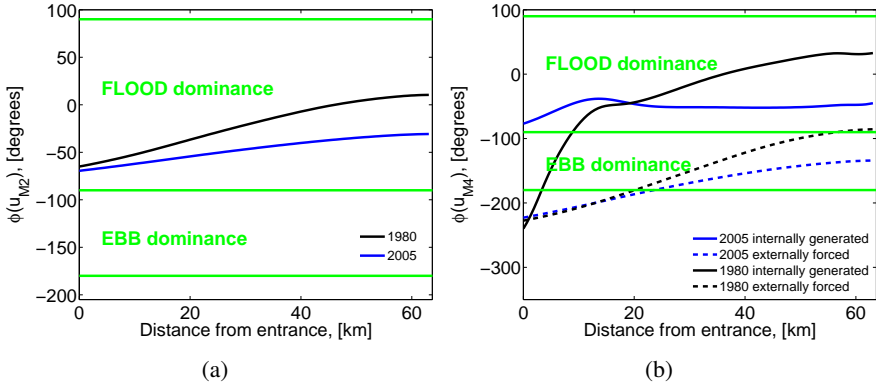


Figure 2.8: The left panel shows the M_2 horizontal velocity phase at the surface and the right panel depicts the M_4 horizontal velocity phase at the surface.

between two distinct regions. In a region within 20 km of the entrance the first region, located close to the entrance, the M_4/M_2 ratio has decreased from 1980 to 2005. This is caused by a local decrease of the M_4 internally generated velocity in 1980. Everywhere else we observe the opposite: an increase of the M_4/M_2 ratio in 2005 compared to 1980. This can be explained by a rapid damping of the M_4 externally forced signal towards the end of the estuary in 1980, which is not the case in 2005. Moreover, the internally generated M_4 velocity amplitude is more amplified in 2005 than in 1980 everywhere in the estuary.

Finally, we analyze the residual flow. The residual flow is the sum of five separate contributions, each from an individual forcing mechanism: gravitational circulation, river inflow, tidal return flow, surface contribution and tidal stresses (see Section 2.3.2). In Fig. 2.10, the three largest residual horizontal velocity components are presented. The other two components are negligible. The top row shows the gravitational circulation in 1980 (Fig. 2.10(a)) and 2005 (Fig. 2.10(b)), respectively. These figures suggest that the gravitation circulation has intensified over the years. The reason for that is a combination of increased estuarine depth and a decrease of vertical mixing (Talke et al, 2009a,b). At the same time, the tidal return flow, depicted in Figs. 2.10(c) and 2.10(d), has decreased between 1980 and 2005. One would expect an increase of this contribution due to a decrease of the vertical mixing. On the other hand, the increase of water depth and decrease of the stress parameter s (resulting in a wave with a stronger standing wave character) result in a decrease of the tidal return flow. In this case, based on additional model

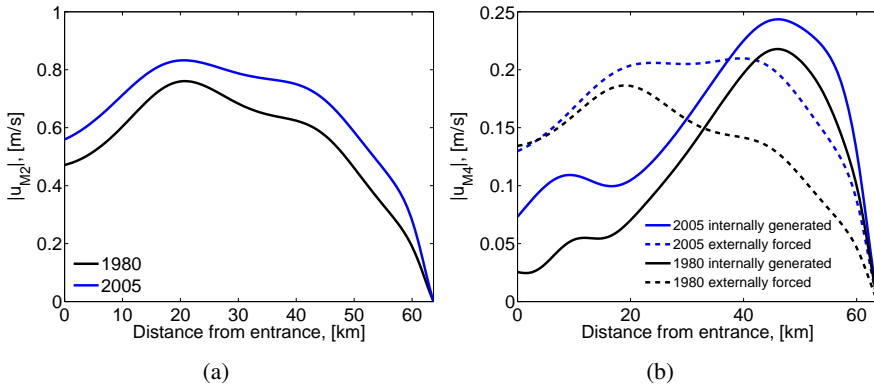


Figure 2.9: The left panel represents M_2 velocity amplitude at the surface and right one the M_4 velocity amplitude at the surface.

computations, the latter effect is stronger. The lower panels, Figs. 2.10(e) and 2.10(f), represent the river velocity in 1980 and 2005, respectively. The river velocity has decreased by less than 5% in 2005 due to deepening but there are no significant changes between 1980 and 2005. Therefore, the combination of the increased gravitational circulation and the decrease of the tidal return flow resulted in the residual flow changes described in Section 2.4.3.

2.5.2 Analysis of the residual sediment transports

In Fig. 2.7, we observe different sediment trapping regions between different years and/or grain sizes. For fine silt the trapping region is found at the classic location in 1980, i.e., near the upward limit of salt intrusion. In 2005, the trapping region has shifted further upstream by 19 km. Coarse silt is trapped at the classical location in 1980 as well, whereas in 2005 two trapping regions are observed. One ETM is located at the classical location and the other trapping region is far upstream into the freshwater zone. To understand the physical mechanisms resulting in these different trapping regions, we analyze the sediment transports discussed in Section 2.3.3.

To clarify our analysis method, we take as an example the sediment transports for fine silt in 1980. These transports are shown in Fig. 2.11. In this figure, the solid red line represents the residual sediment transport due to the transport of the residual concentration by the residual velocity. If this transport is negative (i.e., between approximately 15 and 45 km), the sediment is transported in the

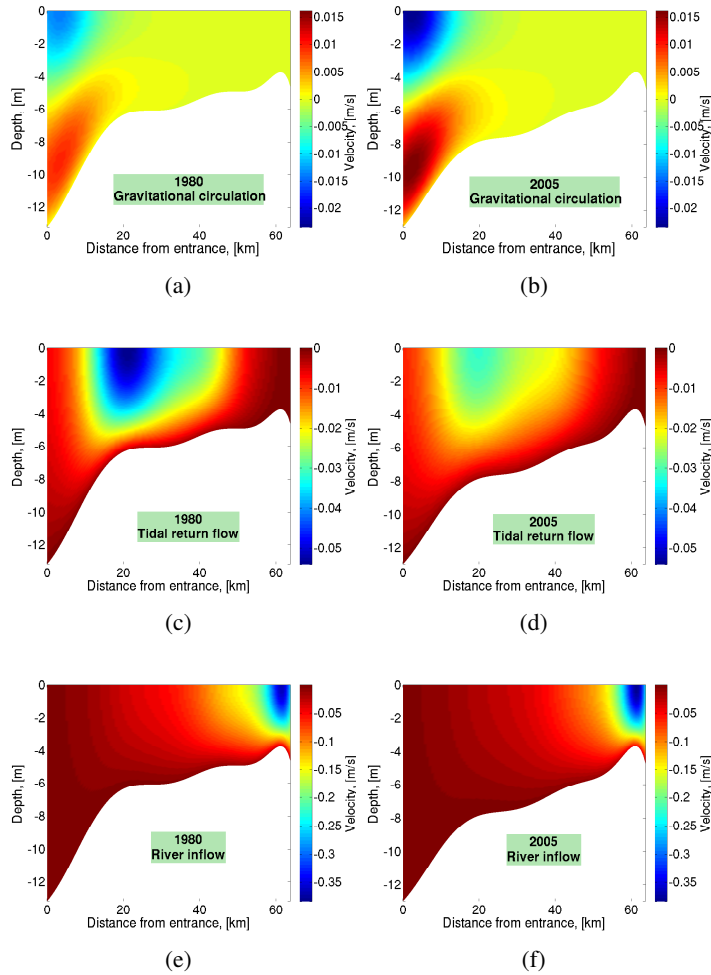


Figure 2.10: The residual velocity constituents, namely, the gravitational circulation is depicted on the upper panels, the tidal return flow is shown on the middle panels and the river outflow on the lower panels.

seaward direction. If the transport is positive (from the entrance up to approximately 15 km), the sediment transport is directed up-stream. Similarly, the solid green, black and magenta lines denote the residual sediment transport due to the interaction of the M_2 concentration with the M_2 velocity, the M_4 concentration and the M_4 velocity and diffusion (i.e., $aT_{\text{diff}} + a_x F$), respectively. Since the system is

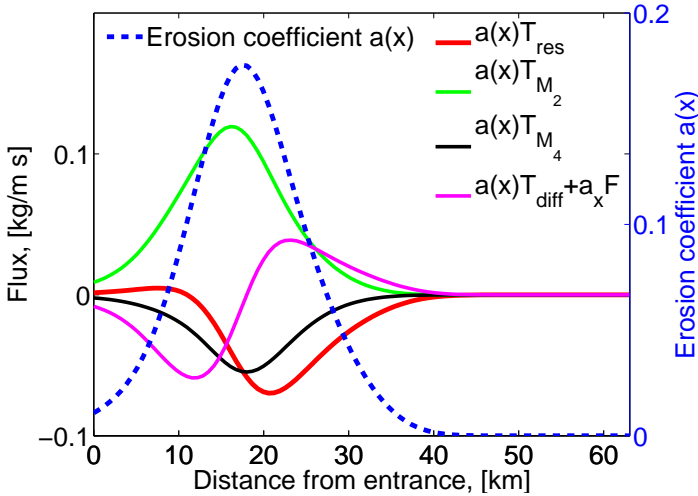


Figure 2.11: Residual sediment transports in morphodynamic equilibrium in 1980 due to: the residual velocity/residual concentration (solid red line), M_2 velocity/ M_2 concentration (solid green line), M_4 velocity/ M_4 concentration interaction (solid black line) and diffusion (solid magenta line). Erosion coefficient $a(x)$ that results in morphodynamic equilibrium is shown with dashed blue line. Results are obtained for the settling velocity of 0.5 mm s^{-1} and river discharge $65 \text{ m}^3 \text{ s}^{-1}$.

in morphodynamic equilibrium these transports balance, i.e., the sum of the different contributions vanishes everywhere in the estuary, resulting in no residual sediment transport anywhere. The erosion coefficient that results in this morphodynamic equilibrium (and is calculated using Eq. (2.42)) is the dashed blue line in Fig. 2.11. The location of the maximum corresponds to the location of the ETM and is at the classical location. In the sediment balance all transports have a significant contribution. There is no approximate balance between the diffusive transport $a(x)T_{\text{diff}} + a_x F$ and the $a(x)T_{\text{res}}$ transport as used in Talke et al (2009b).

From Eq. (2.42), it follows that a (local) maximum or minimum in sediment concentration is found in the vicinity of the location where the transport function $T = 0$. At these locations $da/dx = 0$, and, since $a(x)$ itself is non zero, $T(x)$ has to be zero. Hence, to determine the ETM locations (i.e., a (local) maximum of sediment concentration) one has to investigate the zeros of T . Differences in trapping regions, as observed in Fig. 2.7, result from an up- or downstream shift of the convergence point or the occurrence of a new location with $T = 0$.

The physical reason for changes in trapping location can be found by study-

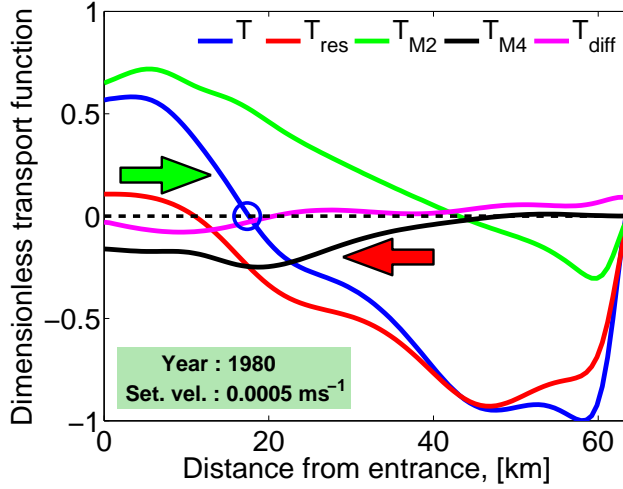


Figure 2.12: Dimensionless transport function T (solid blue line) in 1980. Results are obtained for the settling velocity of 0.5 mm s^{-1} . Red, green, black and magenta lines depict contributions of T that result from: the residual velocity/residual concentration, M_2 velocity/ M_2 concentration, M_4 velocity/ M_4 concentration interaction and diffusion, respectively. The two arrows show the direction of the residual export and import of sediment, respectively. The color of the arrows represents the main contribution, responsible for the sediment transport, i.e., the residual import of sediment is mainly due to T_{M_2} (represented by the green arrow) and the residual export is primarily caused by T_{res} (shown with the red arrow).

ing the different contributions of T (see Eq. (2.42)). As an example of such a decomposition of the dimensionless transport function T (i.e., T divided by its maximum absolute value) and its components for 1980 (fine sediment) are shown in Fig. 2.12. The blue line represents the total residual transport T and its zero crossing (marked with a blue circle) corresponds to the location of the ETM in Fig. 2.11. The red, green, black and magenta lines in Fig. 2.12 are the contributions to the residual transport T , which result from the interaction of the residual velocity with the residual concentration (T_{res}), M_2 velocity with M_2 concentration (T_{M_2}), M_4 velocity with M_4 concentration (T_{M_4}) and diffusion (T_{diff}), respectively. From the seaward boundary up to approximately 18 km, the sediment is transported up-estuary mainly by T_{M_2} (the arrows in Fig. 2.12 show the direction of the sediment transport, with its color representing the main transport mechanism. Here, the green arrow indicates the import of sediment), while from 18 to 63 km transport is down-estuary mainly by T_{res} (the export of sediment is indicated by

the red arrow). Hence, there is a convergence of sediment around 18 km.

By analyzing the sediment transport components and comparing them for different grain sizes and/or years, we can conclude which transports are responsible for the sediment trapping and the observed differences in the sediment trapping between the years (Section 2.5.2.1) and for different grain size (Section 2.5.2.2).

2.5.2.1 Changes between 1980 and 2005

From Fig. 2.13, it follows that for fine sediment in both 1980 and 2005 the main import of sediment into the estuary is due to the M_2 transport (T_{M_2}) and the major export is caused by the residual transport (T_{res}) (see arrows in Figs. 2.13(a) and 2.13(b)). For coarse sediment in 1980 the main import of sediment in the upstream region is due to T_{M_2} (green arrow in Fig. 2.13(c)) and the export is due to a combination of T_{res} , T_{M_2} and T_{M_4} transports (green/red arrow). In 2005, coarse sediment was primarily imported in the upstream reaches by T_{M_2} and exported by T_{res} , whereas sediment to the downstream ETM is imported due to a combined transport of T_{M_2} and T_{M_4} and exported due to T_{res} and T_{M_2} (see arrows in Fig. 2.13(d)).

From Figs. 2.13(a) and 2.13(b) we see that for fine silt the global behavior of the residual transport T changed between 1980 and 2005. Closer inspection shows this change is mainly due to a change in T_{M_2} . In 1980, T_{M_2} is approximately constant and positive up until 20 km, after which it starts to decrease. In 2005, T_{M_2} only starts to decrease after approximately 50 km. Therefore, the transport function T becomes negative farther upstream in 2005 than in 1980. This results in a shift of the convergence point between 1980 and 2005 by approximately 19 km.

For coarser silt, we observe one convergence point in the 1980 case and two convergence points in 2005 (see Figs. 2.13(c) and 2.13(d)). In both cases the first convergence point is still at the classical location, even though its position has shifted upstream by approximately 5 km in 2005 compared to 1980. The second convergence point is well into the freshwater region. The change in the transport function T is again mainly due to changes in the T_{M_2} contribution. In 1980, T_{M_2} becomes negative at approximately km 18, whereas in 2005 this point is located closer to the weir at km 52.

It follows that for both fine and coarse silt the T_{M_2} contribution play an important role in the changes of the sediment trapping location in the Ems estuary between 1980 and 2005. In the next paragraphs we analyze the T_{M_2} contribution in more detail. Detailed analysis of the other components of the transport function are presented in Appendix A8.

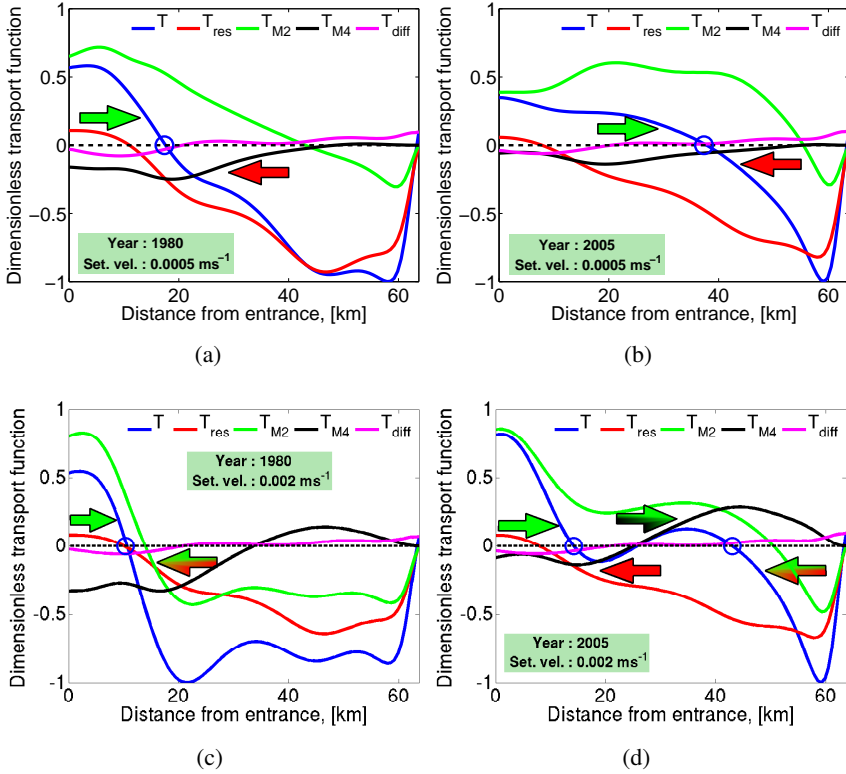


Figure 2.13: Dimensionless transport function T and its components. The upper panels show fine silt and the lower ones coarse silt. The left panels represent 1980 and the right ones 2005. Arrows show the direction of export and import of sediment, their color(s) represent(s) the main contribution(s) responsible for transport.

To understand which mechanism is responsible for this significant change of T_{M_2} , T_{M_2} will be decomposed into different components. The M_2 concentration (see Section 2.3.2.2), is forced by the M_2 component of the bed shear stress. From Eq. (2.39), it follows that the M_2 component of the bed shear stress is a result of the interaction of both the residual and the M_4 velocities with the M_2 velocity. Contributions of T_{M_2} that involve the residual velocity components are denoted by $T_{M_2}^{res}$ and $T_{M_2}^{M_4}$ denotes the contribution of T_{M_2} due to the overtide velocity components (for details, see Appendix A8).

In Fig. 2.14, T_{M_2} and its components $T_{M_2}^{res}$, $T_{M_2}^{M_4}$ are shown by the dashed green, solid red and solid blue lines, respectively. The qualitative change in T_{M_2} is mainly

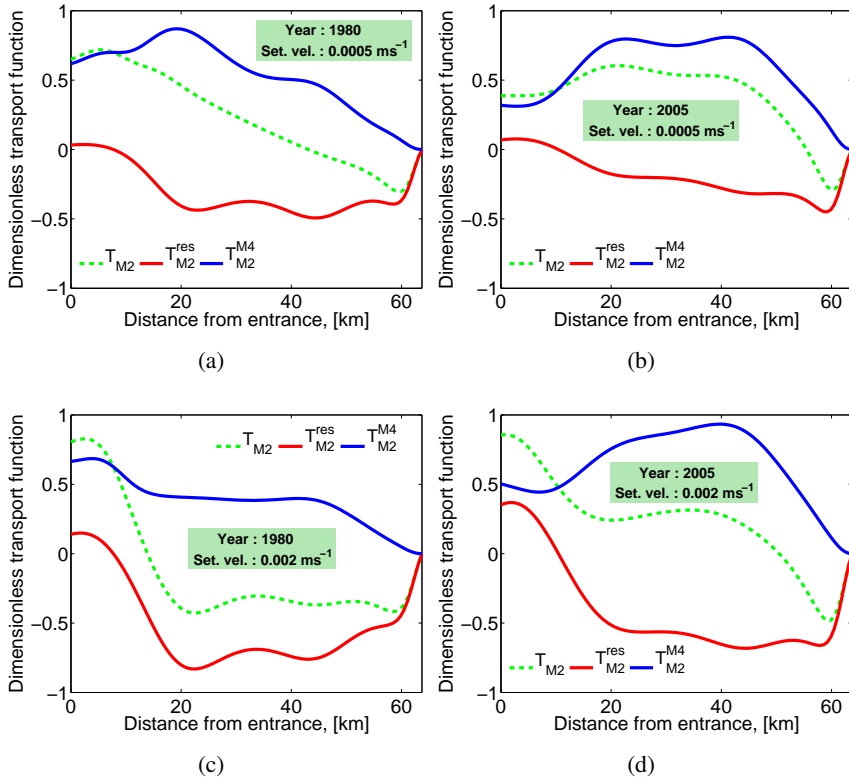


Figure 2.14: Dimensionless transport function T_{M_2} and its components.

determined by the $T_{M_2}^{M_4}$ contribution. In 1980, the $T_{M_2}^{M_4}$ transport begins to decrease at approximately km 20, whereas in 2005 it is elevated over much of the estuary and begins decreasing only upstream of km 50.

The $T_{M_2}^{M_4}$ contribution can be decomposed further into four contributions as $T_{M_2}^{M_4} = T_{M_2}^{AC} + T_{M_2}^{FS} + T_{M_2}^{NS} + T_{M_2}^{EF}$. Here, the M_4 velocity components that contribute to $T_{M_2}^{M_4}$ are advective contributions, denoted by $T_{M_2}^{AC}$; free surface contribution, denoted by $T_{M_2}^{FS}$; no-stress contribution, denoted by $T_{M_2}^{NS}$; and the M_4 external forcing, denoted by $T_{M_2}^{EF}$ (see Eq. (2.38) and Appendix A8 for details). The $T_{M_2}^{M_4}$ components of the transport function T_{M_2} are shown in Fig. 2.15. For both fine silt (Figs. 2.15(a) and 2.15(b)) and coarse silt (Figs. 2.15(c) and 2.15(d)), we see that the changed behavior of $T_{M_2}^{M_4}$ (the dashed blue line) is primarily determined by the $T_{M_2}^{EF}$ contribution which results from the externally forced M_4 tide (the solid magenta

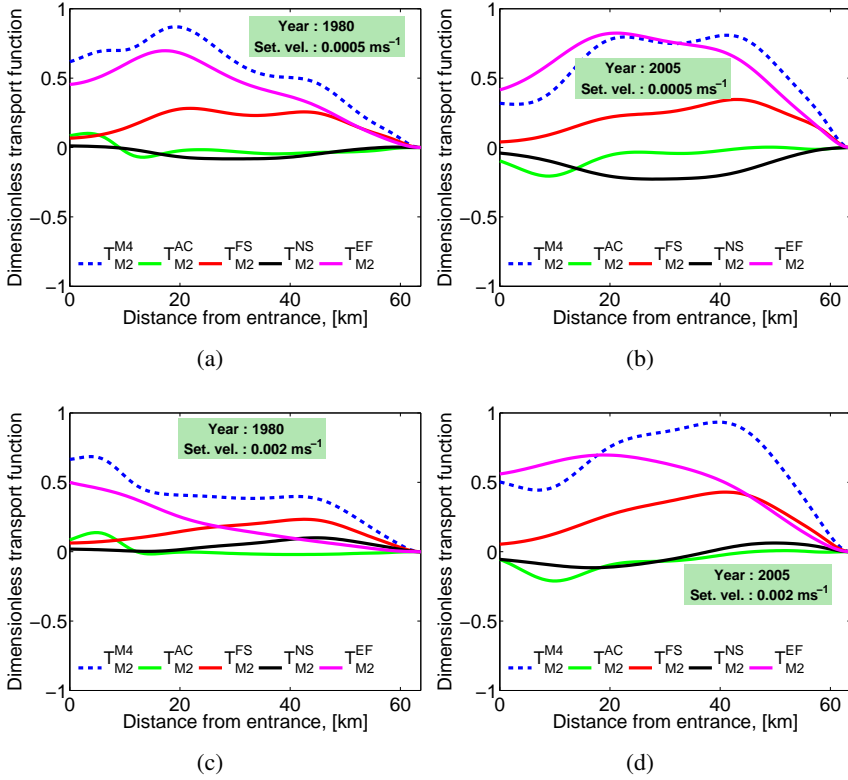


Figure 2.15: Dimensionless transport function $T_{M_2}^{M_4}$ and its components.

line). The other three contributions are much smaller. In 1980, the transport due to the external overtide decreases from km 16, whereas in 2005 an abrupt decrease starts only at approximately km 40. Hence, the main change between 1980 and 2005 is due to the difference in residual sediment transport by tidal asymmetry, resulting in less import of sediment in 1980 compared to 2005, both for fine and coarser silt.

As overall conclusion, it follows that the changes in trapping location between 1980 and 2005, for both years, is a result of changes in the sediment transport due to tidal asymmetry, i.e. changes of the external overtide.

2.5.2.2 Grain size sensitivity

In the previous section, our focus was on the changes between 1980 and 2005 for sediment with the same grain sizes. Here, we analyze the difference in the sediment distribution for different grain sizes for the same year. As shown by Groen (1967), the temporal settling lag mechanism is quite efficient in transporting suspended sediment in one direction (upstream in our case) when there is tidal asymmetry.

In Figs. 2.16(a) and 2.16(b), we show the transport function T with (solid lines) and without (dashed lines) the temporal settling lag (TSL) effects in 1980 and 2005, respectively (see Eq. (2.9)). As we can see from Fig. 2.16(a), in 1980, there is virtually no import of sediment into the estuary in the absence of the temporal settling lag (the dashed lines). Temporal settling lag (the solid lines) results in an import of sediment upstream and is, as expected, more efficient in transporting fine silt (from the entrance up to approximately 20 km) than coarse silt (up to approximately 12 km). In the 2005 case shown in Fig. 2.16(b), we observe two trapping locations for both fine and coarse silt in absence of the temporal settling lag mechanism (the dashed lines). One ETM is located at the classical location and the other one further upstream at km 45. For fine silt, the temporal settling lag (the solid lines in Fig. 2.16(b)) qualitatively changes the trapping locations: instead of two trapping locations, fine silt is deposited only at one location at approximately km 37. For coarse silt, temporal settling lag is not as efficient and we observe an insignificant shift of the trapping locations upstream (the blue dashed and solid lines in Fig. 2.16(b)).

From Fig. 2.16, we conclude that the difference between the sediment distribution of different grain sizes is a result of the temporal settling lag mechanism.

2.5.3 Parameter sensitivity

The analysis of the specific cases with river discharge $Q = 65 \text{ m}^3/\text{s}$ and settling velocity w_s of 0.0005 and 0.002 m s^{-1} (see Section 2.5.2.1) gives a good insight into processes in the estuary, but only for these specific parameters. To study the sensitivity of the turbidity maxima to river outflow and settling velocity, we analyze the transport function T for a range of settling velocity w_s ($0.0002 - 0.002 \text{ m s}^{-1}$) and river discharge Q ($20 - 140 \text{ m}^3 \text{ s}^{-1}$). For each w_s and Q , we constructed a plot, which is similar to Fig. 2.12 and determined the location where an ETM occurs. We summarize these locations in Fig. 2.17(a) for 1980 and Fig. 2.17(b) 2005. On the x -axis, the location in the estuary is plotted, on the y -axis the settling velocity.

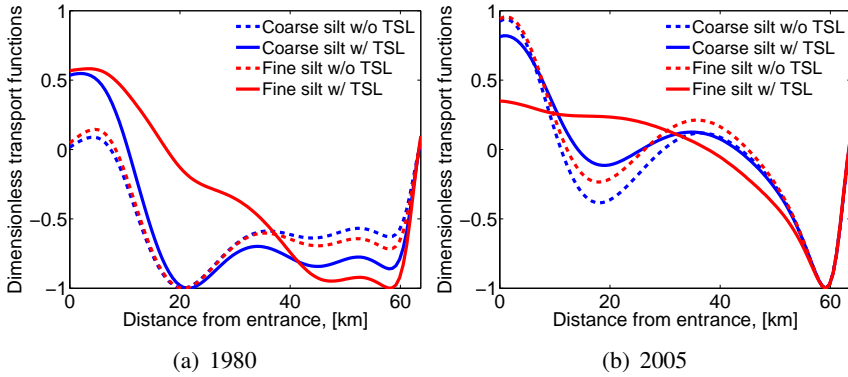


Figure 2.16: Dimensionless transport function T for both fine and coarse silt with and without temporal settling lag (TSL) effect. The blue (red) line represents the coarse (fine) silt. The dashed lines depict the transport function T in the absence of the temporal settling lag effect. The left panel shows 1980 and the right one 2005.

If trapping occurs at a certain location for a specific settling velocity, the associated river outflow is given by the color code. If no trapping occurs for a settling velocity at a certain location for a river outflow between 20 and $150 \text{ m}^3 \text{ s}^{-1}$, then this (x, w_s) coordinate is left blank.

From Fig. 2.17, we conclude that in 1980 the trapping location of both fine and coarse silt is found at the upstream limit of salt intrusion (i.e., the classical location). In 1980, the sediment is found more into the estuary only for very small river outflow (at most $30 \text{ m}^3 \text{ s}^{-1}$). Furthermore, we observe two trapping locations only for coarse silt (with settling velocity between $0.001 - 0.002 \text{ m s}^{-1}$) and river discharge corresponding to low flow conditions (at most $22 \text{ m}^3 \text{ s}^{-1}$). In 2005, fine silt is either trapped at the classical location (for very high river discharge of $100 - 140 \text{ m}^3 \text{ s}^{-1}$) or in the freshwater zone (river discharge of approximately $30 - 80 \text{ m}^3 \text{ s}^{-1}$), which depends on specific magnitude of river discharge Q and settling velocity w_s . For coarser silt in 2005, two trapping regions are observed even for relatively high river outflow ($40 - 75 \text{ m}^3 \text{ s}^{-1}$). One ETM is found at the classical location, the other one is located more upstream in the freshwater zone.

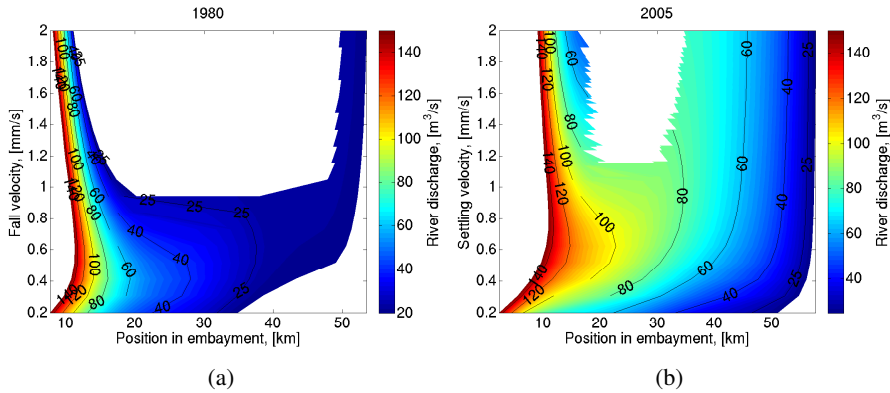


Figure 2.17: Occurrence of ETMs in the estuary. The horizontal axis is the position in the estuary, and the vertical axis represents the settling velocity. If trapping occurs at a certain location for a specific settling velocity, the associated river outflow is given by the color code; otherwise, this (x, w_s) coordinate is left blank. The river outflow is varied between 20 and $150 \text{ m}^3 \text{ s}^{-1}$.

2.6 Conclusions

This chapter presents a width-averaged analytical model of water and sediment dynamics in an estuary constrained upstream by a weir. Using the morphodynamic equilibrium condition, the trapping of sediment can be described in this estuary. The estuary is assumed to be exponentially converging and vertically well-mixed. The water motion is modeled by the width-averaged shallow water equations, the concentration by the width-averaged advection-diffusion equation. The sediment concentration still depends on a spatially varying erosion coefficient which models the availability of erodible sediment, and is found using the condition of morphodynamic equilibrium. Analytic solutions are obtained using a perturbation approach in which physical variables are expanded in power series of the ratio of the semi-diurnal tidal amplitude and the undisturbed water depth at the entrance.

To test the applicability of our model, we consider the Ems estuary. Here, anthropogenic changes altered the water motion and sediment trapping locations significantly between 1980 and 2005. Two distinct bathymetries are considered which represents these two years. Most parameter values are obtained from measurements directly. The vertical eddy viscosity coefficient and stress parameter are obtained by calibrating the model to measured data by minimizing the dif-

ference between the observed and modeled semi-diurnal tidal amplitude and the phase difference between the semi-diurnal horizontal and vertical tide in a least square sense. Other observations are used to validate the model. Model results suggest a 50% and 37% reduction in the stress parameter and vertical eddy viscosity coefficient, respectively, in 2005 compared to 1980. The decreased friction and mixing suggests less hydraulic roughness, possibly because bed forms have been removed by dredging or because of the fluid mud that currently covers much of the turbid zone (Talke et al, 2009b).

The model results indicate that the water motion of the estuary is more amplified in 2005. This occurs both due to the deepening of the estuary and to the decreased vertical eddy viscosity and stress parameter. The shift towards greater flood dominance in 2005 is a result of changes in the internally generated overtides. The increased depth and decreased vertical mixing and stress parameter have intensified the gravitational circulation and weakened the tidal return flow in 2005 compared to 1980.

The modeled concentration profiles show that in 1980 both fine and coarse silt is trapped near the upward limit of salt intrusion, with the ETM moving further upstream only for small river outflow (less than $35 \text{ m}^3 \text{ s}^{-1}$). In 2005, fine silt is either trapped near the upward limit of salt intrusion or in the freshwater zone, depending on the specific magnitude of river discharge and settling velocity. The main import of fine sediment into the estuary is due to the M_2 transport and the major export is caused by the residual transport in both 1980 and 2005. For coarser silt, two trapping regions are observed even for relatively high river outflow ($40 - 75 \text{ m}^3 \text{ s}^{-1}$). One is found at the classical location, the other one upstream in the freshwater zone. In 1980, the main import of coarse sediment to the ETM is due to the M_2 transport and the export is due to a combination of the residual, M_2 and M_4 transports. In 2005, coarse sediment was primarily imported to the upstream ETM by the M_2 transport and exported by the residual transport, whereas sediment is imported to the downstream ETM due to a combined transport of M_2 and M_4 and exported due to the residual and M_2 transport.

Based on presented model, the upstream shift of the estuarine turbidity maximum between 1980 and 2005 and the trapping of sediment in the fresh water zone is primarily a result of changes in tidal asymmetry (the external overtide). The amplification and change of behavior of the externally forced M_4 tide results in a shift of the estuarine turbidity maximum into the freshwater zone in 2005. The difference between the sediment distribution of different grain sizes under the same hydrodynamic conditions (i.e., for the same year) is a result of the temporal settling lag mechanism.

A number of processes that might be important for the trapping of sediment are not taken into account: spatial settling lag, the high sediment concentration, wind waves, flocculation, tidal flats and the SIPS mechanism (strain-induced periodic stratification) discussed for example by [Burchard and Baumert \(1998\)](#). Note that this kind of model does not allow us to explain an increase of the SSC from 400 to 950 mg/l observed between 1980 and 2005. Furthermore, in our model the SSC is not found close to the weir. Preliminary results show that the spatial settling lag effect, for example, is important in a region of approximately 20 km down-stream from the weir and is negligible in the rest of the estuary. Hence, it probably will enhance the shift of the ETM that is located in the freshwater zone up-stream, whereas the ETMs that occur at the classical location will not be affected by this effect.

Influence of high concentration and geometrical characteristics on the estuarine turbidity maxima

In many estuaries such as the Ems and Humber, high sediment concentrations up to tens of grams per liter are found in the turbidity zone. Earlier studies have shown that the location of the turbidity maximum in the Ems could be understood by a detailed study of the residual sediment transports in the morphodynamic equilibrium. However, the influence of high sediment concentration on the density distribution was not considered. Moreover, the sensitivity of the turbidity zone to various geometrical characteristics and external forcing was not investigated.

To investigate these issues, an idealized model is developed in which density depends on both salinity and suspended sediment concentration. The latter component results in turbidity currents, which produce an additional transport in the morphodynamic balance resulting in a wider spread and enhanced asymmetry of the turbidity region. Furthermore, we demonstrate that there is a competition between two trapping mechanisms: one mechanism that traps suspended sediment at the entrance of the estuary, and the other resulting in trapping near the end of the embayment. The dominant mechanism determines the position of the ETM in the estuary.

If the estuarine length is shorter than the resonance length of the M_4 tidal constituent, the ETM is located in the freshwater region. For longer estuaries, the ETM is found near the upward limit of salt intrusion. For estuaries close to resonance, two ETMs are found. By altering geometrical characteristics and/or external forcing, the dominant mechanism can change and a qualitative change in trapping location can occur.

This chapter is based on Chernetsky AS, Schuttelaars HM Influence of high sediment concentration and geometrical characteristics on the position of estuarine turbidity maxima in tidal estuaries, Journal of Geophysical Research, submitted

3.1 Introduction

Many estuaries are characterized by the presence of turbidity regions. In these zones, the suspended sediment concentration (SSC) in the water column can vary from a few mg/l up to 50 g/l (Uncles et al, 2002). These variations in SSC are observed between different estuaries and within the same estuary at different times. Uncles et al (2002); Uncles and Smith (2005) show that tidal range and tidal intrusion length strongly influence the turbidity, either directly or as surrogates for other physical variables.

Tidal range and intrusion length can vary by natural processes (e.g., the spring-neap cycle, time-dependent river runoff, etc) or as a result of human interferences (e.g., construction of weirs, the streamlining of waterways, deepening or maintenance dredging in estuaries, etc). For example, Garrett (1974); Greenberg (1975) discuss the influence of length of the bay of Fundy on the tidal amplitude. Using empirical data Greenberg (1975); Shaw et al (2010) argue that a natural barrier across the eastern end of Minas Channel, and its natural breakdown (thus changing the length of the system) had a profound influence on mean high water. An example of an estuary where changes in both water motion and SSC due to human interference are observed, is the Ems estuary. The Ems river has sustained human interference since the sixteenth century. However, the major changes were introduced into the Ems system over the course of the twentieth century. In 1900, a tidal weir was constructed near the city of Herbrum (100 km from the North Sea), thus, splitting the river into the tidally influenced Ems/Dollard estuary and the river itself. Since the late 1950's, the shipping channel in the estuary has been streamlined and maintenance dredging of the navigation channels has started. Furthermore, in 1980's, successive deepening of the Ems estuary has begun. These changes have significantly influenced the tidal and sediment dynamics. The tidal range in the upstream reaches has increased by 1.5 m (Talke et al, 2009a), and the surface sediment concentration has increased from approximately 400 mg/l in 1980 (De Jonge, 1983) up to approximately 1 g/l in 2006. Furthermore, the position of the turbidity zone has broadened into the freshwater zone.

When the suspended sediment concentration in the water column becomes large (a few g/l), the water density is affected by both the salinity and suspended sediment concentration (see for example Talke et al (2009b)), and the SSC is not passive anymore. Talke et al (2009b) show that turbidity currents can strongly influence the ETM dynamics. The idealized model, used in (Talke et al, 2009b), is a tidally averaged model, i.e., processes taking place on the tidal time-scale were not taken into account explicitly. Recent literature (Simpson et al, 1990; Geyer,

1993; Jay and Musiak, 1994; Burchard and Baumert, 1998) strongly suggests that these processes are important to get a good description of the residual sediment transports. Indeed, Chernetsky et al (2010) showed that processes on the tidal timescale are essential in modeling and understanding the ETM dynamics in the Ems estuary: tidal asymmetry and temporal settling lag have a significant effect on the sediment trapping in this estuary. However, in Chapter 2 (Chernetsky et al, 2010) the effect of turbidity currents was not taken into account. First results that include the influence of high sediment concentration on the hydrodynamics, presented in Chernetsky and Schuttelaars (2010), showed the importance of this mechanism. Therefore, the first aim of this chapter is to investigate the influence of high sediment concentration on the water motion, sediment concentration and location of sediment trapping in a model that resolves processes on the tidal timescale. The proposed model is an extension of the model, discussed in Chernetsky et al (2010), in which the influence of suspended sediment concentration on density is taken into account, resulting in turbidity currents. By varying the total amount of SSC in the estuary, we are able to investigate the influence of turbidity currents on the position, shape and width of estuarine turbidity maxima (ETM) in morphodynamic equilibrium.

This extension is not a simple linear superposition of the results published in Chernetsky et al (2010) and Talke et al (2009a). In Talke et al (2009a), the influence of tidally averaged high sediment concentration resulted in an additional velocity contribution. Multiplying this turbidity current with the tidally averaged concentration profile, resulted in a tidally averaged sediment flux that contributed to the trapping of sediment. When taking the presence of high sediment concentration into account in a tide-resolving model, both a tidally averaged and M_4 velocity component will be induced. Furthermore, these turbidity currents will result in enhanced shear stresses, resulting in an extra contribution to the M_2 suspended sediment concentration. Apart from these contributions, there are new contributions to the suspended sediment transport (compared to the tidally averaged model presented in Talke et al (2009b)), which are due to spatial dependencies in the along-channel velocities. The relative importance of these transports and the physical processes involved in them will be investigated in detail. Note that we assume density variations in the vertical to be small. This implies that we neglect suspended sediment transport due to internal tidal asymmetry, which is motivated as a first step by the results of Winterwerp (2011) that suggest that this transport mechanism was neither in the '80s nor at present the dominant transport mechanism.

As discussed above, the influence of geometrical parameters, bathymetry, and

tidal forcing on the turbidity zone is evident from observations, but their influence on the location of trapping of sediment has not been systematically investigated. The sensitivity study to the estuarine length, presented in [Schuttelaars et al \(2012\)](#), is a good motivation for a more detailed study of the effect of geometrical parameters on the ETM. Therefore, the second aim of this chapter is to investigate the influence of these parameters on the location of the turbidity zone.

In Section 3.2, we discuss the governing equations which are used to construct the model. A perturbation analysis of these equations and an analytical solution scheme are outlined in Section 3.3. The results and discussion are given in Section 3.4, followed by conclusions in Section 3.5.

3.2 Model

We consider an exponentially converging estuary with the width prescribed by $B(x) = B_0 e^{-x/L_b}$. B_0 is the width of the estuary at the seaward side and L_b is the exponential convergence length. A Cartesian coordinate system (x, z) is used, where x is the along-channel coordinate, and z is the vertical coordinate. The embayment is constrained by a weir at the landward side at $x = L$. The bathymetry is prescribed with the depth at the entrance denoted by H_{ent} , and the depth at the weir by H_{end} . The estuary is forced at the seaward side by a prescribed external tide and at the landward side by a river discharge. The model geometry is sketched in Fig. 3.1.

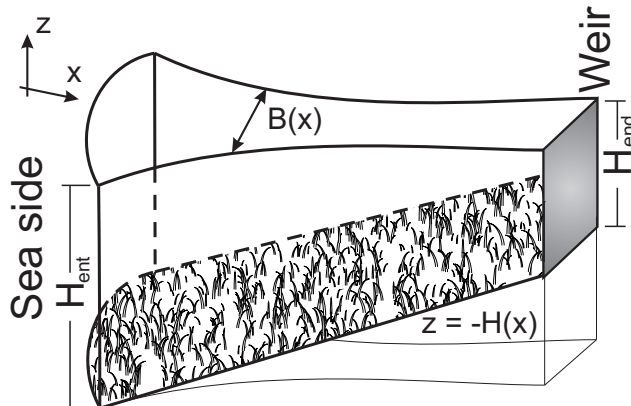


Figure 3.1: Sketch of the model geometry. A Cartesian coordinate system is used, with x the along-channel coordinate directed landwards and z the vertical coordinate pointing upwards. The depth at the entrance is H_{ent} and H_{end} is the depth at the weir.

The water motion in the longitudinal direction is modeled by the width-averaged shallow water equations

$$u_x + w_z - \frac{u}{L_b} = 0, \quad (3.1a)$$

$$u_t + uu_x + wu_z + g\zeta_x - \frac{g\rho_x}{\rho_0}(z - \zeta) - (A_v u_z)_z = 0, \quad (3.1b)$$

where u , w are the along-channel and vertical velocity, and ζ is the sea surface elevation and subscripts x , z and t denote the derivative with respect to coordinates x , z and time t . The along-channel water density is denoted by $\rho(x, z, t)$. The difference with the hydrodynamic equations used in [Chernetsky et al \(2010\)](#), is that the water density depends on both the salinity and suspended sediment concentration (SSC). The temporal variations of the salinity field are assumed to be small compared to the time-averaged salinity field and the salinity is vertically well-mixed. Hence, the along-channel density ρ is modeled as

$$\rho(s, c, t) = \rho_0 \left(1 + \underbrace{\beta \langle s(x) \rangle}_{\text{Salinity term}} + \underbrace{\gamma c(t, x, z) / \rho_0}_{\text{SSC term}} \right), \quad (3.2)$$

where $c(t, x, z)$ is the width-averaged suspended sediment concentration and $\langle s(x) \rangle$ is the observed along-channel time- and depth-averaged salinity profile ([Talke et al, 2009a](#); [Chernetsky et al, 2010](#)). In the remainder of this chapter, the angular brackets $\langle \cdot \rangle$ denote a tidal average. Furthermore, $\beta \sim 7.6 \times 10^{-4} \text{ psu}^{-1}$ is the haline contraction coefficient and $\gamma = (\rho_s - \rho_0) / \rho_s \sim 0.62$ is the relative density of the suspended sediment ρ_s to water density ρ_0 .

The vertical eddy viscosity function A_v is modeled following ([Friedrichs and Aubrey, 1996](#))

$$A_v(x) = A_{v0} \frac{H(x)}{H_{\text{ent}}}, \quad (3.3)$$

where H_{ent} is the local water depth at the entrance of the estuary and A_{v0} is the reference eddy viscosity coefficient.

At the free surface, $z = \zeta$, we impose the no stress condition and the kinematic boundary condition:

$$A_v u_z = 0 \quad \text{and} \quad w = \zeta_t + u \zeta_x. \quad (3.4)$$

We assume that the bed is impermeable at $z = -H(x)$,

$$w = -u H_x, \quad (3.5)$$

and a partial slip condition is prescribed,

$$A_v u_z = s(x)u \quad \text{at} \quad z = -H(x), \quad (3.6)$$

where the stress parameter $s(x)$ is parametrized as (for details, see [Chernetsky et al \(2010\)](#)),

$$s(x) = s_0 \frac{H(x)}{H_0}. \quad (3.7)$$

At the seaward side, $x = 0$, the estuary is forced by a prescribed tidal elevation

$$\zeta(t, 0) = A_{M_2} \cos \sigma t + A_{M_4} \cos(2\sigma t - \phi). \quad (3.8)$$

The prescribed tide consists of a semi-diurnal (M_2) tidal constituent and its first overtide (M_4). The amplitudes of these constituents are denoted by A_{M_2} and A_{M_4} , respectively. Moreover, $\sigma = 1.4 \cdot 10^{-4} \text{ s}^{-1}$ is the tidal frequency of the M_2 tidal constituent and ϕ is the M_4 phase. In this study, we will distinguish between the externally prescribed M_4 tidal constituent, resulting from the M_4 forcing in Eq. (3.8), and the internally generated M_4 tide, which is produced within the estuary due to nonlinear interactions.

At the riverine side, $x = L$, the estuary is forced only by a constant river discharge Q and the depth integrated tidal velocity is required to vanish, i.e.,

$$B(L) \int_{-H}^{\zeta} u(L, z) dz = Q. \quad (3.9)$$

The sediment is assumed to be mainly transported as suspended load and consists of noncohesive fine particles. The sediment dynamics is governed by the width-averaged advection-diffusion equation

$$c_t + uc_x + wc_z = w_s c_z + (K_h c_x)_x + (K_v c_z)_z - \frac{1}{L_b} K_h c_x, \quad (3.10)$$

where w_s is the settling velocity, and K_h and K_v are the horizontal and vertical diffusivity, respectively. For simplicity, the vertical diffusivity is assumed to be equal to A_v .

We assume that no particles can enter or leave the domain through the free surface, $z = \zeta$,

$$w_s c + K_v c_z - K_h c_x \zeta_x = 0. \quad (3.11)$$

At the bottom, $z = -H(x)$, the boundary condition is given by

$$-K_v c_z n_z - K_h c_x n_x = \frac{w_s \rho_s s}{g' d_s} |u(t, x)| a(x), \quad (3.12)$$

where n_x and n_z are the components of the unit normal vector at the bottom, ρ_s is the density of sediment, d_s is the grain size of the sediment and g' is the reduced gravity. Moreover, $a(x)$ is the erosion coefficient that models the along-channel distribution of easily erodible sediment at the bottom, which has to be determined yet.

To obtain the along-channel spatial distribution of the erosion coefficient, we require the estuarine system to be in morphodynamic equilibrium, i.e., there is no evolution of the bed over a tidal period. This means a balance between the tidally averaged erosion $\langle E \rangle$ and deposition $\langle D \rangle$ (defined in Section 2.2), resulting in a morphodynamic equilibrium condition (see Friedrichs et al (1998); Chernetsky et al (2010))

$$\left\langle \int_{-H}^{\zeta} (uc - K_h c_x) dz \right\rangle = 0. \quad (3.13)$$

The suspended sediment concentration $c(t, x, z)$ in Eq. (3.13) depends on the erosion coefficient, and the morphodynamic equilibrium condition can be rewritten as a first order differential equation (ODE) for $a(x)$. The main difference with Chernetsky et al (2010) is that the condition (3.13) depends in a nonlinear way on $a(x)$, resulting in a nonlinear ODE with respect to the erosion coefficient $a(x)$. This equation is derived and explained in Section 3.3.

3.3 Solution Method

The aim of this section is to illustrate the procedure used to construct a (semi-) analytic solution for the system of equations given in Section 3.2. This section will only give a brief overview of this procedure, details can be found in Chernetsky et al (2010).

The solution is constructed using a perturbation approach. First, we perform a scaling analysis of the equations to estimate the relative importance of the various contributions. This is done by ordering different terms with respect to a small dimensionless parameter ε , which is the ratio of the M_2 tidal amplitude A_{M_2} and the local water depth at the entrance H_{ent} , i.e., $\varepsilon = A_{M_2}/H_{\text{ent}} \ll 1$. Next, we expand

the physical variables in power series of this small parameter, i.e.,

$$\psi = \psi^0 + \varepsilon^1 \psi^1 + \varepsilon^2 \psi^2 + \dots, \quad (3.14)$$

with $\psi = (u, w, \zeta, c)$.

Finally, we substitute expansion (3.14) into the scaled equations and boundary conditions, and collect terms of equal order of ε . This results in a system of hydrodynamic and concentration equations, together with appropriate boundary conditions, at each order. In this study, we consider the zeroth (leading) and first order system of equations.

The leading order system ($\mathcal{O}(\varepsilon^0)$) of the hydrodynamic and concentration equations and its solution method is identical to the one discussed in Chernetsky et al (2010) and, hence, is not repeated here. The first order system of equations has changed. The hydrodynamic equations are discussed in Section 3.3.1 and the concentration equation is provided in Section 3.3.2. The resulting condition of morphodynamic equilibrium is presented in Section 3.3.3.

3.3.1 First Order Hydrodynamics

The first order velocity field and free surface elevation consist of a residual and M_4 contribution. For example, the horizontal first order velocity reads $u^1 = u^{10} + u^{14}$. Here the first superscript denotes the order of ε and the second one represents the corresponding tidal constituent (u^{10} and u^{14} are the first order residual and M_4 horizontal velocity field, respectively). Due to linearity of the hydrodynamic equations, these contributions can be studied separately. Therefore, we will discuss the first order systems of hydrodynamics equations for the residual and M_4 flow separately.

Residual flow. The forced linear system of equations that describes the residual water motion reads

$$u_x^{10} + w_z^{10} - \frac{u^{10}}{L_b} = 0, \quad (3.15a)$$

$$\underbrace{\langle u_x^{02} u_x^{02} + w_z^{02} u_z^{02} \rangle}_{\text{TS}} + g \zeta_x^{10} - \underbrace{g \beta \langle s \rangle_x z}_{\text{GC}} - \underbrace{g \gamma c_x^{00} z}_{\text{HC}} = (A_v u_z^{10})_z \quad (3.15b)$$

with the underbrace $\underbrace{\quad}$ denoting individual forcing terms, which are known expressions that will be discussed later. At this order the leading order residual sediment concentration c^{00} enters the momentum equation (3.15b). The residual

sediment concentration has a linear dependence on the erosion coefficient $a(x)$ (see Chernetsky et al (2010)),

$$c^{00} = a(x)c^{00a}, \quad (3.16)$$

where c^{00a} is independent of $a(x)$.

At the free surface, $z = 0$, the boundary conditions read

$$w^{10} = - \underbrace{\langle \zeta^{02} w_z^{02} - u^{02} \zeta_x^{02} \rangle}_{\text{SD}} \quad \text{and} \quad A_v u_z^{10} = - \underbrace{\langle A_v \zeta^{02} u_{zz}^{02} \rangle}_{\text{SC}}, \quad (3.17)$$

and at the bottom, $z = -H(x)$,

$$w^{10} = -u^{10} H_x \quad \text{and} \quad A_v u_z^{10} = s u^{10}. \quad (3.18)$$

The boundary conditions at the entrance and riverine side are given by

$$\zeta^{10} = 0 \quad \text{at} \quad x = 0, \quad (3.19)$$

$$\int_{-H}^0 u^{10} dz = \underbrace{\frac{Q}{B}}_{\text{RI}} \quad \text{at} \quad x = L. \quad (3.20)$$

The system of equations (3.15) and boundary conditions are linear, which allows us to construct a solution for each forcing term separately. This results in 6 different contributions to χ^{10} :

$$\chi^{10} = \chi_{\text{TS}}^{10} + \chi_{\text{GC}}^{10} + \chi_{\text{SD}}^{10} + \chi_{\text{SC}}^{10} + \chi_{\text{RI}}^{10} + \chi_{\text{HC}}^{10}, \quad (3.21)$$

where $\chi^{10} = (u^{10}, w^{10}, \zeta^{10})$. The subscript TS denotes the contribution due to the tidally averaged advective contribution of the leading order velocity fields, the GC term is the contribution due to the along-channel salinity gradient. The contribution denoted by SD is the tidal return transport (Stokes drift), the SC contribution is a result of the no-stress condition at the surface and a prescribed river discharge at the weir results in a residual contribution RI. The contribution HC is due to the influence of SSC on the water density. All contributions, except for HC, are discussed in detail in Chernetsky et al (2010). Hence, we will only focus on the solution for the forcing contribution HC, which follows from solving the system of equations

$$u_x^{10} + w_z^{10} - \frac{u^{10}}{L_b} = 0, \quad (3.22a)$$

$$g \zeta_x^{10} - g \gamma (a(x) c^{00a})_{xz} = (A_v u_z^{10})_z, \quad (3.22b)$$

with the boundary conditions

$$w^{10} = 0 \quad \text{at} \quad z = 0, \quad (3.23a)$$

$$A_v u_z^{10} = 0 \quad \text{at} \quad z = 0, \quad (3.23b)$$

$$w^{10} = -u^{10} H_x \quad \text{at} \quad z = -H(x), \quad (3.23c)$$

$$A_v u_z^{10} = s u^{10} \quad \text{at} \quad z = -H(x), \quad (3.23d)$$

$$\int_{-H}^0 u^{10} dz = 0 \quad \text{at} \quad x = L, \quad (3.23e)$$

$$\zeta^{10} = 0 \quad \text{at} \quad x = 0. \quad (3.23f)$$

Note that Eq. (3.16) was used in Eq. (3.22b).

Integration of the momentum equation (3.22b) over z , using the known expression for c^{00a} and boundary conditions (3.23b) and (3.23c), yields a solution for the along-channel residual velocity u_{HC}^{10} . This solution still depends on the unknown erosion coefficient $a(x)$ and gradient of the sea surface elevation ζ_x^{10} . The sea surface gradient and the vertical velocity w^{10} are determined from the continuity equation (3.22a) together with boundary conditions (3.23a) and (3.23c). Finally, using boundary conditions (3.23e) and (3.23f), we obtain the expression for the sea surface elevation, which depends on $a(x)$. Back-substitution of this expression into the along-channel residual velocity u_{HC}^{10} yields

$$u_{\text{HC}}^{10} = u_{\text{HC}}^{10a} a(x) + u_{\text{HC}}^{10ax} a_x(x), \quad (3.24)$$

where $u_{\text{HC}}^{10a}(x, z)$ and $u_{\text{HC}}^{10ax}(x, z)$ are known functions independent of $a(x)$. The function u_{HC}^{10a} , proportional to the erosion coefficient, is due to the influence of the along-channel variations of the bottom velocity. Note that this contribution was not considered in Talke et al (2009b), as c^{00a} was independent of the along-channel coordinate in that paper. The second function u_{HC}^{10ax} , proportional to the gradient of the erosion coefficient, is the result of the dependence of the sediment availability on the position in the estuary.

Based on Eqs. (3.21) and (3.24), the first order residual along-channel velocity can be written as

$$u^{10} = u^{10a} a(x) + u^{10ax} a_x(x) + u^{10*}, \quad (3.25)$$

where $a(x)$ is the unknown erosion coefficient and

$$\begin{aligned} u^{10a} &= u_{\text{HC}}^{10a}, \\ u^{10ax} &= u_{\text{HC}}^{10ax}, \\ u^{10*} &= u_{\text{TS}}^{10} + u_{\text{GC}}^{10} + u_{\text{SD}}^{10} + u_{\text{SC}}^{10} + u_{\text{RI}}^{10}. \end{aligned}$$

M₄ flow. Using a similar method as described above, the M_4 velocities and sea surface elevation are constructed. Apart from the contributions described in Section 3.2.1 in Chernetsky et al (2010), there is an extra contribution due to high sediment concentration. Taking this into account, the resulting solution for the M_4 velocity fields and free surface elevation can be written similar to Eq. (3.21) as

$$\chi^{14} = \chi_{\text{AC}}^{14} + \chi_{\text{FS}}^{14} + \chi_{\text{NS}}^{14} + \chi_{\text{EF}}^{14} + \chi_{\text{HC}_1}^{14}, \quad (3.26)$$

where $\chi^{14} = (u^{14}, w^{14}, \zeta^{14})$. The contribution AC is the M_4 constituent of the advective contribution of the leading order velocity fields, the FS term is due to a compensation for the correlation between the horizontal and vertical water motion, the NS contribution is a result of the no-stress condition and the term HC_1 is due to the influence of high suspended sediment concentration on the water density. These four components are produced within the estuary due to nonlinear interactions of the leading order M_2 tide or the leading order concentration, and they are referred to as the internally generated overtide. The forcing term EF is a result of an externally prescribed overtide.

The solution for the forcing terms AC, FS, NS and EF is discussed in detail in Chernetsky et al (2010) and is not duplicated here. In the remainder, we will only illustrate the solution for the high sediment concentration constituent HC_1 . The M_4 water motion, forced by the HC_1 term, is governed by

$$u_x^{14} + w_z^{14} - \frac{u^{14}}{L_b} = 0, \quad (3.27a)$$

$$u_t^{14} + g \zeta_x^{14} - \underbrace{g\gamma(a(x)c^{04a})_{xz}}_{\text{HC}_1} = (A_v u_z^{14})_z, \quad (3.27b)$$

with the appropriate boundary conditions. Here c^{04a} is the known leading order M_4 concentration independent of the erosion coefficient.

To derive a solution, first, we substitute

$$(u^{14}, w^{14}, \zeta^{14}) = \Re \left\{ \left(\hat{u}^{14}(x, z), \hat{w}^{14}(x, z), \hat{\zeta}^{14}(x) \right) e^{2i\sigma t} \right\} \quad (3.28)$$

into (3.27) and the corresponding boundary conditions, where $\Re\{\cdot\}$ denotes the real part of the expression. The resulting time independent problem has to be solved following the solution scheme, used for the residual problem. This yields a solution for the spatial along-channel velocity $\hat{u}_{\text{HC1}}^{14}(x, z)$ of the following structure

$$\hat{u}_{\text{HC1}}^{14} = \hat{u}_{\text{HC1}}^{14a} a(x) + \hat{u}_{\text{HC1}}^{14ax} a_x(x). \quad (3.29)$$

This solution still depends on the erosion coefficient $a(x)$, which has to be determined yet.

Based on Eqs. (3.26) and (3.29), the M_4 along-channel velocity u^{14} can be written as

$$u^{14} = \Re\left\{ \left[\hat{u}^{14a} a(x) + \hat{u}^{14ax} a_x(x) + \hat{u}^{14*} \right] e^{2i\sigma t} \right\}, \quad (3.30)$$

where $a(x)$ is the unknown erosion coefficient and the spatial velocity components are

$$\begin{aligned} \hat{u}^{14a} &= \hat{u}_{\text{HC1}}^{14a}, \\ \hat{u}^{14ax} &= \hat{u}_{\text{HC1}}^{14ax}, \\ \hat{u}^{14*} &= \hat{u}_{\text{AC}}^{14} + \hat{u}_{\text{FS}}^{10} + \hat{u}_{\text{NS}}^{14} + \hat{u}_{\text{EF}}^{14}. \end{aligned}$$

3.3.2 First Order Sediment Dynamics

The first order, i.e. $\mathcal{O}(\varepsilon^1)$, concentration equation reads

$$c_t^1 - w_s c_z^1 = (K_v c_z^1)_z. \quad (3.31)$$

with boundary conditions given by

$$w_s c^1 + K_v c_z^1 = 0 \quad \text{at} \quad z = 0, \quad (3.32)$$

and

$$-K_v c_z^1 = \frac{w_s \rho_s S}{g' d_s} u^1 \frac{u^{02}}{|u^{02}|} a(x) \quad \text{at} \quad z = -H(x). \quad (3.33)$$

Note that, similar to Chapter 2, we assume the nonlinear terms $uc_x + wc_z$, resulting in the spatial settling lag effect, are of $\mathcal{O}(\varepsilon^2)$ and they do not enter into the first order concentration equation.

From Eq. (3.33), it follows that the first order concentration c^1 is a result of the interaction of the leading (u^{02}) and first order (u^1) flows. A Fourier analysis of the right hand side of bottom boundary condition (3.33) shows that c^1 consists of all tidal components, i.e., $c^1 = c^{10} + c^{12} + c^{14} + \dots$. However, to get

the morphodynamic equilibrium condition in leading order, we only need the M_2 component c^{12} (see Section 3.3.3). This component is obtained by substituting $c^{12} = \Re\{\hat{c}^{12}(x, z)e^{i\sigma t}\}$ into Eqs. (3.31) - (3.33) and approximating boundary condition (3.33) by its Fourier series, retaining only the contribution that oscillates at the M_2 frequency σ . The resulting spatial problem is solved using the appropriate boundary conditions yielding a solution, which has the following structure

$$c^{12} = \Re\left\{\left(c^{12a}a(x) + c^{12aa}a^2(x) + c^{12aax}a(x)a_x(x)\right)e^{i\sigma t}\right\}. \quad (3.34)$$

Here, $a(x)$ is the undetermined erosion coefficient and c^{12a} , c^{12aa} and c^{12aax} are known functions that are obtained analytically. The first M_2 contribution is linear in $a(x)$ and is described in Chernetsky et al (2010). The other two terms enter this equation due to the influence of SSC on the horizontal velocity u^1 (see Eqs. (3.24), (3.29) and (3.33)). The term c^{12aa} , proportional to the squared erosion coefficient, is due to the presence of the first order horizontal velocity constituent proportional to $a(x)$, and the c^{12aax} term (proportional to the product of the erosion coefficient and its gradient) is the result of the u^1 constituent proportional to the gradient of the erosion coefficient. Due the last two terms, Eq. (3.34) is nonlinear in $a(x)$.

3.3.3 Morphodynamic equilibrium condition

Following Chernetsky et al (2010), the leading order morphodynamic equilibrium condition reads

$$\int_{-H}^0 \left(u^{10}c^{00} + \langle u^{02}c^{12} \rangle + \langle u^{14}c^{04} \rangle - K_h \langle c_x^{00} \rangle\right) dz + \langle \zeta^0 [u^{02}c^0]_{z=0} \rangle = 0. \quad (3.35)$$

Using Eqs. (3.16), (3.25), (3.30) and (3.34), Eq. (3.35) transforms into a nonlinear ordinary differential equation for the unknown erosion coefficient $a(x)$

$$F(x)a_x + T(x)a + \underbrace{T_1(x)a^2 + T_2(x)aa_x}_{\text{TCM}} = 0, \quad (3.36)$$

where

$$\begin{aligned}
 F &= - \int_{-H}^0 K_h c^{00a} dz, \\
 T &= \underbrace{\int_{-H}^0 c^{00a} u^{10*} dz + \left\langle \zeta^0 [u^{02} c^{0a}]_{z=0} \right\rangle}_{T_{\text{res}}} + \underbrace{\int_{-H}^0 \langle c^{12a} u^{02} \rangle dz}_{T_{M_2}} \\
 &\quad + \underbrace{\int_{-H}^0 \langle c^{04a} u^{14*} \rangle dz}_{T_{M_4}} - \underbrace{\int_{-H}^0 K_h \langle c_x^{00a} \rangle dz}_{T_{\text{diff}}} \\
 T_1 &= \int_{-H}^0 \left(c^{00a} u^{10a} + \underbrace{\langle c^{12aa} u^{02} \rangle}_{T_1^{M_2}} + \langle c^{04a} u^{14a} \rangle \right) dz, \\
 T_2 &= \int_{-H}^0 \left(c^{00a} u^{10ax} + \underbrace{\langle c^{12aax} u^{02} \rangle}_{T_2^{M_2}} + \langle c^{04a} u^{14ax} \rangle \right) dz.
 \end{aligned}$$

Here, the underbraces $\underbrace{\quad}$ denote different contributions to the residual transport T , induced by various interactions between the velocity field and suspended sediment concentration: T_{res} is the transport, which results from the interaction of the residual velocity with the residual concentration, T_{M_2} is the residual transport due to the M_2 velocity and M_2 concentration interaction, T_{M_4} is the transport due to the M_4 velocity and M_4 concentration interaction. The behavior of the diffusion in the domain is described by a linear combination of a diffusive transport T_{diff} and the transport F (i.e., the diffusive transport equals $aT_{\text{diff}} + a_x F$). These transport functions are discussed in detail in [Chernetsky et al \(2010\)](#). The transport function TCM is a result of the influence of high SSC on the water density and it comprises of two transports, denoted by T_1 and T_2 . The T_1 transport, proportional to the squared erosion coefficient and the T_2 transport, proportional to the product of the erosion coefficient and its gradient. In the residual model of [Talke et al \(2009b\)](#), the counterpart of the TCM transport consists only of the first contribution of the T_2 transport, the T_1 transport equals zero.

From Eq. (3.36) the erosion coefficient is determined up to a constant, which governs the total amount of sediment available in the estuary. In this study, we use

a boundary condition at the seaward side $a(0) = a_*$, to prescribe the total amount of sediment available for resuspension in the domain. The constant a_* is chosen in such a way, that a prescribed maximum concentration at the surface is reached, i.e., we can vary between low and high SSC conditions in the estuary.

3.4 Results

As a reference estuary we take the Ems/Dollart estuary. Most parameter values, used in this chapter, are derived directly from measurements, carried out in the Ems estuary between 2005 and 2006 and are summarized in Table 3.1. For more information on the Ems estuary, see De Jonge (1983, 1992); Talke et al (2009b); Chernetsky et al (2010). Following Chernetsky et al (2010), the model bathymetry is prescribed by the measured bathymetry, smoothed using a lowpass filter.

Table 3.1: *Set up model parameters which represent the Ems estuary (based on 2005-2006 measurements)*

Parameter	Symbol	Dimension	Magnitude
Semi-diurnal angular tidal frequency	σ	s^{-1}	1.4×10^{-4}
Gravitational acceleration	g	$m s^{-2}$	9.8
β	β	psu^{-1}	7.6×10^{-4}
Ref. density	ρ_0	$kg m^{-3}$	1020
Sediment density	ρ_s	$kg m^{-3}$	2650
Length of the estuary	L	km	63.7
Convergence length	L_b	km	30
M_2 tidal amplitude at the entrance	A_{M_2}	m	1.35
M_4 tidal amplitude at the entrance	A_{M_4}	m	0.19
Relative phase at the entrance	ϕ	degrees	-174.6
Vertical eddy viscosity coefficient	A_{v0}	$m^2 s^{-1}$	0.012
Stress coefficient	s_0	$m s^{-1}$	0.049
River discharge	Q	m^3/s	53
Settling velocity	w_s	$m s^{-1}$	0.0002 - 0.002
Horizontal eddy diffusivity	K_h	$m^2 s^{-1}$	100

In Section 3.4.1, we analyze the influence of turbidity currents on the position and shape of the ETM in the Ems estuary. Next, in Section 3.4.2, we investigate the sensitivity of model results to different bathymetric profiles and influence of the estuarine length on the position of the ETMs. In Section 3.4.3, the effect of the externally prescribed M_4 tide on the ETM is discussed.

3.4.1 Turbidity currents

Using parameters representative for the Ems estuary, the along-channel distribution of SSC in morphodynamic equilibrium is obtained by solving the equations given in Section 3.3. Figs. 3.2a and 3.2c show the SSC distribution for fine and coarse silt for parameter values representative for 1980 (given in Chernetsky et al (2010)), and Figs. 3.2b and 3.2d for 2005, respectively. The amount of sediment in the estuary available for resuspension is prescribed in such a way, that the modeled maximum surface SSC is approximately equal to the surface SSC observed in 1980 (0.4 g/l) and 2005 (2 g/l). For fine silt (Fig. 3.2a and 3.2b) in both 1980 and 2005, there is one ETM which is located at the upward limit of salt intrusion. For coarse silt in 1980, the single ETM is located at the entrance of the estuary (Fig. 3.2c), whereas there are two ETMs in 2005. These results are consistent with those obtained in Chernetsky et al (2010), in which turbidity currents were neglected. We may thus conclude that the turbidity current mechanism (TCM) does not change the location where sediment is deposited qualitatively, it rather modifies the spatial distribution of the SSC. To demonstrate this, we consider the coarse silt case in 2005 and compare the SSC in morphodynamic equilibrium with and without the effect of turbidity currents (see Fig. 3.3).

The blue contour lines in Fig. 3.3 show the turbidity zone in the absence of the TCM and the black contour lines in case turbidity currents are considered. The concentration is plotted in g/l and in both cases, the maximum surface SSC is taken to be 2 g/l. The dashed lines depict local maxima of SSC. We can see that the turbidity currents result in a slight downstream shift of the ETM by approximately 2 km and a more asymmetric shape of the ETMs. Moreover, we observe a turbidity zone rather than two distinct ETMs. To understand and explain these changes, we analyze individual sediment transports in morphodynamic equilibrium (see Eq. (3.36) and Chernetsky et al (2010)).

In Fig. 3.4, the residual sediment transports in morphodynamic equilibrium are depicted. Fig. 3.4a shows the results when the water density is affected by the salinity only, and Fig. 3.4b when the influence of the SSC on the density is accounted for. In both figures, the red line represents the residual sediment

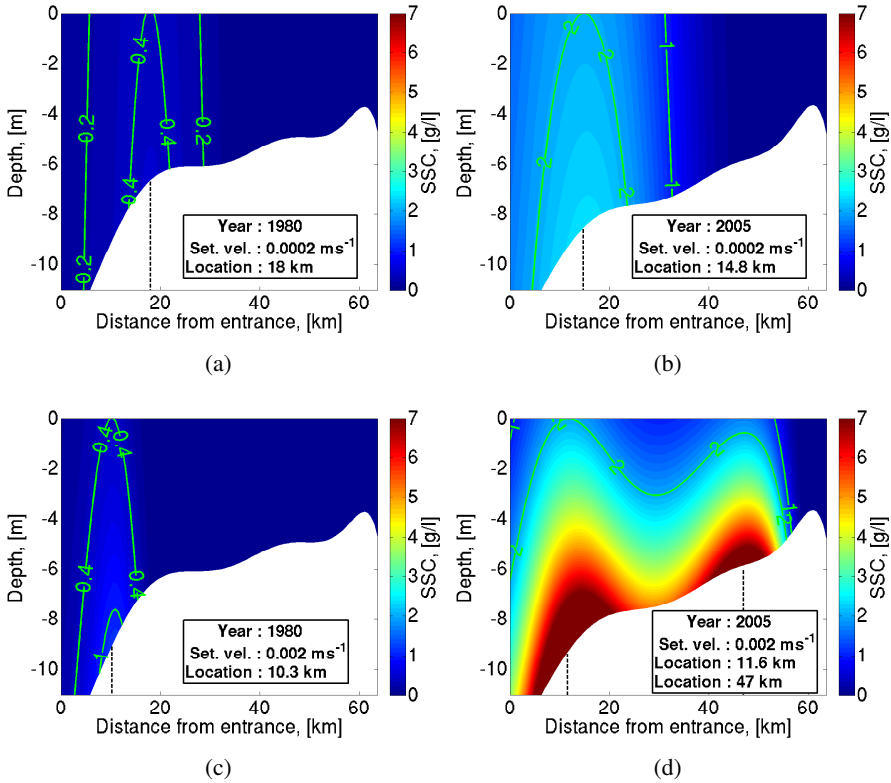


Figure 3.2: Tidally averaged SSC in morphodynamic equilibrium accounting the turbidity currents mechanism. The left panels represent the 1980 case with the maximum SSC at the surface of 0.4 g/l and the right panels show the 2005 case with the maximum SSC of 2 g/l. The upper panels depict fine silt and the lower ones coarse silt

transport due to the residual velocity/residual concentration interaction, the green line depicts the residual sediment transport due to the M_2 velocity/ M_2 concentration interaction, the black line shows the residual sediment transport due to the M_4 velocity/ M_4 concentration interaction, and the diffusive transport is depicted by the magenta line. Because we consider morphodynamic equilibrium, these transports must balance, i.e., their sum vanishes everywhere in the estuary. If the transport is positive, the sediment is transported upstream. If it is negative, the transport is directed seawards. The arrows in Figs. 3.4a and 3.4b show the direction of the sediment transport and their color represents the corresponding transports. For example, the green arrow shows the residual import of sediment

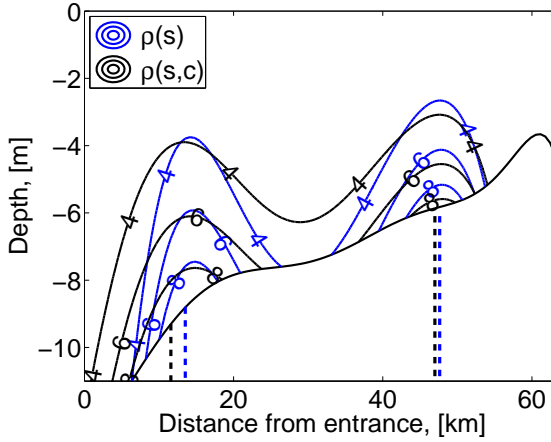


Figure 3.3: The tidally averaged SSC (in g/l) with and without the turbidity current mechanism (TCM). The blue contour lines show the turbidity zone in the absence of the TCM and the black contour lines represent the influence of high suspended sediment concentration. The dashed blue and black lines depict the maximum SSC of the ETMs

by the M_2 sediment transport. From Fig. 3.4a, we may conclude that the M_2 sediment transport is primarily responsible for the import of sediment, while the residual sediment transport transports the sediment out of the system. The M_4 sediment transport is exporting near the entrance and importing farther upstream. The diffusive transport balances the other sediment transports.

The turbidity currents generate an additional sediment transport (the nonlinear terms TCM in Eq. (3.36)), which is referred to as the TCM transport and represented by the cyan line in Fig. 3.4b. Cyan arrows show the direction of transport. At the locations of maximum concentration (km 12 and 47 in Fig. 3.3), this transport the sediment in opposite directions, thus, acting like a diffusive transport. This results in a wider spread of the ETMs and their downstream shift. Moreover, the ETM asymmetry seems to be slightly enhanced. In the remainder of this section, we will focus on the analysis and physical interpretation of this transport.

The TCM sediment transport consists of two contributions. One transport, denoted by T_1 is proportional to the squared erosion coefficient and depicted by the solid green line in Fig. 3.5. The other one, denoted by T_2 is proportional to $a(x)a_x(x)$ and is represented by the solid red line. These transports result from three residual contributions, induced by the residual, M_2 and M_4 velocity/concentration interactions (see the expressions for T_1 and T_2 in Eq. (3.36)). The $T_1^{M_2}$ and $T_2^{M_2}$ constituents, shown by the dashed lines in Fig. 3.5, are the ma-

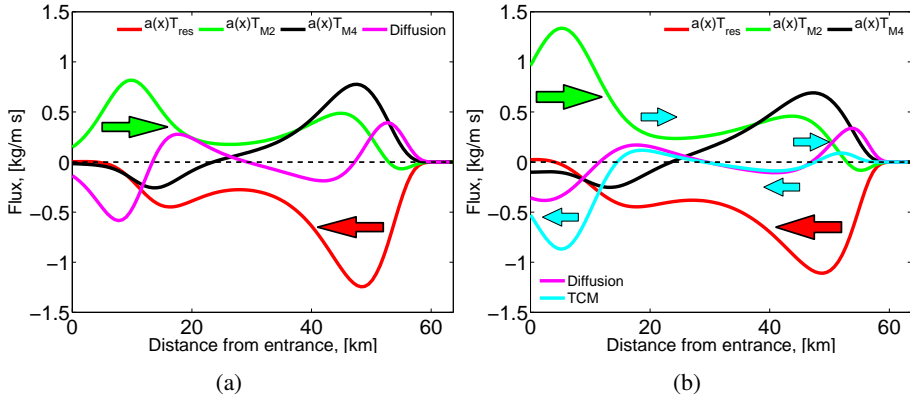


Figure 3.4: Residual sediment transports in morphodynamic equilibrium. The density is affected by the salinity only (left panel) and by both the salinity and SSC (right panel). The red line represents the residual sediment transport due to the residual velocity/residual concentration interaction, the green line depicts the M_2 sediment transport due to the M_2 velocity/ M_2 concentration interaction, the black line shows the M_4 sediment transport due to the M_4 velocity/ M_4 concentration interaction, and the diffusive transport is depicted by the magenta line. The cyan line in the right panel represents the sediment transport generated by the nonlinear terms. Results represent the 2005 case and are obtained for the settling velocity of 0.002 m s^{-1}

major contributors to the T_1 and T_2 transports. Therefore, the physical explanation of the influence of turbidity currents on the ETM formation can be achieved by investigating these transports.

The residual sediment transports $T_1^{M_2}$ and $T_2^{M_2}$ are due to the transport of the M_2 concentration constituents c^{12aa} and c^{12aax} by the M_2 velocity u^{02} , respectively (see Sections 3.3.2 and 3.3.3). The M_2 velocity field is the leading order component and is not influenced by the turbidity currents. On the contrary, the first order M_2 concentrations c^{12aa} and c^{12aax} , forced by the bed-shear stress, are induced by the nonlinear interaction between the leading order (u^{02}) and first order velocity field ($u^1 = u^{10} + u^{14}$), which contains contributions due to turbidity currents (see Eqs. (3.25), (3.30) and Section 3.3.1). Focusing on the contributions to the bed-shear stress due to the velocity components that are proportional to the erosion coefficient, it is found that the M_4 velocity contributions u^{14a} and u^{14ax} have a negligible influence on c^{12aa} and c^{12aax} . These contributions are mainly due to the interaction of the residual velocities u^{10a} and u^{10ax} and the M_2 velocity field u^{02} . Therefore, the $T_1^{M_2}$ transport (and thus T_1) is primarily governed by the contribu-

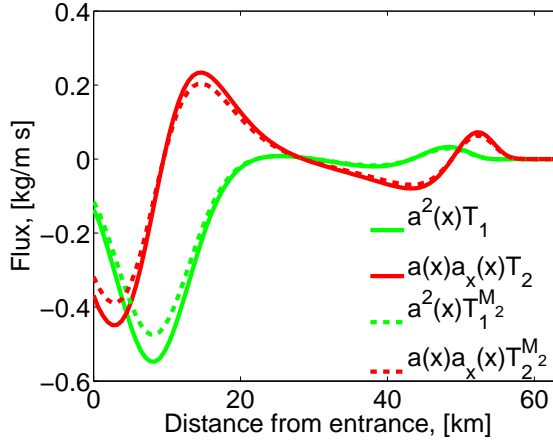


Figure 3.5: Constituents of the TCM transport. The red solid line depicts the T_1 constituent, which is proportional to the squared erosion coefficient, and the solid green line represents the T_2 transport, proportional to the product of the erosion coefficient and its gradient. The dashed lines show the major (M_2) contribution to the T_1 and T_2 transports

tions proportional to the residual velocity constituent u_{HC}^{10a} and $T_2^{M_2}$ (and thus T_2) by contributions proportional to u_{HC}^{10ax} (see Eq. (3.24)). These velocity components are shown in Fig. 3.6, where the left panel shows u_{HC}^{10a} which is proportional to the erosion coefficient $a(x)$, and the right one depicts u_{HC}^{10ax} , proportional to the gradient of $a(x)$.

Using these figures, the influence of high sediment concentration on the trapping locations can be understood. First, we focus on the influence of the velocity u_{HC}^{10a} , proportional to the erosion coefficient. During the ebb tide, the M_2 velocity at the bottom in the first 20 km region near the entrance is enhanced by the residual velocity u_{HC}^{10a} (left panel in Fig. 3.6) resulting in a higher shear stress, thus, inducing higher sediment concentrations in the water column. This sediment is transported seawards by the M_2 tide. During the flood, the bed-shear stress is smaller, which results in lower concentrations and, hence, less transport into the estuary. Averaging over a tidal period, sediment is exported, resulting in a negative T_1 transport (see Fig. 3.5), which pushes the ETM slightly to the seaward side. A similar mechanism determines the behavior of the T_2 transport. During the ebb (flood) tide, the M_2 velocity at the bottom is enhanced by the residual velocity constituent u_{HC}^{10ax} at the left (right) hand side of the ETMs. During the flood (ebb), the M_2 velocity is reduced at the left (right) hand side of the ETM resulting

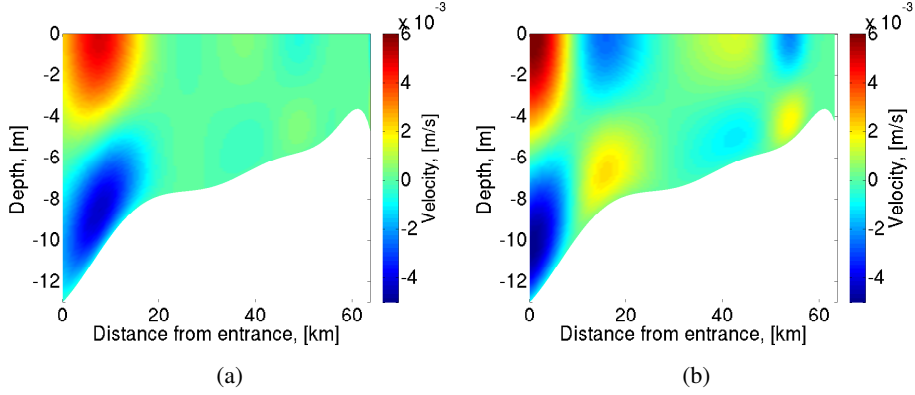


Figure 3.6: Constituents of the residual velocity u_{HC}^{10} , induced by turbidity currents. The left panel shows the constituent proportional to the erosion coefficient, and the right one depicts the component proportional to its gradient

in downstream (upstream) direction of the T_2 transport. Hence, averaged over a tidal cycle, this transport acts like a diffusive transport, resulting in a wider ETM profile.

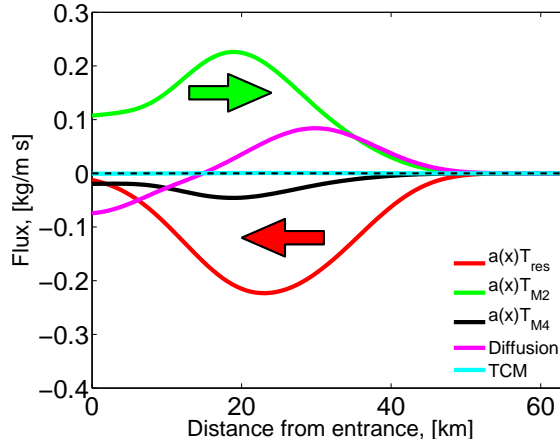


Figure 3.7: Residual sediment transports in morphodynamic equilibrium for fine sediment with the settling velocity of 0.0002 m s^{-1}

In case of fine sediment, shown in Fig. 3.7, the sediment transport generated by the turbidity currents is negligible. Compared to coarse sediment, it requires

less fine sediment to reach the same surface concentration. Thus, the concentration in the water column is much lower and does not significantly affect the water density.

3.4.2 Sensitivity to bathymetry

In this section, we investigate the effect of the bathymetry on the occurrence and location of the estuarine turbidity maxima. This is done by substituting the Ems bottom profiles of 1980 and 2005 with a linear fit of these bathymetries. Figs. 3.8a and 3.8b show the tidally averaged SSC for fine silt (the settling velocity is 0.0002 m s^{-1}), whereas coarse silt (the settling velocity is 0.002 m s^{-1}) is depicted in Figs. 3.8c and 3.8d for 1980 and 2005, respectively. For the 1980 case, the bathymetry is prescribed by $H_{\text{ent}} = 10.2 \text{ m}$ and $H_{\text{end}} = 3.1 \text{ m}$, and in 2005, $H_{\text{ent}} = 10.2 \text{ m}$ and $H_{\text{end}} = 4.2 \text{ m}$. The amount of sediment is prescribed such, that the maximum SSC at the surface is approximately 0.4 and 2 g/l in 1980 and 2005, respectively.

By comparing the locations of sediment trapping in corresponding cases for the linear (Fig. 3.8) and varying bathymetry (Fig. 3.2), we can see that the obtained results are qualitatively similar. The substitution of a smoothed historical bathymetry by its linear fit results in an insignificant up- or downstream shift of the ETM by 3.5 km at most. Hence, the presence of the bed formations has a minor effect on the location of the turbidity region and the linearly fitted bathymetry can be used as a sound initial approximation.

The assumption of linear bathymetry allows to investigate the influence of the embayment length and various deepening scenarios on the position of the ETM in the embayment. Fig. 3.9 depicts the along-channel suspended sediment concentration at the bottom as a function of estuarine length (y -axis). On the x -axis the location in the estuary is shown (with 0 the seaward entrance), and the color code indicates the magnitude of the suspended sediment concentration shown in g/l, with warmer (cooler) colors being higher (lower) suspended sediment concentration. The trapping locations are the locations where the suspended sediment concentration has its maximum (the dark red patch in Fig. 3.9). The sediment is assumed to be coarse with a settling velocity of 0.002 m s^{-1} .

To clarify Fig. 3.9 further, consider the Ems estuary with a length of approximately 63.7 km, i.e., this corresponds to the value of 63.7 on the y -axis. The color code between 0 and 63.7 in x -direction indicate the suspended sediment concentration at the bottom (see Fig. 3.8d) between the entrance (km 0) and the tidal weir (km 63.7).

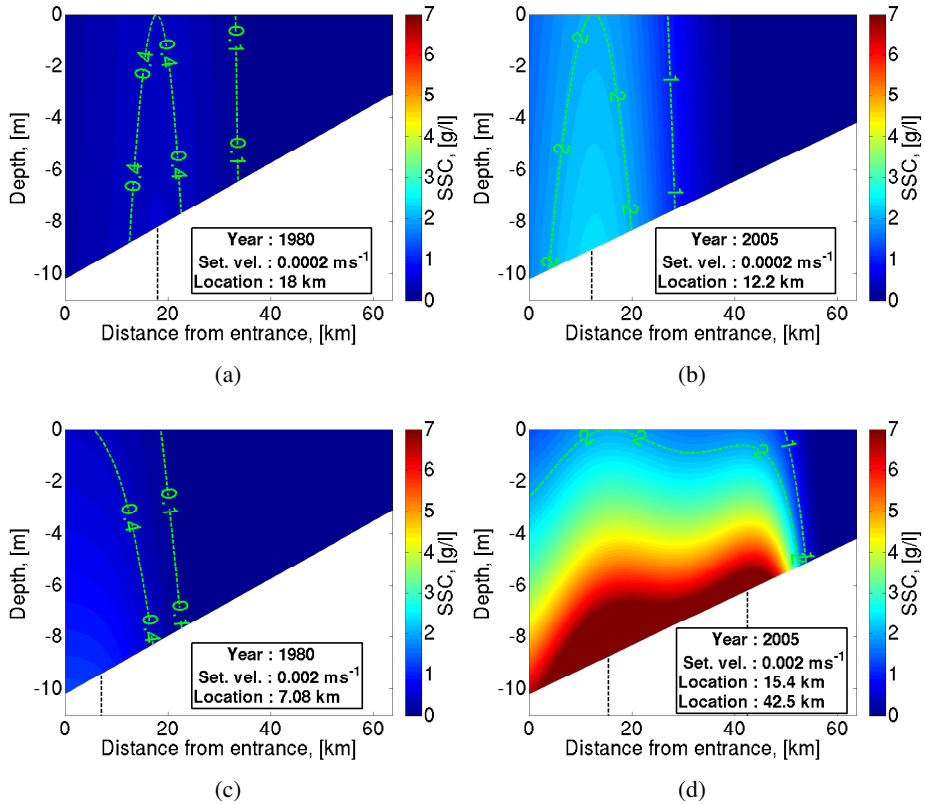


Figure 3.8: Tidally averaged suspended sediment concentration (SSC) in morphodynamic equilibrium. The upper panels show the SSC for fine silt and the lower ones depict coarse silt. The bottom profile at the left panels is prescribed by $H_{ent} = 10.2$ m and $H_{end} = 3.1$ m, and at the right panels is $H_{ent} = 10.2$ m and $H_{end} = 4.2$ m. The maximum SSC at the surface is prescribed to 0.4 g/l in 1980 and 2 g/l in 2005

For short embayments, i.e., the estuarine length between approximately 20 and 60 km, a single ETM is observed which is located near the tidal weir. For a length between 60 and 66 km, two ETMs occur: one at the entrance and the other one close to the weir. The Ems estuary, with length of approximately 63.7 km, falls into this range. When the estuary becomes longer than 66 km, a single trapping region is found which is located downstream near the entrance of the embayment.

These changes in sediment trapping can be again explained by analyzing in-

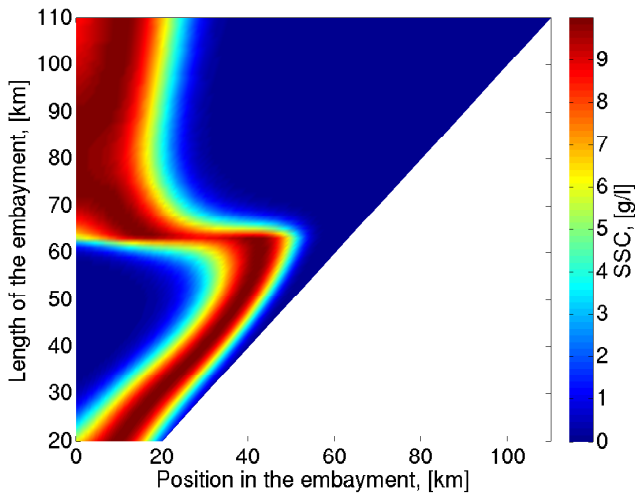


Figure 3.9: *Trapping locations of the suspended sediment concentration as a function of estuarine length. The color code indicates the magnitude of the suspended sediment concentration shown in g/l. Coarse sediment is considered with settling velocity of 0.002 m s^{-1}*

dividual sediment transports in morphodynamic equilibrium for every estuarine length. In [Chernetsky et al \(2010\)](#), we showed two primary mechanisms resulting in trapping of suspended sediment. The ETM at the entrance results from the interaction of the various contributions of the T_{M_2} and T_{res} transports (in the remainder of this chapter, this is called mechanism *I*), whereas the one upstream is due to the import resulting from tidal asymmetry and the export due to river outflow. The suspended sediment is primarily trapped by the strongest mechanism and multiple trapping locations occur when both mechanism are of equal strength. From a detailed analysis of sediment transports for various estuarine lengths, it follows that the transition from one mechanism to the other happens mainly due to a strong decrease of the tidal asymmetry for an estuarine length between approximately km 60 and 66. To understand this transition, we have to analyze the changes in tidal asymmetry.

The M_2 and M_4 tidal amplitude of the sea surface elevation are shown as a function of estuarine length in [Fig. 3.10a](#) and [3.10b](#), respectively. The plotting procedure is similar to [Fig. 3.9](#), the y-axis represents the length of the estuary and the x-axis shows the position within the embayment. The color code in x-direction indicate the magnitude of the tidal amplitude between the entrance (km 0) and the

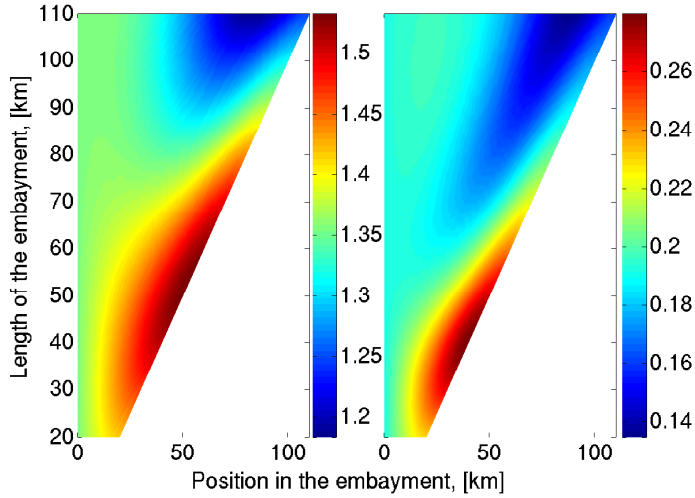


Figure 3.10: *The amplitude of the sea surface elevation in the estuary as a function of estuarine length. The left panel depicts the M_2 tidal constituent and the left one shows the externally prescribed M_4 constituent. The amplitude is shown in meters*

tidal weir in meters. If the amplitude towards the end of the estuary increases (decreases), this is reflected by warmer (cooler) colors at the tidal weir.

From Fig. 3.10, it is seen that the tidal amplitude in estuaries with a length between 20 and 60 km is amplified: both the M_2 and M_4 amplitude of the sea surface elevation is maximum at the landward side for these lengths of the estuary. The resonance for the M_2 and M_4 tides occurs for an embayment length of approximately 53 and 41 km, respectively, i.e., the magnitude of the M_2 and M_4 amplitude at the landward side is maximum for these estuarine lengths. This length of the estuary is called the resonance length (see also Appendix A6). Note that the M_2 resonance length is larger than that of the M_4 .

In Chernetsky et al (2010), it was shown that the sediment trapping resulting from the tidal asymmetry is mainly determined by the behavior of the residual transport of the M_2 concentration by the M_2 velocity, forced by the externally prescribed M_4 velocity (see the $T_{M_2}^{EF}$ transport constituent). For short embayments (the length shorter than the M_4 resonance length of 41 km), the M_4 tidal amplitude is enhanced and the tidal wave has mainly the character of a standing wave, i.e., the relative phase difference between the M_2 tidal velocity and the M_2 sea surface elevation is approximately 90° . Therefore, for short estuaries, the influence of the

tidal asymmetry is strong, and suspended sediment is trapped near the end of the estuary. For an embayment length between 41 and 60 km, the M_4 tidal amplitude near the weir starts to decrease gradually and the character of the tidal wave begins to change more towards that of a traveling wave. The tidal asymmetry starts to get weaker, however, it is still strong enough to be the dominant trapping mechanism. In the transition region (the estuarine length is between 60 and 66 km), the strength of the tidal asymmetry trapping mechanism is of the same order as the mechanism I . This results in two trapping regions: one at the entrance and the other one at the tidal weir. For embayments longer than 66 km, the tidal wave behaves in a large part of the estuary as a traveling wave and the tidal asymmetry is not strong enough to trap suspended sediment at the end of the estuary. It is worth mentioning that the natural length of the Ems estuary (~ 63.7 km) is close to the resonance length and falls into the transition region, thus, both trapping mechanisms are active, which results in two trapping regions.

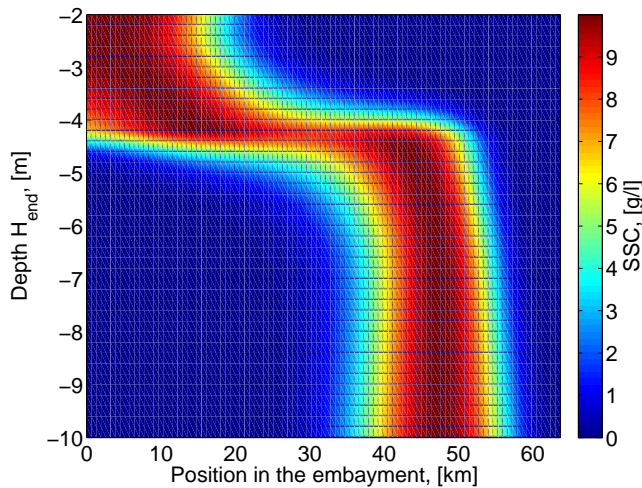


Figure 3.11: Trapping locations of the suspended sediment concentration as a function of depth at the tidal weir. The color code indicates the magnitude of the suspended sediment concentration shown in g/l. The depth at the entrance $H_{ent} = 10.2$ m and coarse sediment is considered with settling velocity of 0.002 m s^{-1} . The length of the estuary is 63.7 km

A similar competition between the trapping mechanisms is also observed for various deepening scenarios of the embayment. Figs. 3.11 and 3.12 depict the trapping locations of the suspended sediment concentration as a function of depth

at the tidal weir and at the entrance, respectively. In the first case, the depth at the entrance is kept constant, $H_{\text{ent}} = 10.2$ m, and in the other case, the depth at the entrance and the weir is increased by the same increment. We consider coarse sediment with a settling velocity of 0.002 m s^{-1} and the length of the basin corresponds to the Ems length of 63.7 km. It is seen that for deep basins, the water motion has the character of a standing wave and the tidal asymmetry is the dominant trapping mechanism. Note, that the resonance length changes with depth and is different for all these embayments. For shallow estuaries, the tidal wave behaves more as a traveling wave, the tidal asymmetry gets weaker and sediment is trapped near the upward limit of salt intrusion. In both scenarios, a transition region is observed.

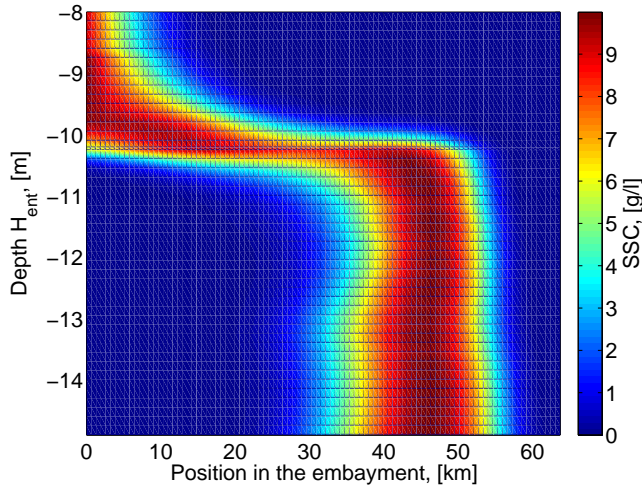


Figure 3.12: *Trapping locations of the suspended sediment concentration as a function of depth at the entrance. The color code indicates the magnitude of the suspended sediment concentration shown in g/l. Coarse sediment is considered with settling velocity of 0.002 m s^{-1} . The length of the estuary is 63.7 km*

The influence of high sediment concentration can be demonstrated using a plot, similar to Fig. 3.9. Fig. 3.13 depicts the trapping region, outlined by the solid lines, as a function of the estuarine length (y-axis). The black curves show the location of the ETM in case the TCM is taken into account, with the black dashed line being the location of maximum suspended sediment concentration. The red curves represent the trapping locations when the influence of high sediment concentration on the water column is neglected. The sediment is assumed to

be coarse and the settling velocity is prescribed to 0.002 m s^{-1} .

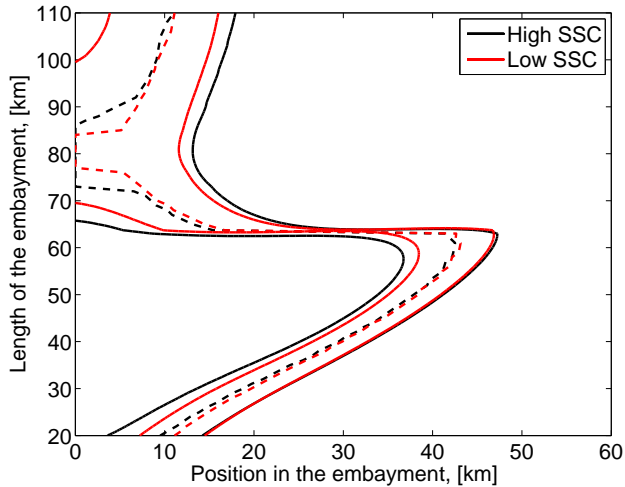


Figure 3.13: *Trapping locations of the suspended sediment concentration as a function of estuarine length for high (black lines) and low (red lines) suspended sediment concentration. The dashed lines represent the maximum concentration for a given estuarine length and the solid lines depicts the associated turbidity region. Coarse sediment is considered with settling velocity of 0.002 m s^{-1}*

Fig. 3.13 shows that the location and occurrence of the turbidity zone is not very sensitive to the presence of turbidity currents, there is a small shift towards the entrance of the estuary. However, comparing the width of the ETM between a situation when high sediment concentration is taken into account (the black solid lines) and neglected (the red solid lines), it is clear that the TCM widens the trapping region towards the seaward side and enhances the asymmetry: the distance between the black solid lines is larger than for the red solid lines (indicating a wider ETM), and the seaward black solid line has shifted more towards the entrance of the estuary than the other black solid line has shifted landwards, resulting in a slight increase of the asymmetry of the turbidity region.

3.4.3 Sensitivity to the external forcing

As discussed above, suspended sediment is mainly trapped by two mechanisms. The mechanism due to the tidal asymmetry, resulting in an ETM in the fresh water zone, is driven predominantly by the presence of an M_4 external tidal component. Therefore, the occurrence of an ETM near the tidal weir is quite sensi-

tive to changes of this tidal constituent. In this section, we present a sensitivity analysis of trapping locations in the estuary to the M_4 externally prescribed tidal constituent.

Fig. 3.14 shows the trapping locations of the suspended sediment concentration (x-axis) as a function of the prescribed M_4 tidal amplitude at the entrance (y-axis), i.e., A_{M_4} in Eq. (3.8). The color code indicates the magnitude of the suspended sediment concentration, shown in g/l. The trapping locations are the locations where the suspended sediment concentration is maximum (the dark red patch in the figure). The sediment is assumed to be coarse and the settling velocity is prescribed to 0.002 m s^{-1} . The length of the embayment corresponds to the Ems estuary and is 63.7 km.

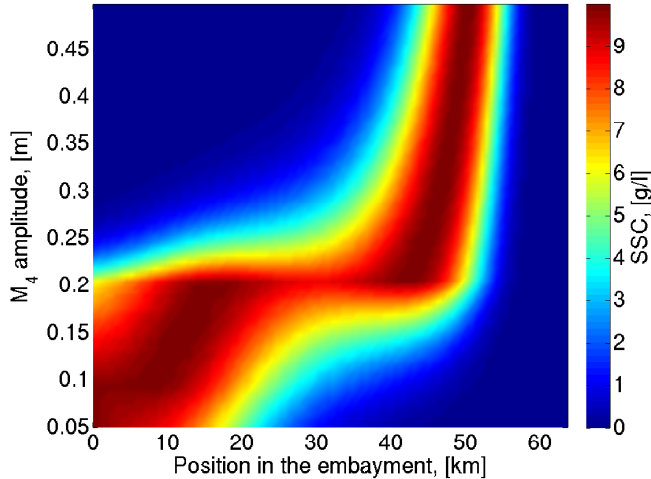


Figure 3.14: Trapping locations of the suspended sediment concentration as a function of the prescribed M_4 tidal amplitude at the entrance. The color code indicates the magnitude of the suspended sediment concentration at the bottom shown in g/l. Coarse sediment is considered with settling velocity of 0.002 m s^{-1} . The length of the estuary is 63.7 km

From Fig. 3.14, it is seen that when the amplitude of the externally prescribed M_4 tide is low, i.e., between approximately 0.05 and 0.18 m, there is only one ETM located near the entrance of the estuary resulting from the classical mechanism. For this amplitude range, the tidal asymmetry is insignificant and not effective enough to capture sediment at the end of the estuary. As the amplitude increases, the tidal asymmetry gets stronger and becomes the dominant trapping mechanism

in the estuary. Similar to the cases discussed in Section 3.4.2, we observe a transition region (A_{M_4} is between 0.18 – 0.21 m), where both mechanisms are of the same order. This results in two trapping locations, one near the entrance and the other one close to the end of the embayment. The M_4 tidal amplitude for the Ems estuary, measured in 2005, was approximately 0.19 m. For this magnitude, both mechanisms are effective and two trapping regions occur. An increase (decrease) of the M_4 tidal amplitude will result in an upstream (downstream) shift of the suspended sediment trapping region.

Apart from the tidal amplitude, the M_4 external tide is characterized by the phase shift relative to the M_2 tidal constituents, i.e., ϕ in Eq. (3.8). The sensitivity of the trapping locations to the M_4 tidal phase is presented in Fig. 3.15. The prescribed M_4 tidal phase is shown in degrees on the y-axis of the plot. The corresponding relative phase between the M_4 and M_2 surface velocity at the entrance ($\phi_{u_{M_4}} - 2\phi_{u_{M_2}}$), (Van de Kreeke and Dunsbergen, 2000) is depicted on the right y-axis. The relative phase allows to determine the ebb/flood dominance at the entrance. If the relative phase is between -90° and 90° , the water motion near the entrance of the estuary is flood dominated; otherwise, the water motion near the entrance is ebb dominated (see also Aubrey and Speer (1985); Chernetsky et al (2010)).

For the M_4 tidal phase between 155° and 173° , the water motion is flood dominated. This phase is a good indication for the relative phase, related to the externally forced M_4 tide everywhere in the estuary, only if the tidal wave behaves as a standing wave. Since this is the case for the parameter values we consider here, it can be inferred that the trapping region is located upstream near the tidal weir. During the flood, the suspended sediment is transported upstream, the ebb velocities are smaller and less sediment is transported out of the estuary. This results in a residual import of sediment. When the water motion near the entrance of the estuary is ebb dominated, i.e., the M_4 tidal phase is more than 177° , the suspended sediment is trapped near the entrance, i.e., the ebb velocity is larger than the flood velocity. During ebb, the sediment from the upper reaches is eroded and transported downstream, where it is trapped by the mechanism *I*. There is a transition region where the M_4 phase is between 173° and 177° . In this case, two ETMs are observed. This region is located close to the relative phase of -90° , the point where the ebb and flood dominance at the entrance of the estuary change.

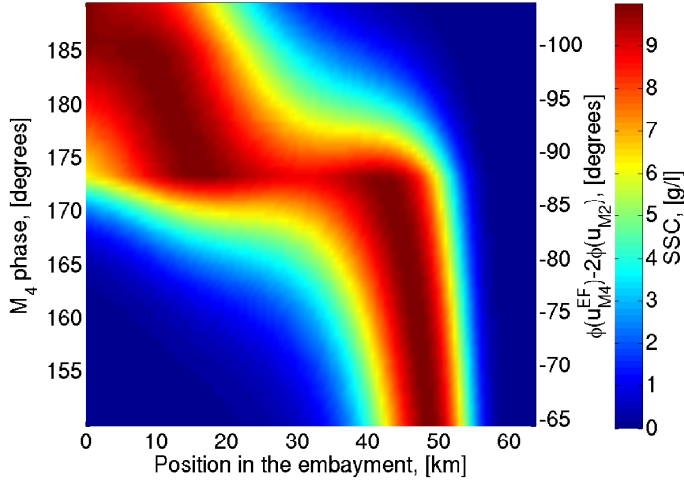


Figure 3.15: *Trapping locations of the suspended sediment concentration as a function of the prescribed M_4 tidal phase at the entrance (shown on the left y-axis). The right y-axis represents the modeled relative phase between the M_4 and M_2 surface velocity at the entrance. The color code indicates the magnitude of the suspended sediment concentration at the bottom shown in g/l. Coarse sediment is considered with settling velocity of 0.002 m s^{-1} . The length of the estuary is 63.7 km.*

3.5 Conclusions

The influence of high sediment concentration on the sediment trapping in tidal estuaries is investigated using an analytical 2DV model. The presented hydro- and sediment dynamic model is an extension of the model introduced in [Chernetsky et al \(2010\)](#). The hydrodynamic conditions in the estuary are modeled using the width-averaged shallow water equations, and the suspended sediment concentration in the water column is governed by the width-averaged advection-diffusion equation. In these equations, the water density depends on both the salinity and variations of the density due to nonhomogeneous distribution of the suspended sediment concentration in the estuary. The condition of morphodynamic equilibrium is assumed, which allows to obtain the spatial distribution of the sediment availability at the bottom. The model equations are solved analytically by making a regular expansion of the various physical variables in a small parameter, which is the ratio of the tidal amplitude over the water depth at the entrance. As a reference estuary, we use the Ems/Dollart estuary and measurements which represent

2005.

We have showed that turbidity currents, resulting from high sediment concentration, produce an additional transport in the morphodynamic balance. This additional transport does not change the balance between the other fluxes significantly, but rather modifies it: this flux results in a wider spread of the turbidity zone, a slight asymmetry enhancement and an insignificant up- or downstream shift of the ETM. The flux consists of six different contributions. In a tidally averaged model, e.g., [Talke et al \(2009a\)](#), only one of these contributions can be taken into account, the contribution due to the transport of tidally averaged suspended sediment concentration by the residual turbidity current. It turns out that this contribution is of minor importance in a tide-resolving model. In such a model, the contribution of the tidally-averaged turbidity current to the M_2 suspended sediment concentration results in the dominant suspended sediment transport contribution by its correlation with the M_2 velocity field. This contribution consists of two parts, one part, related to the spatial variation of the residual concentration field itself, results in the slight shift of the location of the ETM. The second contribution, related to the longitudinal dependency of the sediment availability function results in the wider spread of the turbidity zone.

Furthermore, we have shown that bed formations have a minor effect on the location of the ETMs and a linear fit of an observed bathymetry can be used as a sound first approximation. Based on this approximation, we have made a sensitivity analysis of the suspended sediment trapping locations to the length of the embayment and depth at the entrance and the weir. It was shown that there is a competition between two trapping mechanisms: the mechanism *I* (defined in Section 3.4.2), which traps suspended sediment at the entrance of the estuary, and the trapping mechanism due to the import of sediment by tidal asymmetry and export due to river outflow, resulting in trapping near the end of the embayment. The dominant mechanism, which can change when either geometrical characteristics or external forcing is altered in the estuary, determines the position of the ETM in the estuary. Two ETMs are observed when both mechanisms are of equal strength. Moreover, we have showed the influence of tidal resonance on the position of the suspended sediment trapping in the Ems estuary. When the M_4 resonance length is close or coincides with the estuarine length, the water motion is enhanced towards the end of the estuary, the character of the wave is of a standing type and the tidal asymmetry trapping mechanism becomes active. It either becomes a dominant mechanism in the estuary (sediment is trapped at the end of the embayment) or is of the same order as the mechanism *I* (i.e., two ETMs are produced). Therefore, by changing the resonance characteristics of the basin (e.g., depth or the length of

the embayment), the trapping mechanism and, thus, the trapping location within the estuary changes as well. Note that a newly chosen length or depth of the embayment may result in either enhancement/weakening of the existing ETM or shift of the ETM to a new location: at the entrance or at the end of the estuary.

A similar sensitivity analysis has been conducted for the externally prescribed M_4 tidal constituent. It revealed that for small M_4 tidal amplitude, the trapping of sediment occurs near the entrance of the embayment because the tidal asymmetry is too weak to transport sediment into the estuary. Moreover, it was shown that the ebb/flood dominance at the entrance of the estuary, governed by the phase between the M_2 and M_4 tidal constituent, also affects the sediment trapping locations.

All results given in this chapter are based on the presented model. The model is constructed based on several assumptions. That there are no tidal flats, the model is diagnostic in salinity and the straining of concentration is included, however, straining of salinity is not. A number of processes, which might be important, are not included in the model: spatial settling lag, flocculation, wind waves and lateral advection.

Influence of viscosity parametrization and strain-induced periodic stratification on the ETM

In this chapter, we present an analysis of the influence of different vertical eddy viscosity formulations on the trapping locations in a tidal estuary. The vertical mixing is represented by four different horizontally and vertically varying eddy viscosity functions: horizontally and vertically constant; longitudinally varying, constant in the vertical; longitudinally varying, parabolic in vertical; and time- and longitudinally varying, parabolic in vertical.

Moreover, we investigate the influence of time-variation of the vertical mixing on the location of the turbidity zone. The structure of the water column changes from well-mixed during flood to stratified during ebb, resulting in the so-called strain-induced periodic stratifications (SIPS). The SIPS mechanism is responsible for an additional import of suspended sediment in the estuary and can be as efficient as the gravitational circulation: it will be shown that suspended sediment import can be enhanced due to the presence of asymmetric mixing.

Representative parameters for these different vertical viscosity profiles are obtained by calibrating the model predictions to the measured data. The Ems estuary is considered as a reference case. The along-channel suspended sediment distribution for these eddy viscosity formulations is studied. The physical reason for changes in suspended sediment deposition locations is investigated by analyzing contributions of the transport function.

4.1 Introduction

The hydrodynamics in a tidal basin depends on the formulation of vertical mixing in the water column. A similar observation holds for the sediment dynamics. This implies that the estuarine turbidity maxima location may change with changes in viscosity parametrization. Therefore, a thorough analysis is required to determine the influence of different vertical eddy viscosity models on the trapping locations in a tidal estuary.

Another significant aspect, related to the vertical mixing, is a concept that the vertical mixing (eddy viscosity) does not remain constant throughout the tidal cycle and is different during ebb and flood. During flood conditions, an enhanced mixing occurs, i.e., higher vertical eddy viscosity and diffusivity. Increased mixing results in additional erosion of suspended sediment higher into the water column than during ebb. The water column structure changes from well-mixed during flood to stratified during ebb. Hence, during flood more sediment is transported upstream into the estuary than exported out of the estuary during ebb. This mechanism is called the internal tidal asymmetry (tidal mixing asymmetry) and its significant effect on the transport of sediment has been acknowledged by a number of researchers. [Burchard and Baumert \(1998\)](#) demonstrated that the tidal mixing asymmetry results in an additional importing transport of suspended sediment upstream. Moreover, [Winterwerp \(2011\)](#) shows that for the Ems estuary the internal tidal asymmetry plays a major role in suspended sediment transport and its effect is larger than the influence of the gravitational circulation.

In this chapter, the vertical mixing is modeled by four different horizontally and vertically varying eddy viscosity functions. We consider the following eddy viscosity profiles: horizontally and vertically constant; longitudinally varying, constant in the vertical; longitudinally varying, parabolic in vertical; and time- and longitudinally varying, parabolic in vertical. The latter vertical eddy viscosity formulation takes into account the effect of asymmetry in tidal mixing during ebb and flood tidal cycle. Representative parameters for these different vertical viscosity profiles are obtained by calibrating the model predictions to the measured data using a least square method. The Ems estuary is considered as a reference case. The along-channel suspended sediment distribution in morphodynamic equilibrium for these eddy viscosity formulations is studied. The physical reason for changes in suspended sediment deposition locations is investigated by analyzing different contributions of the transport function.

In this chapter, we focus on along-channel processes and, extend the 2DV model discussed in previous chapters. The hydrodynamic conditions in a tidal

basin are modeled by the width-averaged shallow water equations, the sediment dynamics is governed by the width-averaged sediment mass balance equation. The condition of morphodynamic equilibrium is assumed to obtain the along-channel erosion coefficient. The (semi-) analytic solutions are derived using a perturbation approach. Using these analytic solutions, we compare the sediment distribution along the estuary for various formulations of the vertical eddy viscosity.

4.2 Modeling Approach

The model estuary is assumed to be partially or well-mixed with exponentially converging width. A Cartesian coordinate system is used, where x is the along-channel coordinate and z is the vertical coordinate with $z = 0$ being the undisturbed water level. The local width of the estuary at location x is given by $B(x) = B_0 e^{-x/L_b}$, where L_b is the exponential convergence length, B_0 is the width at the entrance of the basin. The seaward side of the basin is located at $x = 0$ and is forced by a prescribed external tide. At the landward side, $x = L$, the estuary is separated from the river by a tidal weir and we assume a constant river discharge. The bottom profile is prescribed by an arbitrary function $z = -H(x)$.

The water motion in the basin is governed by the width-averaged shallow water equations

$$u_x + w_z - \frac{u}{L_b} = 0, \quad (4.1a)$$

$$u_t + uu_x + wu_z + g\zeta_x - \frac{g\rho_x}{\rho_0}(z - \zeta) - (A_v(t, x, z)u_z)_z = 0, \quad (4.1b)$$

where u and w are the along-channel and vertical velocities, respectively, ζ is the sea surface elevation, and $\rho(x)$ is the along-channel density. In general, the density depends on both the salinity and suspended sediment concentration (SSC) in the water column. In this chapter, we assume that the influence of SSC is negligible, thus, the density is prescribed as

$$\rho(s, c, t) = \rho_0(1 + \beta \langle s(x) \rangle), \quad (4.2)$$

where density varies due to the influence of the prescribed time- and width-averaged salinity gradient $\langle s(x) \rangle$ only (see [Talke et al \(2009a\)](#); [Chernetsky and Schuttelaars \(2012\)](#)). Here $\rho_0 = 1020 \text{ kg m}^{-3}$ is the water density, $\beta \sim 7.6 \times 10^{-4} \text{ psu}^{-1}$ is the haline contraction coefficient, and the angular brackets $\langle . \rangle$ denote a tidal average.

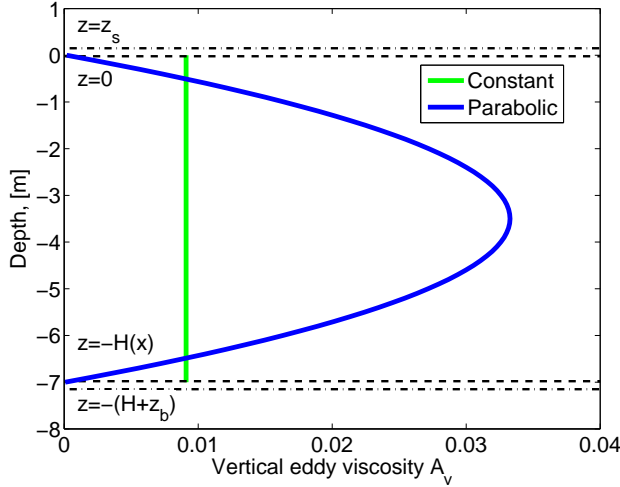


Figure 4.1: Sketch of the vertical eddy viscosity A_v parametrization.

The vertical mixing term in Eq. (4.1b) depends on the vertical eddy viscosity $A_v(t, x, z)$. Following Bowden (1965); Ianniello (1977) and Friedrichs and Aubrey (1996), the vertical eddy viscosity is parametrized by a longitudinally varying function, which is either constant in the vertical (Eq. (4.3a)) or has a parabolic profile (Eq. (4.3b)), i.e.,

$$A_v(x) = A_{v0} \left(\frac{H(x)}{H_0} \right)^n, \quad (4.3a)$$

$$A_v(x, z) = A_{v0}^{\text{par}} (z_s - z)(H(x) + z + z_b), \quad (4.3b)$$

where H_0 is the depth at the entrance and n is an exponential coefficient. These vertical eddy viscosity profiles are shown in Fig. 4.1. Moreover, A_{v0} and A_{v0}^{par} are the eddy viscosity coefficients, and z_s , z_b are geometrical characteristics (see Fig. 4.1), which are obtained from a model calibration (for details, see Section 2.4.2). In Chernetsky et al (2010); Chernetsky and Schuttelaars (2012), the constant vertical eddy viscosity formulation (4.3a) was used, with $n = 1$.

Apart from stationary formulations, we also consider a time-varying formulation of the vertical eddy viscosity. This is motivated by the observation that towards the end of flood, the water column is usually more mixed than during ebb (see Simpson et al (1990); Stacey et al (2001, 2008)). Hence, the water column structure changes from stratified during ebb to well-mixed during the end

of flood (estuarine stratification is explained in Section 1.1). This effect is called the strain-induced periodic stratification (SIPS) (see Nunes and Simpson (1985); Simpson et al (1990); Sharples and Simpson (1995)). This interaction between the tide and horizontal density gradient results in a temporary varying eddy viscosity and diffusivity, driving additional velocity components (Jay and Musiak, 1994) and sediment fluxes in tidal estuaries. In Burchard and Baumert (1998), it was argued that this mechanism played an important role in the formation of an ETM. Following Cheng et al (2010), we prescribe the vertical eddy viscosity function as

$$A_v(t, x, z) = A_{v0}^{\text{par}}(z_s - z)(H(x) + z + z_b) \left(1 + \eta \left\langle \frac{ds}{dx} \right\rangle e^{i(\sigma t - \mu)} \right), \quad (4.4)$$

where η is a coefficient, which is calibrated in such a way that the resulting magnitude of residual flow due to the SIPS mechanism is of the same order as the magnitude of the gravitation circulation for a periodically stratifying estuary (Burchard and Hetland, 2010; Cheng et al, 2011). If tidal straining is not that efficient, this coefficient is much smaller. Inspired by Simpson et al (1990); Stacey et al (2001), the phase μ is chosen such that maximum mixing occurs near the end of flood.

The no-stress and kinematic boundary condition are imposed at the free surface, $z = \zeta$,

$$A_v(t, x, z)u_z = 0 \quad \text{and} \quad w = \zeta_t + u\zeta_x. \quad (4.5)$$

At the bottom, $z = -H(x)$, the impermeability of the bed is imposed

$$w = -uH_x. \quad (4.6)$$

The second boundary condition at the bed depends on the vertical viscosity profile used. If the eddy viscosity is assumed to be constant in the vertical, i.e., boundary condition (4.3a), a partial slip condition (4.7a) is prescribed, otherwise, a no slip condition (4.7b) is used,

$$A_v(t, x, z)u_z = s(x)u \quad \text{at} \quad z = -H(x), \quad (4.7a)$$

$$u = 0 \quad \text{at} \quad z = -H(x). \quad (4.7b)$$

Here, $s(x)$ is the stress parameter, parametrized by

$$s(x) = s_0 \left(\frac{H(x)}{H_0} \right)^n, \quad (4.8)$$

where s_0 is the stress coefficient (see Chernetsky et al (2010)).

A tidal elevation consisting of the M_2 and M_4 tidal constituents is prescribed at the seaward side of the estuary, i.e.,

$$\zeta(t, 0) = A_{M_2} \cos \sigma t + A_{M_4} \cos(2\sigma t - \phi) \quad \text{at } x = 0, \quad (4.9)$$

where A_{M_2} and A_{M_4} are the M_2 and M_4 tidal amplitudes, respectively, $\sigma = 1.4 \cdot 10^{-4} \text{ s}^{-1}$ is the M_2 tidal frequency and ϕ is the relative phase.

The estuary is forced by a constant river discharge Q at the riverine side which is given by

$$B(L) \int_{-H}^{\zeta} u dz = Q \quad \text{at } x = L. \quad (4.10)$$

The sediment is assumed to consist of noncohesive fine particles, which are mainly transported as suspended load. The suspended sediment concentration is described by the width-averaged concentration equation which reads

$$c_t + uc_x + wc_z = w_s c_z + (K_h c_x)_x + (K_v(t, x, z) c_z)_z - \frac{1}{L_b} K_h c_x, \quad (4.11)$$

where w_s is the settling velocity, K_h is a constant horizontal diffusivity coefficient and $K_v(t, x, z)$ is the vertical diffusivity function. Following [Winterwerp et al \(2009\)](#), we take the vertical diffusivity a factor two smaller than the vertical eddy viscosity, i.e., the Prandtl-Schmidt number is set to two ($K_v(t, x, z) = A_v(t, x, z)/2$).

At the free surface, it is assumed that no particles can enter or leave the domain

$$w_s c + K_v(t, x, z) c_z - K_h c_x \zeta_x = 0 \quad \text{at } z = \zeta, \quad (4.12)$$

and at the bottom, $z = -H(x)$, the boundary condition is given by

$$-K_v(t, x, z) c_z n_z - K_h c_x n_x = \frac{w_s \rho_s S(x)}{g' d_s} |u(t, x, z)| a(x), \quad (4.13)$$

where n_x and n_z are the components of the unit normal vector at the bottom, ρ_s is the density of sediment, d_s is the grain size of the sediment and g' is the reduced gravity. Moreover, $a(x)$ is the erosion coefficient that models the along-channel distribution of easily erodible sediment at the bottom, which has to be determined yet.

The longitudinal distribution of the erosion coefficient is obtained using the condition of morphodynamic equilibrium. When the estuarine system is in the

morphodynamic equilibrium, there is no evolution of the bed over a tidal period. This condition reads (see [Friedrichs et al \(1998\)](#) and Chapters 3 and 4)

$$\left\langle \int_H^\zeta (uc - K_h c_x) dz \right\rangle = 0. \quad (4.14)$$

The suspended sediment concentration $c(t, x, z)$ in Eq. (4.14) depends on the erosion coefficient, and the morphodynamic equilibrium condition can be rewritten as a linear first order differential equation (ODE) for $a(x)$. This method is explained in detail in [Chernetsky et al \(2010\)](#).

4.3 Solution Method

A (semi-) analytic solution of the hydrodynamic and concentration equations, presented in Section 4.3, is derived using a perturbation technique. As an initial step, a scaling analysis of Eqs. (4.1), (4.11) and the appropriate boundary conditions is performed. The scaling analysis allows to estimate the relative contribution of various terms with respect to a small dimensionless parameter, denoted by ε . In this chapter, the small parameter is the ratio of the M_2 tidal amplitude A_{M_2} and the local water depth H_0 at the entrance, i.e., $\varepsilon = A_{M_2}/H_0 \ll 1$ (for the Ems estuary $\varepsilon = 0.1$). As a next step, the physical variables (the horizontal and vertical velocity, the sea surface elevation and the concentration) are expanded in power series of this small parameter

$$\psi = \psi^0 + \varepsilon^1 \psi^1 + \varepsilon^2 \psi^2 + \dots, \quad (4.15)$$

where $\psi = (u, w, \zeta, c)$.

By collecting terms of equal order of ε , we obtain a system of hydrodynamic and concentration equations at each order. In this analysis, we retain the components up to the first order of ε . The resulting leading and first order systems of equations and boundary conditions are identical to the equations discussed in [Chernetsky et al \(2010\)](#), with the vertical eddy viscosity $A_v(x, z)$ prescribed by either Eq. (4.3a), (4.3b). These equations and corresponding boundary conditions are not repeated here. If the eddy viscosity profile is chosen to be parabolic (formulation (4.3b)), unlike equations in Chapter 2, the obtained equations are ordinary differential equations of a hypergeometric type and an analytic solution is found in terms of hypergeometric functions.

For the time-varying eddy viscosity formulation (4.4), the perturbation analysis (see Section 2.3) shows that the time-varying term enters the equations as a first order term ($\mathcal{O}(\varepsilon^1)$). Therefore, it does not enter into the leading order system of hydro- and sediment dynamic equations and they are identical to Eqs. (2.16) and (2.20) and not repeated here. However, the first order system of hydrodynamic equations has an additional term due to the time-varying eddy viscosity formulation and reads

$$u_x^1 + w_z^1 - \frac{u^1}{L_b} = 0, \quad (4.16a)$$

$$u_t^1 + \underbrace{u_x^{02} u_x^{02} + w_z^{02} u_z^{02}}_{\text{AC + TS}} + g \zeta_x^1 - \underbrace{g \beta \langle s \rangle_x z}_{\text{GC}} = (A_{v0}^{\text{par}}(z_t - z)(H + z + z_b)u_z^1)_z \quad (4.16b)$$

$$+ \underbrace{(A_{v0}^{\text{par}}(z_s - z)(H + z + z_b)\eta \langle s \rangle_x e^{i(\sigma t - \mu)} u_z^{02})_z}_{\text{SIPS}}.$$

Here the underbraces $\underbrace{\quad}$ denote individual forcing terms. Detailed inspection of the SIPS term in Eq. (4.16b) shows that it consists of a residual and M_4 contribution (i.e., $\text{SIPS} = \text{SIPS}_{\text{res}} + \text{SIPS}_{M_4}$). Due to linearity, these contributions can be studied separately and the system of equations (4.16) breaks into two separate systems of equations for the residual velocity fields u^{10} , w^{10} and sea surface elevation ζ^{10} and the M_4 counterparts u^{14} , w^{14} and ζ^{14} (for more details, see Chapter 2.3.2, where a similar technique was used). Here, we will only focus on the residual contributions due to the time variations in eddy viscosity.

The boundary conditions for the residual flow are identical to (3.17) - (3.20) and the general solution can be written as

$$\chi^{10} = \chi_{\text{TS}}^{10} + \chi_{\text{GC}}^{10} + \chi_{\text{SIPS}_{\text{res}}}^{10} + \chi_{\text{SD}}^{10} + \chi_{\text{SC}}^{10} + \chi_{\text{RI}}^{10}, \quad (4.17)$$

where $\chi^{10} = (u^{10}, w^{10}, \zeta^{10})$. Comparing to the residual solutions in Chapters 2 and 3, here we have an additional residual contribution due to the SIPS $\chi_{\text{SIPS}_{\text{res}}}^{10}$.

The first order concentration equation in the case of time-varying vertical diffusion is given by

$$c_t^1 - w_s c_z^1 = (K_{v0}^{\text{par}}(z_t - z)(H + z + z_b)c_z^1)_z \quad (4.18)$$

$$+ \underbrace{((K_{v0}^{\text{par}}(z_s - z)(H + z + z_b)\eta \langle s \rangle_x e^{i(\sigma t - \mu)}(c^{00} + c^{04}))_z)}_{\text{SIPS}_c},$$

where c^{00} and c^{04} are the residual and M_4 leading order concentrations. Note that terms resulting the spatial settling lag effect are considered of the order $\mathcal{O}(\varepsilon^2)$ and does not enter the equation (see Section 2.3.2.2).

The boundary condition at the surface reads

$$w_s c_z^1 + K_{v0}^{\text{par}} z_s (H + z_b) c_z^1 = 0, \quad (4.19)$$

and at the bottom are

$$-K_{v0}^{\text{par}} c_z^1 = \frac{w_s \rho_s A_{v0}^{\text{par}}}{g' d_s} u_z^1 \frac{u_z^{02}}{|u_z^{02}|} a(x). \quad (4.20)$$

Note that the first order residual velocity field $u_{\text{SIPS}_{\text{res}}}^{10}$ enters the first order concentration via the bottom boundary condition (4.20). Hence the M_2 SIPS component of the concentration consists of 3 contributions, one from the perturbed bottom velocity, and two contributions related to c^{00} and c^{04} .

The solution method for these additional constituents is similar to the one described in Sections 3.3.1 and 3.3.2, and is not repeated here.

4.4 Results

As a case study, we consider the upper Ems estuary between the cities of Herbrum and Knock (see Fig. 1.3). The general description of the Ems system is given in Sections 1.3 and 2.4.1. The bathymetry of the system and most parameter values are obtained directly from observations, conducted in 2005. They are summarized in Tables 2.1 and 3.1. The eddy viscosity coefficients A_{v0} , A_{v0}^{par} , stress coefficient s_0 and geometrical parameters z_s , z_b are obtained from a model calibration to the measured data. We minimize the difference between the observed and modeled semi-diurnal tidal amplitude (ζ_{M_2}), and the phase difference between the semi-diurnal free surface elevation and velocity ($\phi_{\zeta_{M_2}} - \phi_{u_{M_2}}$) in a least square sense. Note that if the formulation of eddy viscosity (4.3a) is used, every magnitude of n and m corresponds to a different set of A_{v0} and s_0 coefficients. Hence, a new model calibration has to be made, if n and m are altered. More details about the model calibration procedure can be found in Section 2.4.2. In this chapter, we consider the following eddy viscosity profiles:

- (a) Horizontally and vertically constant,
- (b) Longitudinally varying, constant in vertical,

- (c) Longitudinally varying, parabolic in vertical,
- (d) Time- and longitudinally varying, parabolic in vertical.

For simplicity, we assume that $m = n$. Corresponding parameters, obtained from the model calibration, are summarized in Table 4.1.

Table 4.1: *Parameters, obtained from model calibrations, representing a constant, longitudinally varying and parabolic eddy viscosity profile*

Viscosity profile	m, n	A_{v0} , [m ² s ⁻¹]	s_0 , [m s ⁻¹]	z_b , [m]	z_s , [m]
Constant	0	0.009	0.031	-	-
Longitudinally varying	1	0.012	0.049	-	-
Parabolic	-	0.003	-	0.004	0.01

Using these parameter values, the resulting longitudinal distribution of suspended sediment in morphodynamic equilibrium is obtained based on the solutions in Section 4.2. The tidally averaged suspended sediment concentration (SSC) for a constant, longitudinally varying, parabolic and time-varying eddy viscosity profile are shown in Fig. 4.2. The maximum SSC at the surface is prescribed to 0.4 g/l. Coarse silt with a settling velocity of 0.002 m s⁻¹ is modeled.

From Fig. 4.2, it is immediately seen that the model for different eddy viscosity parametrization, calibrated to the same observations, results in different spatial distribution and trapping locations of suspended sediment. For the vertically and horizontally constant eddy viscosity profile, presented in Fig. 4.2(a), one turbidity zone is observed near the entrance of the estuary at km 13.5. For the longitudinally varying but constant in vertical eddy viscosity profile, shown in Fig. 4.2(b), two ETMs are produced. One ETM is located near the entrance at km 14.2 and the other one is located in the freshwater region near the tidal weir at km 47. This eddy viscosity parametrization was used in Chapters 2 and 3 and the obtained results are qualitatively consistent (see Figs. 2.7(d) and 3.2(d), however, note that different SSC at the surface is prescribed in these cases). Fig. 4.2(c) depicts the along-channel SSC distribution for the longitudinally varying, parabolic vertical eddy viscosity profile. For this parametrization, we observe one ETM, located in the freshwater zone at km 41.8. If the time-varying vertical eddy viscosity parametrization is used, see Fig. 4.2(d), a single ETM is observed at km 44.4.

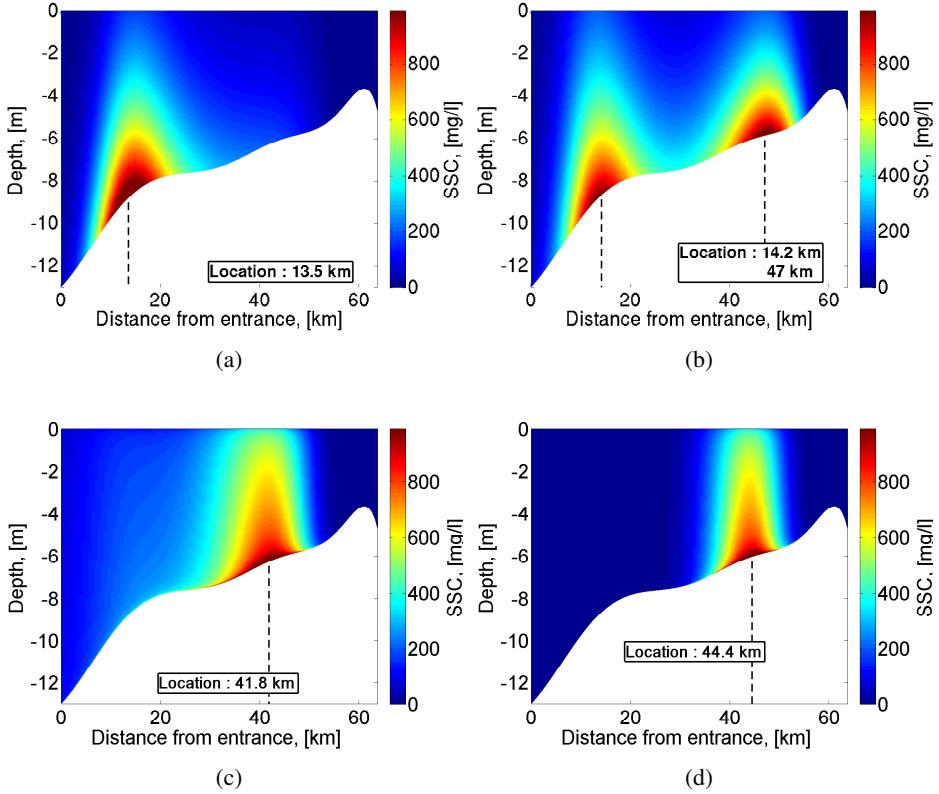


Figure 4.2: Along-channel distribution of suspended sediment concentration in morphodynamic equilibrium for a constant (a), longitudinally varying (b), parabolic eddy viscosity (c) and time-varying profile (d) are shown. The maximum SSC at the surface is prescribed to 0.4 g/l . Coarse silt with a settling velocity of 0.002 m s^{-1} is modeled

To investigate the changes in suspended sediment trapping, we analyze the behavior of residual sediment transports in morphodynamic equilibrium. This technique was applied in Chapters 2 and 3, and detailed explanation can be found in Section 2.5.2. In Fig. 4.3, the dimensionless residual transport T and its components are presented (for definition, see Section 3.3.3). The red line represents the residual sediment transport due to the residual velocity/residual concentration interaction, the green line shows the residual sediment transport due to the M_2 velocity/ M_2 concentration interaction, the black line shows the residual sediment transport due to the M_4 velocity/ M_4 concentration interaction. The diffusive resid-

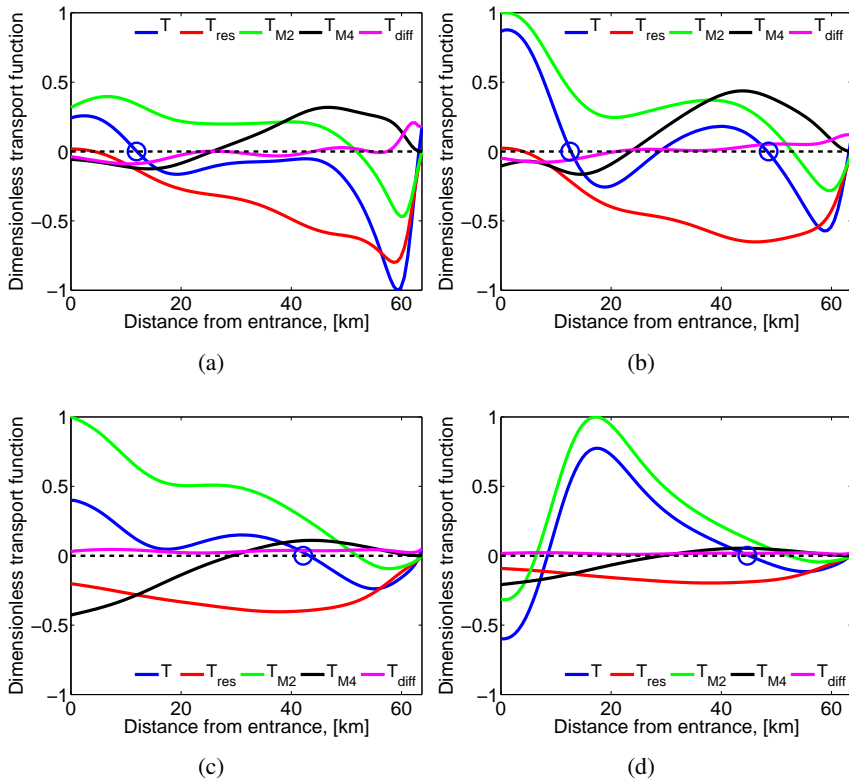


Figure 4.3: Dimensionless residual transport T , depicted by the solid blue line, and its components for a constant (a), longitudinally varying (b), parabolic eddy viscosity (c) and time-varying profile (d). The circle marker indicates a point of sediment convergence in the estuary

ual transport is shown by the magenta line. As it was explained in Section 2.5.2, a point $T = 0$ corresponds to a local maximum or minimum of the suspended sediment concentration. The points of local maxima are shown with blue marks.

Closer inspection of Fig. 4.3 shows that the behavior of all transport function is different for various vertical eddy viscosity formulations. However, the main qualitative change occurs due to a change in T_{M2} . To deeper understand which mechanism is the most sensitive to the vertical eddy viscosity formulation, this transport will be decomposed further into different components (for detailed explanation in Section 2.5.2.1, where transports are decomposed into separate components). The major components of the transport T_{M2} are presented in Fig. 4.4.

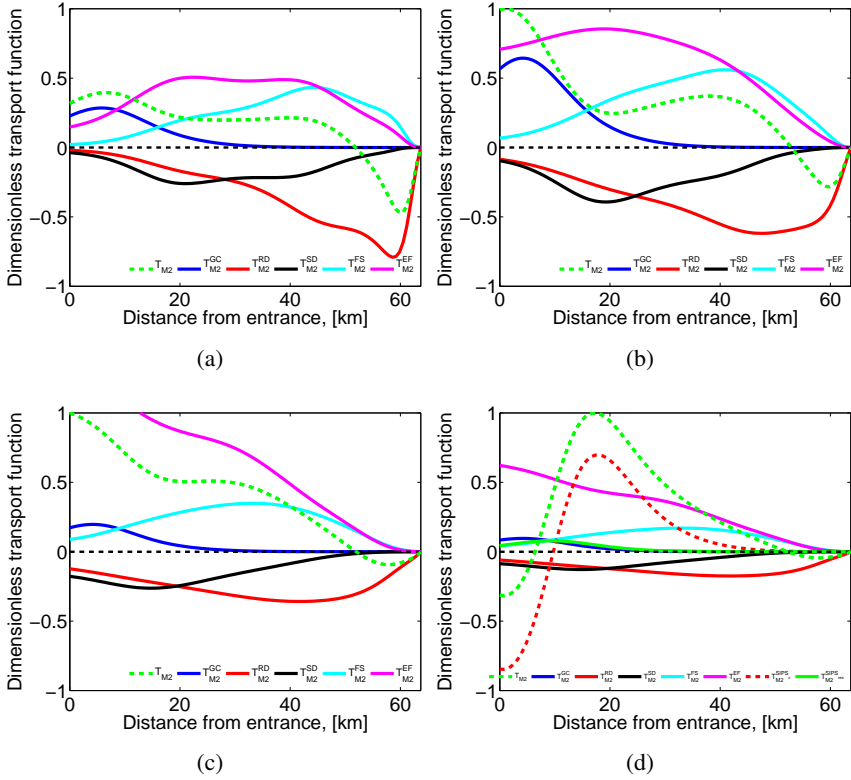


Figure 4.4: Dimensionless residual transport T_{M_2} , depicted by the green dashed line, and its components for a constant (a), longitudinally varying (b), parabolic eddy viscosity (c) and time-varying profile (d)

From Fig. 4.4, we can distinguish two regions where the T_{M_2} transport function changes significantly: one is located at the entrance of the estuary and the other one near the tidal weir. For the constant, longitudinally varying and parabolic viscosity profiles (Figs. 4.4(a)-4.4(c), respectively) different transport behavior near the entrance is attributed to changes of the transport $T_{M_2}^{GC}$, forced by the gravitational circulation, and $T_{M_2}^{EF}$, induced by the externally prescribed M_4 tidal constituent. Note that these velocity components enter the first order concentration indirectly via the boundary conditions for the M_2 concentration (for details, see Section 3.3.2).

Amplification and change of behavior of the M_2 residual transport due to the externally prescribed M_4 tide is a known mechanism, referred to as tidal asym-

metry. This mechanism, which is responsible for a shift of the estuarine turbidity maximum into the freshwater zone, was observed and investigated in Chapters 2 and 3. It is evident that for a constant eddy viscosity profile this transport mechanism is not strong enough, resulting in no trapping of sediment near the landward end. For the parabolic and time-varying eddy viscosity formulations this mechanism turns out to be very efficient.

The residual velocity field, induced by the gravitational circulation, for a constant, longitudinally varying and parabolic viscosity is presented in Figs. 4.6(d), 4.6(e) and 4.6(f), respectively. By comparing corresponding transport function T_{M2}^{GC} , induced by the gravitational circulation, with the gravitational circulation velocity for different eddy viscosity formulations, we see that a stronger residual velocity field results in a stronger transport. The total residual velocity for various eddy viscosity formulation and its significant constituents are presented in Fig. 4.6. For other residual velocity constituents, we observe similar qualitative behaviour: a stronger residual flow results in a stronger transport.

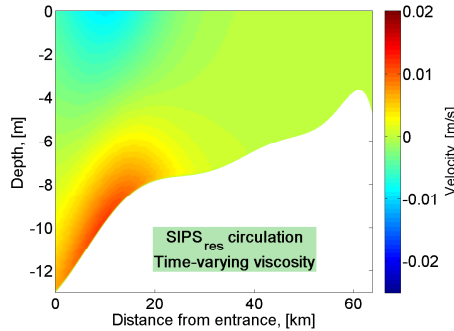


Figure 4.5: *The residual SIPS velocity constituent for the time-varying eddy viscosity profile*

For the time-varying eddy viscosity profile, presented in Fig. 4.4(d), two additional transport constituents are produced. These transports are $T_{M2}^{SIPS_c}$, induced by the forcing term $SIPS_c$ in Eq. 4.18, and a transport function $T_{M2}^{SIPS_{res}}$, which is due to the forcing terms $u_{SIPS_{res}}^{10}$ (see Eq. (4.17)). The latter first order velocity field enters the first order concentration indirectly via the bottom boundary condition (4.20). It appears that the behavior of the $T_{M2}^{SIPS_{res}}$ transport is similar to the T_{M2}^{GC} transport. The residual velocity field, which induce the $T_{M2}^{SIPS_{res}}$ transport is shown in Fig. 4.5. It has the same pattern as the gravitational circulation shown in Fig. 4.6(f), and is of the order of magnitude of the gravitational circulation where

$\langle s_x \rangle$ is minimal (see Eq. (4.4), where the choice of the SIPS coefficient is discussed). However, the dominant transport for the time-varying viscosity near the entrance is the new transport $T_{M_2}^{\text{SIPS}_c}$, which is not present in other viscosity formulations. It is responsible for a strong import of sediment into the estuary. This importing residual transport is due to the enhanced mixing of sediment during flood conditions. This results in more sediment higher in the water column than during ebb. Hence, during flood, more sediment is transported upstream than during ebb exported downstream, resulting in an efficient tidally-averaged transport of suspended sediment into the estuary. This residual transport, combined with a strong import flux due to the externally prescribed M_4 tide determines the behaviour of the T_{M_2} transport.

Near the weir, the change of the transport function T_{M_2} is driven by the change of the M_2 residual transport induced by the river discharge. The correspondent velocity fields are presented in Figs. 4.6(g), 4.6(h) and 4.6(i). It is seen that for a parabolic eddy viscosity, the velocity magnitude of the river discharge is lower than for a constant or longitudinally varying viscosity formulation. Thus near the weir, the net sediment transport by this contribution is also smaller.

4.5 Conclusions

In this chapter, we investigated how different vertical eddy viscosity parametrization affects the ETM locations in tidal estuaries. As a reference estuary we considered the Ems estuary. The following vertical eddy viscosity profiles were studied:

- (a) Horizontally and vertically constant,
- (b) Longitudinally varying, constant in vertical,
- (c) Longitudinally varying, parabolic in vertical,
- (d) Time- and longitudinally varying, parabolic in vertical.

We have shown that different viscosity formulations result in slightly different location(s) of suspended sediment deposition in the estuary and even different number of ETMs. However, observed trapping patterns are similar. For the vertically and horizontally constant eddy viscosity, there is one turbidity zone near the entrance of the estuary at km 13.5. For the longitudinally varying but constant in vertical eddy viscosity, we observe two ETMs: one is located near the entrance at km 14.2 and the other one is located in the freshwater region near the tidal weir

at km 47. The longitudinally varying, parabolic vertical eddy viscosity results in one ETM, located in the freshwater zone at km 41.8. For the time-varying vertical eddy viscosity parametrization, a single ETM is observed at km 44.4.

To investigate the changes between the viscosity formulation, we have analyzed the difference between the transport functions, their constituents and forcing velocity fields. It was shown that the M_2 residual transport has the most significant contribution to the overall changes between the viscosity profiles. There are two characteristic regions where this transport function changes significantly: one near the entrance of the estuary and the other one upstream near the tidal weir. We have shown that the change of the M_2 transport behaviour near the entrance is mainly results from changes of transport due to the gravitational circulation and externally prescribed M_4 tidal constituent. Close to the weir, the change of the M_2 transport is mainly attributed to changes due to the river discharge.

For the time-varying vertical eddy viscosity formulation, two additional M_2 transport constituents are produced: $T_{M_2}^{\text{SIPS}_c}$ and $T_{M_2}^{\text{SIPS}_{\text{res}}}$. The transport constituent $T_{M_2}^{\text{SIPS}_c}$, which is not present for other eddy viscosity formulations, becomes dominant near the entrance of the estuary and is responsible for a strong import of sediment upstream. This landward (importing) transport is due to the enhanced mixing of suspended sediment during flood. This leads to higher concentration of suspended sediment in the water column and more sediment is transported upstream during flood than transported downstream during ebb. This is a so-called strain-induced periodic stratification (SIPS) mechanism. The SIPS transport is an important mechanism which significantly affects the suspended sediment distribution and the location of ETM near the entrance of the estuary.

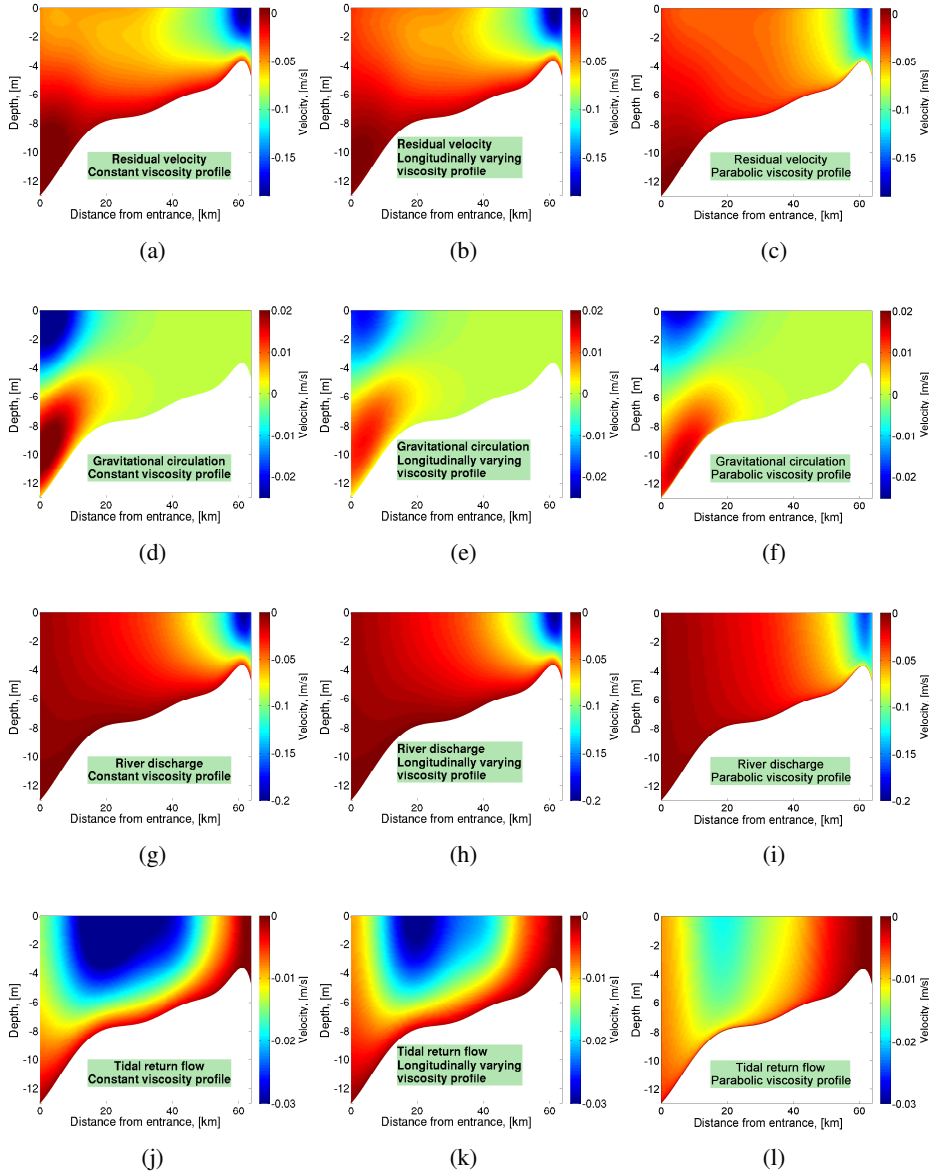


Figure 4.6: The residual velocity and its major constituents for a constant (Figs. a, d, g, j), longitudinally varying (Figs. b, e, h, k) and parabolic eddy viscosity parametrization (Figs. c, f, i, l). The residual velocity is shown in the upper panels, the gravitational circulation constituent and river discharge are depicted in the upper- and lower-middle panels, respectively, and the tidal (Stokes) return flow is presented in the lower panels

Conclusions

5.1 Main conclusions

The main aim of this thesis was to investigate longitudinal estuarine processes and determine the main mechanisms that result in suspended sediment trapping in tidal estuaries using an idealized analytical model. Major conclusions of the conducted research and answers to the research questions, stated in Section 1.5, are summarized below in a question/answer form.

- $\mathcal{Q}1$: Is it possible to reproduce the hydro- and sediment dynamics, observed in partially mixed tidal estuaries, using an idealized analytical width-averaged model?

$\mathcal{A}1$. This question was addressed in all chapters of this thesis. As a reference estuary, the Ems/Dollart system has been considered. In Chapters 2-4, most parameter values and bathymetry for the model were directly taken from observations of 1980 and/or 2005. However, unknown parameters (e.g., the vertical eddy viscosity coefficient, stress parameter, z_b , etc.) were obtained indirectly by calibrating the model to the measured data: the M_2 horizontal and vertical tide (see details in Section 2.4.2). Other observations, such as the residual and M_4 tidal amplitude and the velocity at the surface, were used to validate the model. The comparison of the model results and observations showed a qualitatively good agreement between model results and observations, see Appendix A7. Therefore, we may conclude that an idealized analytical model is able to qualitatively reproduce the dynamics of a real tidal estuary.

- $\mathcal{Q}2$: What are the dominant physical mechanisms resulting in suspended

sediment trapping? And what physical mechanisms can result in multiple estuarine turbidity maxima?

A2. The occurrence of ETM and its location are determined by a complex interaction between various components of exporting and importing suspended sediment contributions. Multiple ETMs are observed when certain components (different for various vertical eddy viscosity formulations) of downstream and upstream directed (exporting and importing) residual transport balance each other at different locations in the estuary (see Sections 2.4.4, 3.4.1 and 4.4). It was observed that an ETM at the entrance of the estuary results from an interaction of various contributions of the residual and M_2 transport, and an ETM near the end of the estuary results from the import of sediment by tidal asymmetry and export due to river outflow. Therefore, based on the results of the presented model, there is no single dominant physical mechanism that solely controls the formation of a turbidity region in an estuary.

- *Q3:* What is the influence of the high turbidity in the water column on the location of the estuarine turbidity maximum?

A3. In Chapter 3, we have shown that high sediment concentration results in the formation of turbidity currents, which produce an additional flux in the morphodynamic equilibrium. This flux does not significantly change the existing balance between other fluxes, but modifies it: high suspended sediment concentration results in a wider spread of the turbidity zone, a slightly enhanced asymmetry and an insignificant shift of the ETM.

- *Q4:* What is the effect of geometrical characteristics of the estuary and external forcing on the position of the ETM?

A4. In this research, we have observed the formation of the either one or two ETMs in the estuary. The first turbidity region is located at the entrance of the estuary and the second one near the weir. The sensitivity analysis, conducted in Sections 3.4.2 and 3.4.3, reveals that there is a competition between trapping mechanisms that results in these ETMs. The dominant mechanism determines the position of the ETM. Two ETMs are observed when both mechanisms are of equal strength (also see *Q3/A3*). The dominance of both mechanisms can change when either geometrical characteristics of the estuary or external forcing is altered. This means that any change of the geometrical characteristics or/and external forcing will influence either the position or the occurrence of an ETM in the estuary.

- *Q5*: How do different vertical eddy viscosity parametrizations affect the turbidity zone? What is the influence of the SIPS mechanism on the turbidity zone.

A5. In Chapter 4, it was shown that various vertical eddy viscosity formulations result in slightly different deposition location(s) of suspended sediment. Based on the viscosity formulation, the number of EMT(s) can range between 1 and 2. The main changes in deposition locations occur due to changes of the M_2 transport.

We have shown that the strain-induced periodic stratification (SIPS) is a very important mechanism which is responsible for the import of suspended sediment into the estuary upstream. The effect of the SIPS mechanism on the location(s) of the turbidity zone is of the same order or can exceed the influence of the gravitational circulation.

5.2 Recommendations

The presented modeling approach and the results described in this research give a clear insight into the longitudinal estuarine processes and provide an essential framework for a better understanding of trapping mechanisms of suspended sediment in tidal estuaries. Nonetheless, there are many directions for further extension and development of the presented model. Possible extension directions and research questions are listed below.

- **An idealized analytical 3D model.** This research is focused on the investigation of longitudinal exporting/importing mechanisms that results in the along-channel suspended sediment trapping. It would be of great interest to investigate the influence of cross-sectional trapping mechanisms on the turbidity region and trapping locations, obtained with the along-channel model. This can be done by coupling the presented model with an idealized transversal model into a 3D idealized analytical model. For example, the transversal model presented in [Huijts et al \(2006, 2011\)](#).
- **Go from the morphodynamic equilibrium to time-development.** A condition of morphodynamic equilibrium, used to obtain the along-channel distribution of the erosion coefficient, allows to observe an estuarine system only in an initial (prescribed) state and a final state, when the system has reached the morphodynamic equilibrium. However, the time development of the system towards the equilibrium state remains unknown. The understanding of the system time-development towards its equilibrium state can

provide additional insight into physical processes that results in suspended sediment trapping.

- **Comparison of idealized and numerical model results.** In derivation of the presented model, a number of assumptions have been used. A comparison of model results with historical observations in the Ems estuary has proved the applicability of the model (the research question $\mathcal{Q}1$). However, a comparison of the analytical model with a numerical model is necessary to accurately estimate the influence of these assumption. Moreover, it will allow to determine additional mechanisms which might be important for further extension of the model.
- **Analyze the influence of other estuarine processes.** The presented model does not take into account some physical processes which might have some influence on the trapping of suspended sediment. These processes are spatial settling lag, wind waves, flocculation, tidal flats, fluid mud, etc. The extension of the model and the sensitivity analysis to these processes will enable to gain a deeper understanding of complex estuarine processes.

A1 Derivation of Width-Averaged Shallow Water Equations

A1.1 Continuity equation

Continuity equation is derived from the fundamental requirement of mass conservation of a system. The most general form of continuity equation can be written as follows

$$\frac{D\rho}{Dt} + \rho \vec{\nabla} \cdot \vec{U} = 0.$$

Here, $\frac{D\rho}{Dt}$ is the total derivative of density, \vec{U} is a three-dimensional velocity vector and $\vec{\nabla}$ is the nabla operator.

Using the Boussinesq approximation, which assumes that the density in the oceans is nearly constant, the continuity equation can be simplified to

$$\vec{\nabla} \cdot \vec{U} = 0.$$

With respect to a Cartesian coordinate system \vec{U} has components u, v, w in the x, y, z -direction and $\vec{\nabla}$ has the components $\frac{\partial}{\partial x}, \frac{\partial}{\partial y}, \frac{\partial}{\partial z}$. Hence,

$$u_x + v_y + w_z = 0.$$

The width-averaged form of the latter equation is derived by integrating from $-B/2$ to $B/2$, where $B(x)$ is the width of the estuary (see sketch of the estuary in

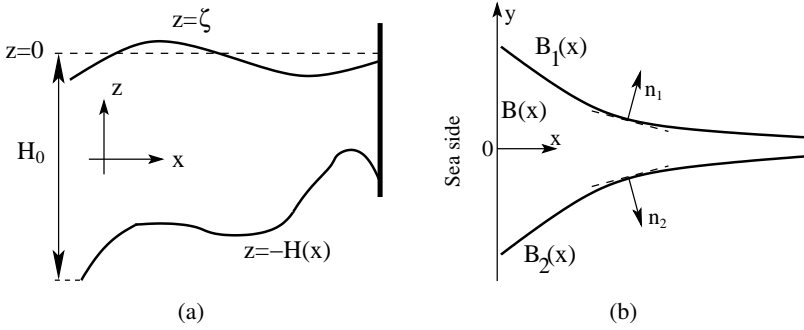


Figure A.1: Sketch of the model geometry. The left panel depicts the side view of the estuary and the right one presents the top view. A Cartesian coordinate system is used, the x axis is along-channel coordinate directed landwards, y axis is transverse coordinate points upwards and z is the vertical coordinate.

Fig. A.1(b)

$$\int_{-B(x)/2}^{B(x)/2} \frac{\partial u}{\partial x} dy + \int_{-B(x)/2}^{B(x)/2} \frac{\partial v}{\partial y} dy + \int_{-B(x)/2}^{B(x)/2} \frac{\partial w}{\partial z} dy = 0.$$

The Leibnitz integral rule yields

$$\begin{aligned} \frac{\partial}{\partial x} \int_{-B(x)/2}^{B(x)/2} u dy - \frac{1}{2} u|_{y=-B/2} \frac{dB(x)}{dx} - \frac{1}{2} u|_{y=B/2} \frac{dB(x)}{dx} + \\ v|_{y=B/2} - v|_{y=-B/2} + \frac{\partial}{\partial z} \int_{-B(x)/2}^{B(x)/2} w dy = 0. \end{aligned} \quad (\text{A.1})$$

There is no flow through the side boundaries $\vec{n} \cdot \vec{U} = 0$. This condition can be written for the both banks as follows:

$$\begin{aligned} n_1 &= \left(-\frac{1}{2} \frac{dB(x)}{dx}, 1 \right) & -\frac{1}{2} u|_{y=B/2} \frac{dB(x)}{dx} + v|_{y=B/2} &= 0 \\ n_2 &= \left(\frac{1}{2} \frac{dB(x)}{dx}, 1 \right) & \frac{1}{2} u|_{y=-B/2} \frac{dB(x)}{dx} + v|_{y=-B/2} &= 0 \end{aligned}$$

Eq. (A.1), taking into account the expressions above, reads

$$\frac{\partial}{\partial x} \int_{-B(x)/2}^{B(x)/2} u dy + \frac{\partial}{\partial z} \int_{-B(x)/2}^{B(x)/2} w dy = 0.$$

The width-averaged velocities (\sim) are defined as follows

$$\tilde{u} = \frac{1}{B(x)} \int_{-B(x)/2}^{B(x)/2} u dy, \tilde{w} = \frac{1}{B(x)} \int_{-B(x)/2}^{B(x)/2} w dy.$$

The width of the estuary is prescribed as

$$B(x) = B_0 e^{-x/L_b}.$$

Eventually, the width-averaged continuity equation reads

$$\frac{\partial}{\partial x} \tilde{u} + \frac{\partial}{\partial z} \tilde{w} - \frac{\tilde{u}}{L_b} = 0. \quad (\text{A.2})$$

A1.2 Momentum equation

This equation is obtained from momentum balance. The equation has the following form

$$\rho \left(\frac{D\vec{U}}{Dt} + f \vec{e}_z \times \vec{U} \right) = \vec{\nabla} \cdot \boldsymbol{\sigma} + \rho \vec{g}. \quad (\text{A.3})$$

Here, $\frac{D\vec{U}}{Dt}$ is the total time derivative, f is the Coriolis parameter (Coriolis effects are left out due to the width of the estuary is small compared to the Rossby deformation radius), \vec{e}_z is a unity vector in the vertical direction, $\boldsymbol{\sigma}$ is the stress tensor, given by

$$\boldsymbol{\sigma} = -P\boldsymbol{\delta} + \boldsymbol{\tau},$$

with P the pressure, $\boldsymbol{\delta}$ unity tensor and $\boldsymbol{\tau}$ the shear stress tensor. The elements of the latter tensor are called the Reynolds stresses. To close the system the turbulent Reynolds stresses must be expressed in terms of the state variables. A simple closure scheme, which is commonly used, is to relate the turbulent shear stresses to velocity gradients (Pedlosky, 1987).

The differential form of hydrostatic balance of the fluid reads

$$\frac{\partial P}{\partial z} = -\rho g.$$

At the water surface, $z = \zeta$ (see Fig. A.1(a)), the pressure equals to the atmospheric pressure P_a . Hence, the solution of hydrostatic balance can be written as

$$P = P_a + \rho g(\zeta - z).$$

Using the Boussinesq approximation, the density ρ is replaced by its constant reference value ρ_* and the pressure gradient reads

$$P_x = P_{ax} + \rho_* g \zeta_x + g P_x(\zeta - z) = P_{ax} + \rho_* g \zeta_x + g \int_z^\zeta \rho_x dz. \quad (\text{A.4})$$

It consist of three parts: a contribution due to spatial variations of the atmospheric pressure; a barotropic part, independent of depth, related to variations of the free surface; and baroclinic part, depth-dependent, due to density gradients.

By expanding the total derivative in Eq. (A.3) and writing the components in a Cartesian coordinate system using Eq. (A.4) and corresponding elements of the Reynolds stress tensor, we obtain

$$u_t + uu_x + vu_y + wu_z + g\zeta_x + \frac{g}{\rho_*} \int_z^\zeta \rho_x dz - (A_v u_z)_z = 0,$$

and the width-averaged form of the momentum equation is given by

$$\tilde{u}_t + \tilde{u}\tilde{u}_x + \tilde{w}\tilde{u}_z + g\zeta_x + \frac{g}{\rho_*} \int_z^\zeta \rho_x dz - (A_v \tilde{u}_z)_z = 0.$$

A2 The Width-Averaged Sediment Concentration Equation

Conservation of mass for the sediment is given by

$$\frac{\partial c}{\partial t} + \vec{\nabla} \cdot \vec{F} = 0. \quad (\text{A.5})$$

Here, c is the 3D concentration, \vec{F} is the total sediment flux which consists of an advective \vec{F}_a , settling \vec{F}_s and diffusive \vec{F}_d flux. They are given by

$$\begin{aligned}\vec{F}_a &= c\vec{u} + cw\vec{e}_z, \\ \vec{F}_s &= -cw_s\vec{e}_z, \\ \vec{F}_d &= -K_h\vec{\nabla}c - K_v\frac{\partial c}{\partial z}\vec{e}_z.\end{aligned}$$

where \vec{u} is the horizontal velocity field, w the vertical velocity component, \vec{e}_z the unit vector in the z direction. Finally, K_h and K_v the horizontal and vertical eddy diffusivity coefficient, respectively.

Eq. (A.5) yields the sediment concentration equation

$$c_t + (uc)_x + (vc)_y + (c(w - w_s))_z = (K_h c_x)_x + (K_h c_y)_y + (K_v c_z)_z. \quad (\text{A.6})$$

The width-integrated sediment concentration equation is obtained by integrating Eq. (A.6) over the width and using the Leibniz integral rule. It yields

$$\begin{aligned}& \frac{\partial}{\partial t} \int_{B_2}^{B_1} c dy + \frac{\partial}{\partial x} \int_{B_2}^{B_1} u c dy + \frac{\partial}{\partial z} \int_{B_2}^{B_1} c(w - w_s) dy - \frac{\partial}{\partial x} \int_{B_2}^{B_1} K_h c_x dy \\ & - \frac{\partial}{\partial z} \int_{B_2}^{B_1} K_v c_z dy - \underbrace{[ucB_{1x} - vc - K_h c_x B_{1x} + K_h c_y]_{y=B_1}}_1 \\ & + \underbrace{[ucB_{2x} - vc - K_h c_x B_{2x} + K_h c_y]_{y=B_2}}_2 = 0.\end{aligned} \quad (\text{A.7})$$

Next, we use the boundary conditions at the transversal sides of the estuary. The estuary sketch is shown in Fig. A.1. There is no flux through the side boundaries, i.e.

$$\vec{n} \cdot (c\vec{u} - K_h\vec{\nabla}c) = 0 \quad \text{at} \quad y = B_1(x) \text{ and } B_2(x), \quad (\text{A.8})$$

where $\vec{n}_1 = (-B_{1x}, 1)$ is a normal outward pointing vector at $y = B_1$, and $\vec{n}_2 = -(-B_{2x}, 1)$ the normal vector at $y = B_2$.

Using the boundary condition (A.8), terms 1 and 2 in Eq. (A.7) drop out and

the equation reduces to

$$\begin{aligned} \frac{\partial}{\partial t} \int_{B_2}^{B_1} c dy + \frac{\partial}{\partial x} \int_{B_2}^{B_1} u c dy + \frac{\partial}{\partial z} \int_{B_2}^{B_1} c(w - w_s) dy - \\ \frac{\partial}{\partial x} \int_{B_2}^{B_1} K_h c_x dy - \frac{\partial}{\partial z} \int_{B_2}^{B_1} K_v c_z dy = 0. \end{aligned} \quad (\text{A.9})$$

Next, we assume that the concentration $c = \tilde{c} + c'$, with \tilde{c} the width-averaged concentration, defined as

$$\tilde{c} = \frac{1}{B(x)} \int_{B_2}^{B_1} c dy,$$

and c' are fluctuations in the y -direction, defined as $c' = c - \tilde{c}$. Here $B(x) = B_1(x) - B_2(x)$ is the width of the estuary. Similarly write $u = \tilde{u} + u'$. Using the Leibniz integral rule, the width-integrated sediment concentration equation (A.9) reads

$$(\tilde{c})_t + (B\tilde{u}\tilde{c})_x + (B\tilde{c}(\tilde{w} - w_s))_z - (K_h B\tilde{c}_x)_x - (K_v B\tilde{c}_z)_z = 0, \quad (\text{A.10})$$

where we assumed that the sediment concentration at the transversal boundaries equals the width-averaged concentration, i.e. $c|_{y=B_1} = c|_{y=B_2} = \tilde{c}$. Moreover, we

assume that correlations $\frac{\partial}{\partial x} \int_{B_2}^{B_1} u' c' dy$ can be modeled as a dispersive contribution.

Finally, using continuity equation (A.2) and assuming that the width of the estuary is exponentially converging (i.e., $B(x) = B_0 e^{-x/L_b}$), the width-averaged concentration equation (A.10) becomes

$$\tilde{c}_t + \tilde{u}\tilde{c}_x + \tilde{c}_z(\tilde{w} - w_s) = (K_h \tilde{c}_x)_x + (K_v \tilde{c}_z)_z - \frac{1}{L_b} K_h \tilde{c}_x. \quad (\text{A.11})$$

A3 Morphodynamic Equilibrium Condition

The time evolution equation for the bed (Van Rijn, 1993) reads

$$\rho_s(1-p) \frac{\partial z_b}{\partial t} = D - E_s, \quad (\text{A.12})$$

with ρ_s the density and p the porosity of the sediment. The depositional sediment flux D normal to the bottom is given by

$$D \equiv w_s c n_z \quad \text{at} \quad z = -H,$$

or the width-averaged expression

$$B\tilde{D} = Bw_s \tilde{c} n_z. \quad (\text{A.13})$$

The erosional sediment flux reads $E_s = -K_h \vec{\nabla} c - K_v \frac{\partial c}{\partial z} \vec{n}_z$. By integrating this equation over the width, neglecting the transversal bottom variations and assuming that the concentration at the transversal boundaries equals the width-averaged concentration, i.e. $c|_{y=B_1} = c|_{y=B_2} = \tilde{c}$, we obtain the width-averaged erosional sediment flux

$$\tilde{E}_s = -K_h \tilde{c}_x n_x - K_v \tilde{c}_z n_z \quad \text{at} \quad z = -H. \quad (\text{A.14})$$

Note that here, $n_x = H_x/|\vec{n}|$ and $n_z = 1/|\vec{n}|$ denote the components (not derivatives) of the unit normal vector \vec{n} at the bottom.

A relation between deposition and erosion is derived from the sediment concentration equation (A.10) by integrating it over the depth and using the Leibniz integral rule

$$\begin{aligned} & \frac{\partial}{\partial t} \int_{-H}^{\zeta} B \tilde{c} dz + \frac{\partial}{\partial x} \int_{-H}^{\zeta} B \tilde{u} \tilde{c} dz - \frac{\partial}{\partial x} \int_{-H}^{\zeta} K_h B \tilde{c}_x dz = \\ & -B \underbrace{(w_s \tilde{c} + K_h \tilde{c}_x H_x + K_v \tilde{c}_z)_{z=-H}}_I + B \tilde{c} \underbrace{(\zeta_t + \tilde{u} - \tilde{w})_{z=\zeta}}_II + \\ & B \tilde{c} \underbrace{(\tilde{u} H_x + \tilde{w})_{z=-H}}_III + B \underbrace{(w_s \tilde{c} - K_h \tilde{c}_x \zeta_x + K_v \tilde{c}_z)_{z=\zeta}}_IV \end{aligned} \quad (\text{A.15})$$

Terms *II*, *III*, *IV* are eliminated due to boundary conditions, i.e.,

$$\tilde{w} = \zeta_t + \tilde{u} \zeta_x \quad \text{at} \quad z = \zeta, \quad (\text{A.16a})$$

$$\tilde{w} = -\tilde{u} H_x \quad \text{at} \quad z = -H, \quad (\text{A.16b})$$

$$-w_s \tilde{c} - K_v \tilde{c}_z + K_h \tilde{c}_x \zeta_x = 0 \quad \text{at} \quad z = \zeta, \quad (\text{A.16c})$$

and term *I*, according to Eqs. (A.13) and (A.14), can be expressed as $-B(\tilde{D} - \tilde{E}_s)$. Therefore, Eq. (A.15) reduces to

$$\frac{\partial}{\partial t} \int_{-H}^{\zeta} B \tilde{c} dz + \frac{\partial}{\partial x} \int_{-H}^{\zeta} B \tilde{u} \tilde{c} dz - \frac{\partial}{\partial x} \int_{-H}^{\zeta} B K_h \tilde{c}_x dz = B(-\tilde{D} + \tilde{E}_s). \quad (\text{A.17})$$

Next, we average the result over a tidal period and require that the bed does not change over a tidal period. This means that there is a tidally averaged balance between erosion and deposition, i.e. $\langle \tilde{D} \rangle - \langle \tilde{E}_s \rangle = 0$. Using this in Eq. (A.17) gives that

$$\left\langle \frac{\partial}{\partial x} \int_{-H}^{\zeta} B \tilde{u} \tilde{c} dz \right\rangle - \left\langle \frac{\partial}{\partial x} \int_{-H}^{\zeta} B K_h \tilde{c}_x dz \right\rangle = 0. \quad (\text{A.18})$$

The condition of morphodynamic equilibrium can be obtained by integrating Eq. (A.18) with respect to x :

$$\left\langle \int_{-H}^{\zeta} (\tilde{u} \tilde{c} - K_h \tilde{c}_x) dz \right\rangle = 0. \quad (\text{A.19})$$

Note that the width B dropped out of the equation. The integration constant is set to zero as we require no mean sediment transport at the weir.

A4 Perturbation Analysis and Solutions

As a first step in perturbation analysis, the variables are scaled by their typical order with dimensionless variables denoted by a tilde (\sim), see Table A.1.

Apart from the velocity scale $U = \sigma A_{M_2} \ell / H_0$ (variables are explained in Table A.1), a second along-channel velocity scale in the model is the typical velocity scale for the density driven residual circulation $U_d = g H_0 \beta S_x / \sigma$. Substituting the scaled variables into the width-averaged shallow water equations yields the dimensionless shallow water equations

$$\tilde{u}_{\tilde{x}} + \tilde{w}_{\tilde{z}} - \frac{\ell}{L_b} \tilde{u} = 0, \quad (\text{A.20a})$$

$$\begin{aligned} \tilde{u}_{\tilde{t}} + \frac{U}{\sigma \ell} (\tilde{u} \tilde{u}_{\tilde{x}} + \tilde{w} \tilde{u}_{\tilde{z}}) + \lambda^{-2} \tilde{\zeta}_{\tilde{x}} - \\ \frac{U_d}{U} \langle \tilde{s} \rangle_x \left(\tilde{z} - \frac{A_{M_2}}{H_0} \tilde{\zeta} \right) = \left(\frac{A_v}{\sigma H_0^2} \tilde{u}_{\tilde{z}} \right)_{\tilde{z}}, \end{aligned} \quad (\text{A.20b})$$

where $\lambda = \ell / L_w$ is the ratio of the convergence length or embayment length (depending on which one is smaller) and the frictionless tidal wavelength L_w . The along-channel density expression has been used to obtain Eq. (A.20b).

Table A.1: Typical scales of various physical variables

<i>Scaling</i>			
Physical Quantity	Typical Scale	Symbol	Variable
Time	M_2 tidal frequency	σ	$t = \sigma^{-1}\tilde{t}$
Sea surface elevation	M_2 tidal amplitude	A_{M_2}	$\zeta = A_{M_2}\tilde{\zeta}$
Vertical coordinate	Water depth at the entrance	H_0	$z = H_0\tilde{z}$
Local water depth			$H = H_0\tilde{H}$
Horizontal coordinate	Minimum of the estuary length or convergence length	ℓ	$x = \ell\tilde{x}$
Horizontal velocity	*	$U = \frac{\sigma A_{M_2} \ell}{H_0}$	$u = U\tilde{u}$
Vertical velocity	**	$W = \frac{H_0}{\ell}U$	$w = W\tilde{w}$
Sediment concentration	Typical magnitude of the quantity	$C = \frac{\rho_s A_v U a_*}{H_0 g' d_s}$	$c = C\tilde{c}$
Salinity gradient	under consideration	S_x	$\langle \frac{s}{S_x} \rangle_x = \langle \tilde{s} \rangle_x$
Erosion coefficient		a_*	$a = a_*\tilde{a}$

*Follows from the integration of the continuity equation over depth and requiring an approximate balance between the resulting contributions

**Obtained from the continuity equation by requiring an approximate balance between the first and second term

The dimensionless boundary condition at the entrance is given by

$$\tilde{\zeta} = \cos\tilde{t} + \frac{A_{M_4}}{A_{M_2}} \cos(2\tilde{t} - \phi) \quad \text{at} \quad \tilde{x} = 0,$$

where A_{M_4} is the amplitude of the M_4 tidal constituent. At the riverine side we impose that

$$\int_{-\tilde{H}}^{\varepsilon\tilde{\zeta}} \tilde{u} d\tilde{z} = \frac{Q}{UH_0B} \quad \text{at} \quad \tilde{x} = L/\ell,$$

with Q being the river discharge.

At the free surface $\tilde{z} = \varepsilon \tilde{\zeta}$ the boundary conditions read

$$A_v \tilde{u}_{\tilde{z}} = 0 \quad \text{and} \quad \tilde{w} = \tilde{\zeta}_{\tilde{t}} + \frac{A_{M_2}}{H_0} \tilde{u} \tilde{\zeta}_{\tilde{x}},$$

at the bottom $\tilde{z} = -\tilde{H}$ they are given by

$$\tilde{w} = -\tilde{u} \tilde{H}_{\tilde{x}} \quad \text{and} \quad \tilde{u}_{\tilde{z}} = \frac{sH_0}{A_v} \tilde{u}.$$

The dimensionless sediment mass balance equation, which is obtained from Eq. (A.11), reads

$$\tilde{c}_{\tilde{t}} + \frac{U}{\sigma \ell} (\tilde{u} \tilde{c}_{\tilde{x}} + \tilde{w} \tilde{c}_{\tilde{z}}) - \frac{w_s}{\sigma H_0} \tilde{c}_{\tilde{z}} - \frac{K_h}{\sigma \ell^2} \tilde{c}_{\tilde{x}\tilde{x}} - \frac{K_v}{\sigma H_0^2} \tilde{c}_{\tilde{z}\tilde{z}} - \frac{K_h}{\sigma \ell L_b} \tilde{c}_{\tilde{x}} = 0. \quad (\text{A.21})$$

The dimensionless boundary conditions for the suspended sediment concentration are given by

$$\frac{w_s}{\sigma H_0} \tilde{c} + \frac{K_v}{\sigma H_0^2} \tilde{c}_{\tilde{z}} - \frac{K_h A_{M_2}}{\sigma \ell^2 H_0} \tilde{c}_{\tilde{x}} \tilde{\zeta}_{\tilde{x}} \quad \text{at} \quad \tilde{z} = \varepsilon \tilde{\zeta},$$

and

$$-\frac{K_v}{\sigma H_0^2} \tilde{c}_{\tilde{z}} - \frac{K_h}{\sigma \ell^2} \tilde{c}_{\tilde{x}} \tilde{H}_{\tilde{x}} = \frac{w_s}{\sigma H_0} |\tilde{u}_{\tilde{z}}| \tilde{a} \quad \text{at} \quad \tilde{z} = -\tilde{H}.$$

The dimensionless morphodynamic equilibrium condition and integral condition read

$$\left\langle \int_{-\tilde{H}}^{\varepsilon \tilde{\zeta}} (\tilde{u} \tilde{c} - \frac{K_h}{\ell U} \tilde{c}_{\tilde{x}}) d\tilde{z} \right\rangle = 0 \quad \text{and} \quad \frac{\int_0^1 \tilde{a} e^{-\frac{\ell}{L_b} \tilde{x}} d\tilde{x}}{\int_0^1 e^{-\frac{\ell}{L_b} \tilde{x}} d\tilde{x}} = 1 \quad (\text{A.22})$$

From observations, it usually follows that the ratio of the M_2 tidal amplitude A_{M_2} and undisturbed water depth H_0 is a small parameter, i.e. $\varepsilon = A_{M_2}/H_0 \ll 1$. In order to construct a solution of the system of equations as a perturbation series, we have to relate the order of magnitude of most non dimensional coefficients in the equations above to ε . These parameters, their order and actual magnitude are provided in Table A.2.

Table A.2: Order of magnitude of dimensionless parameters and their actual values

Nondimensional parameter	Order	Value	
		1980	2005
$\varepsilon \equiv A_{M_2}/H$	$\mathcal{O}(\varepsilon)$	0.14	0.13
$U/\sigma\ell$	$\mathcal{O}(\varepsilon)$	0.14	0.13
ℓ/L_b	$\mathcal{O}(1)$	1	
U_d/U	$\mathcal{O}(\varepsilon)$	0.27	0.29
$A_v/\sigma H_0^2 = K_v/\sigma H_0^2$	$\mathcal{O}(1)$	1.57	0.86
$w_s/\sigma H_0$	$\mathcal{O}(1)$	0.14 – 3.57	
$K_h/\sigma\ell^2$	$\mathcal{O}(\varepsilon^3)$	7.9×10^{-4}	
$K_h/\sigma\ell L_b$	$\mathcal{O}(\varepsilon^3)$	7.9×10^{-4}	
A_{M_4}/A_{M_2}	$\mathcal{O}(\varepsilon)$	0.17	0.14
$K_h/\ell U$	$\mathcal{O}(\varepsilon^2)$	0.006	
$A_{M_2}K_h/\sigma\ell^2 H_0$	$\mathcal{O}(\varepsilon^4)$	1.1×10^{-4}	

The dimensionless slip parameter sH_0/A_v is allowed to vary from zero (free slip) to a large value (no slip) in the model, its actual value is derived from observations. Moreover, we assume that Q/UH_0B is at most of order ε .

We approximate the solution of the dimensionless Eqs. (A.20), (A.21) and (A.22) together with the appropriate boundary conditions by expanding the physical variables in power series of the small parameter ε

$$\begin{aligned}\tilde{u} &= \tilde{u}^0 + \varepsilon^1 \tilde{u}^1 + \varepsilon^2 \tilde{u}^2 + \dots \\ \tilde{w} &= \tilde{w}^0 + \varepsilon^1 \tilde{w}^1 + \varepsilon^2 \tilde{w}^2 + \dots \\ \tilde{\zeta} &= \tilde{\zeta}^0 + \varepsilon^1 \tilde{\zeta}^1 + \varepsilon^2 \tilde{\zeta}^2 + \dots \\ \tilde{c} &= \tilde{c}^0 + \varepsilon^1 \tilde{c}^1 + \varepsilon^2 \tilde{c}^2 + \dots\end{aligned}$$

where superscripts denote the order of ε . After substitution of these expansions in the equations and boundary conditions and collecting terms of equal powers of ε , one can investigate the dynamics of the system at different orders. The resulting reduced systems of the water motion and concentration equations and the morphodynamic equilibrium condition are given in Sections A4.1, A4.2 and A4.3, respectively.

A4.1 Leading order system of equations

From here on, the first superscript of a physical variable denotes the order of ε and the second superscript indicates the frequency of the constituent under consideration, by using the index of the lunar frequency. An analysis of the leading order system of equations revealed that the system is perturbed only by the M_2 tidal forcing, therefore, \tilde{u}^{02} denotes the dimensionless leading order velocity forced by the M_2 forcing.

Using the typical scales given in Table A.1, the dimensional variables can be obtained. In leading order, i.e. $\mathcal{O}(\varepsilon^0)$, the dimensional system of equations describing the water motion reads

$$u_x^{02} + w_z^{02} - \frac{u^{02}}{L_b} = 0, \quad (\text{A.23a})$$

$$u_t^{02} + g \zeta_x^{02} - (A_v u_z^{02})_z = 0, \quad (\text{A.23b})$$

where the first superscript denotes the order of ε .

The boundary condition at the riverine side requires the depth-averaged velocity to be zero at the weir and, at the entrance, the system is forced by the externally prescribed semi-diurnal tide. These conditions read

$$\zeta^{02} = A_{M_2} \cos(\sigma t) \quad \text{at} \quad x = 0, \quad (\text{A.24a})$$

$$\int_{-H}^0 u^{02} dz = 0 \quad \text{at} \quad x = L. \quad (\text{A.24b})$$

At the free surface, $z = 0$, the boundary conditions are given by

$$w^{02} = \zeta_t^{02} \quad \text{and} \quad A_v u_z^{02} = 0. \quad (\text{A.25})$$

At the bottom $z = -H(x)$ the boundary conditions read

$$w^{02} = -u^{02} H_x, \quad (\text{A.26a})$$

$$A_v u_z^{02} = s u^{02}. \quad (\text{A.26b})$$

The dynamics of the sediment concentration in leading order is given by

$$c_t^0 - w_s c_z^0 = (K_v c_z^0)_z. \quad (\text{A.27})$$

Hence, in leading order the evolution of the sediment concentration is governed by the local inertia, settling and vertical mixing of sediments.

The boundary condition at the free surface, $z = 0$, imposes a no flux condition through the boundary,

$$w_s c^0 + K_v c_z^0 = 0. \quad (\text{A.28})$$

At the bottom, $z = -H(x)$, the boundary condition reads

$$-K_v c_z^0 = w_s \rho_s \frac{s|u^{02}(t, x)|}{g' d_s} a(x). \quad (\text{A.29})$$

Since the water motion only consists of an M_2 tidal signal in leading order, it follows that the concentration has a residual component and all constituents with frequencies that are an even multiple of the M_2 tidal frequency, hence,

$$c^0 = c^{00} + c^{04} + \dots \quad (\text{A.30})$$

The sediment concentration c^0 still depends on the unknown erosion coefficient $a(x)$.

Solution. The leading order equations for the water motion (A.23) and sediment concentration (A.27) allow solutions of the following form:

$$(u^{02}, w^{02}, \zeta^{02}) = \Re \left\{ \left(\hat{u}^{02}(x, z), \hat{w}^{02}(x, z), \hat{\zeta}^{02}(x) \right) e^{i\sigma t} \right\}, \quad (\text{A.31})$$

$$c^0 = c^{00}(x, z) + \Re \left\{ \hat{c}^{04}(x, z) e^{2i\sigma t} + \dots \right\}, \quad (\text{A.32})$$

where $\Re\{\cdot\}$ denotes the real part of the expression in braces and i is the imaginary unit.

By substituting (A.31) into Eqs. (A.23), the time-dependent system of equations is transformed into a system of ordinary differential equations for the spatial variables $\hat{u}^{02}(x, z)$, $\hat{w}^{02}(x, z)$ and $\hat{\zeta}^{02}(x)$:

$$\hat{u}_x^{02} + \hat{w}_z^{02} - \frac{\hat{u}^{02}}{L_b} = 0, \quad (\text{A.33a})$$

$$i\sigma \hat{u}^{02} + g \hat{\zeta}_x^{02} - (A_v \hat{u}_z^{02})_z = 0. \quad (\text{A.33b})$$

First, momentum equation (A.33b) is solved using the corresponding boundary conditions for \hat{u}^{02} at $z = 0$ and $z = -H(x)$. The resulting expression for \hat{u}^{02} still depends on the unknown sea surface elevation $\hat{\zeta}^{02}$ and reads

$$\hat{u}^{02} = -\frac{g \hat{\zeta}_x^{02}}{i\sigma} (1 - \alpha(x) \cosh(\beta(x)z)), \quad (\text{A.34})$$

where $\alpha = s / (A_v \beta \sinh(\beta H) + s \cosh(\beta H))$ and $\beta = \sqrt{i\sigma / A_v}$.

Next, the continuity equation (A.33a) is used to solve for \hat{w}^{02} . The boundary condition for \hat{w}^{02} at $z = 0$ is satisfied using the integration constant. This results in

$$w^{02} = \frac{g}{i\sigma} \left(\frac{\zeta_x^{02}}{L_b} - \zeta_{xx}^{02} \right) \left(z - \frac{\alpha}{\beta} \sinh(\beta z) \right) + \frac{g \sinh(\beta z) \zeta_x^{02}}{i\sigma \beta} \left(\alpha_x + \alpha \beta_x \left(z \coth(\beta z) - \frac{1}{\beta} \right) \right) + i\sigma \zeta^{02}.$$

To satisfy the other boundary condition (A.26a), an ordinary differential equation for $\hat{\zeta}^{02}$ has to be solved, usually numerically. This equation reads

$$T_1 \hat{\zeta}_{xx}^{02} - T_2 \hat{\zeta}_x^{02} - T_3 \hat{\zeta}^{02} = 0,$$

with

$$\begin{aligned} T_1 &= \frac{\alpha \sinh(\beta H)}{\beta} - H, \\ T_2 &= \frac{T_1}{L_b} - \frac{\alpha_x \sinh(\beta H)}{\beta} + H_x (1 - \alpha \cosh(\beta H)) + \frac{\alpha \beta_x (\sinh(\beta H) - \beta H \cosh(\beta H))}{\beta^2}, \\ T_3 &= -\frac{\sigma^2}{g}. \end{aligned}$$

By back-substituting $\hat{\zeta}^{02}$, we obtain the spatial velocities \hat{u}^{02} and \hat{w}^{02} .

Next, the sediment concentration equation (A.27) is solved using substitution (A.32). Because Eq. (A.32) is linear, we can construct and solve an ordinary differential equation with respect to each spatial component (i.e. c^{00} , \hat{c}^{04} , etc) of the leading order concentration c^0 separately. As follows from Section A4.3, we only require the spatial variables c^{00} and \hat{c}^{04} to calculate the equilibrium sediment distribution. The solution for these components reads

$$\begin{aligned} c^{00} &= \frac{a(x) \rho_s s a_0}{g' d_s} e^{-\frac{w_s(H+z)}{K_v}}, \\ \hat{c}^{04} &= a(x) \left(A_1 e^{\frac{(\lambda - w_s)z}{2K_v}} + A_2 e^{-\frac{(\lambda + w_s)z}{2K_v}} \right), \end{aligned} \quad (\text{A.35})$$

with $\lambda = \sqrt{w_s^2 + 8i\sigma K_v}$, A_1 and A_2 are integration constants, obtained from boundary conditions (A.28) and (A.29)

$$A_2 = \frac{-2w_s \rho_s s (a_2 - ib_2)(w_s + \lambda)}{g'd_s \left((\lambda - w_s)^2 e^{\frac{(w_s - \lambda)H}{2K_v}} - (w_s + \lambda)^2 e^{\frac{(w_s + \lambda)H}{2K_v}} \right)},$$

$$A_1 = -\frac{A_2(w_s - \lambda)}{w_s + \lambda}.$$

and a_0 , a_2 and b_2 are coefficients of the Fourier series of the absolute value of the M_2 tidal velocity at the bed

$$|\hat{u}^{02}(x, -H)| = a_0 + a_1 \cos(\sigma t) + b_1 \sin(\sigma t) + a_2 \cos(2\sigma t) + b_2 \sin(2\sigma t) + \dots$$

Here, a_1 and b_1 equal to zero due to orthogonality.

A4.2 First order system of equations

In this section the first order system of equations is discussed. The water motion is discussed in subsection A4.2.1 and sediment dynamics in A4.2.2.

A4.2.1 Water motion

The first order dimensional hydrodynamic equations, i.e. $\mathcal{O}(\varepsilon^1)$ is given by

$$u_x^1 + w_z^1 - \frac{u^1}{L_b} = 0, \quad (\text{A.36a})$$

$$u_t^1 + u^{02} u_x^{02} + w^{02} u_z^{02} + g \zeta_x^1 - g \beta \langle s \rangle_x z = (A_v u_z^1)_z, \quad (\text{A.36b})$$

at this order the advective contributions enter the momentum equation (A.36b).

At the free surface, $z = 0$, the boundary conditions read

$$w^1 = \zeta_t^1 - \zeta^{02} w_z^{02} + u^{02} \zeta_x^{02} \quad \text{and} \quad A_v u_z^1 + A_v \zeta^{02} u_{zz}^{02} = 0, \quad (\text{A.37})$$

and at the bottom, $z = -H(x)$,

$$w^1 = -u^1 H_x \quad \text{and} \quad A_v u_z^1 = s u^1. \quad (\text{A.38})$$

The boundary conditions at the riverine side and entrance are given by

$$\zeta^1 = A_{M_4} \cos(2\sigma t - \phi) \quad \text{at} \quad x = 0, \quad (\text{A.39})$$

$$\int_{-H}^0 u^1 dz + \frac{H_0}{A_{M_2}} u^{02} \Big|_{z=0} \zeta^{02} = \frac{Q}{B} \quad \text{at} \quad x = L. \quad (\text{A.40})$$

From Eq. (A.34) and boundary condition (A.24b), we can conclude that $u^{02} = 0$ at $x = L$. Therefore, boundary condition (A.40) reduces to

$$\int_{-H}^0 u^1 dz = \frac{Q}{B} \quad \text{at} \quad x = L.$$

Careful inspection of the higher-order system of equations and the boundary conditions shows that the order ε velocity fields u^1, w^1 and the sea surface elevation ζ^1 consist of the residual contributions ($u^{10}, w^{10}, \zeta^{10}$) and contributions ($u^{14}, w^{14}, \zeta^{14}$) with twice the frequency of the semi-diurnal tide. Hence, the solution of the first order water motion can be expressed as, e.g. $u^1 = u^{10} + u^{14}$.

Residual flow. By averaging over a tidal period, a forced linear system that describe the residual flow is obtained

$$u_x^{10} + w_z^{10} - \frac{u^{10}}{L_b} = 0, \quad (\text{A.41a})$$

$$\langle u^{02} u_x^{02} + w^{02} u_z^{02} \rangle + g \zeta_x^{10} - g \beta \langle s \rangle_x z = (A_v u_z^{10})_z, \quad (\text{A.41b})$$

where the angular brackets $\langle . \rangle$ denote a tidal average.

At the free surface, $z = 0$, the boundary conditions are given by

$$w^{10} = - \langle \zeta^{02} w_z^{02} - u^{02} \zeta_x^{02} \rangle \quad \text{and} \quad A_v u_z^{10} + \langle A_v \zeta^{02} u_{zz}^{02} \rangle = 0. \quad (\text{A.42})$$

At the bottom $z = -H(x)$ the boundary conditions read

$$w^{10} = -u^{10} \frac{\partial H}{\partial x} \quad \text{and} \quad A_v u_z^{10} = s u^{10}. \quad (\text{A.43})$$

The boundary condition at the riverine side is that the depth- and tidally-averaged velocity is related to the river discharge at the weir by

$$\int_{-H}^0 u^{10} dz dt = \frac{Q}{B} \quad \text{at} \quad x = L. \quad (\text{A.44})$$

Furthermore, the residual sea surface elevation is zero at the entrance

$$\zeta^{10} = 0 \quad \text{at} \quad x = 0. \quad (\text{A.45})$$

First overtide (M_4) flow. The M_4 constituent of the water motion is described by the following system of forced equations

$$u_x^{14} + w_z^{14} - \frac{u^{14}}{L_b} = 0, \quad (\text{A.46a})$$

$$u_t^{14} + [u^{02} u_x^{02} + w^{02} u_z^{02}] + g \zeta_x^{14} = (A_v u_z^{14})_z, \quad (\text{A.46b})$$

where braces $[\cdot]$ denote the M_4 contribution.
At the free surface, $z = 0$, the boundary conditions are given by

$$w^{14} = \zeta_t^{14} + [u^{02}\zeta_x^{02} - \zeta^{02}w_z^{02}], \quad (\text{A.47a})$$

$$A_v u_z^{14} + A_v [\zeta^{02} u_{zz}^{02}] = 0. \quad (\text{A.47b})$$

At the bottom the boundary conditions read

$$w^{14} = -u^{14} \frac{\partial H}{\partial x} \quad \text{and} \quad A_v u_z^{14} = s u^{14} \quad \text{at} \quad z = -H(x). \quad (\text{A.48})$$

The first overtide boundary conditions at the entrance and riverine side are identical to those of the leading order conditions, with a difference that the system is forced by the externally prescribed M_4 tide at the entrance. These conditions are

$$\zeta^{14} = A_{M_4} \cos(2\sigma t - \phi) \quad \text{at} \quad x = 0, \quad (\text{A.49a})$$

$$\int_{-H}^0 u^{14} dz = 0 \quad \text{at} \quad x = L. \quad (\text{A.49b})$$

The first order system of equations for the water motion consists of residual contributions, given by Eqs. (A.41)-(A.45), and M_4 contributions (Eqs. (A.46)-(A.49)). The residual and M_4 water motion is forced by various contributions, see the main text for a detailed description of these forcing terms.

Since the Eqs. (A.41) and boundary conditions (A.42)-(A.45) are linear, we can solve the equations for each forcing term separately. The solution method for each forcing term is similar to the method described in Section A4.1.

Similar to (A.31), the M_4 water motion equations (A.46) allow the solution of the following form

$$(u^{14}, w^{14}, \zeta^{14}) = \Re \left\{ \left(\tilde{u}^{14}(x, z), \tilde{w}^{14}(x, z), \tilde{\zeta}^{14}(x) \right) e^{2i\sigma t} \right\}, \quad (\text{A.50})$$

here, $\Re\{\cdot\}$ stands for the real part of an expression in braces and i the imaginary unit. Substitution (A.50) in Eqs. (A.46) results in a system of ODEs with respect to the spatial variables $\tilde{u}^{14}(x, z)$, $\tilde{w}^{14}(x, z)$ and $\tilde{\zeta}^{14}(x)$. The resulting system of equations is linear. Analogous to the method which was employed for the residual water motion, we decompose the system and boundary conditions into three

systems of ODEs with appropriate boundary conditions each induced by the individual forcing. Next, we obtain the solution for each system and construct the final solution as a superposition, i.e.,

$$(\tilde{u}^{14}, \tilde{w}^{14}, \tilde{\zeta}^{14}) = \sum_{i=1}^3 (\tilde{u}_i^{14}, \tilde{w}_i^{14}, \tilde{\zeta}_i^{14}).$$

A4.2.2 Sediment dynamics

In deriving the sediment equation at first order, we assume that the nonlinear terms in Eq. (A.21) are negligible in the dynamics of the suspended sediment concentration, even though they give an order epsilon contribution according to the scaling. The motivation for this choice is that treating these nonlinear terms as order ϵ quantities will result in additional mean and overtide components of the first order. Solving these components will be straightforward, but will also complicate the analysis. Since our goal is to gain understanding of sediment transport, these nonlinear terms are neglected at a first step. Hence, the dynamics of the sediment concentration is governed by

$$c_t^1 - w_s c_z^1 = (K_v c_z^1)_z. \quad (\text{A.51})$$

The first order boundary conditions for the sediment concentration are equivalent to those in leading order, with the first order component of the absolute value of the bed shear stress

$$|\tau_b^1| = \rho_0 s u^1 \frac{u^{02}}{|u^{02}|} \quad \text{at} \quad z = -H. \quad (\text{A.52})$$

The boundary conditions read

$$w_s c^1 + K_v c_z^1 = 0 \quad \text{at} \quad z = 0, \quad (\text{A.53})$$

$$-K_v c_z^1 = w_s \rho_s s u^1 \frac{u^{02}}{|u^{02}| g' d_s} a(x) \quad \text{at} \quad z = -H. \quad (\text{A.54})$$

Hence, the first-order sediment concentration is a result of the leading order and the first order tidal flow interaction. Applying the Fourier analysis to bottom boundary condition (A.54), it can be deduced that the first order concentration consist of all tidal components

$$c^1 = c^{10} + c^{12} + \dots \quad (\text{A.55})$$

The semi-diurnal component of the first order sediment concentration c^{12} is obtained by substituting

$$c^{12} = \Re \{ \hat{c}^{12}(x, z) e^{i\sigma t} \} \quad (\text{A.56})$$

in concentration equation (A.51). This results in an ordinary differential equation for the spatial coefficient $\hat{c}^{12}(x, z)$. Using the appropriate boundary conditions (A.53) and (A.54) the solution to this equation reads

$$\hat{c}^{12} = a(x) \left(B_1 e^{\frac{(\lambda - w_s)z}{2K_v}} + B_2 e^{-\frac{(\lambda + w_s)z}{2K_v}} \right), \quad (\text{A.57})$$

with $\lambda = \sqrt{w_s^2 + 4i\sigma K_v}$, B_1 and B_2 are the integration constants, obtained from boundary conditions (A.28) and (A.29)

$$B_2 = \frac{-2w_s \rho_s s (p_1 - id_1)(w_s + \lambda)}{g'd_s \left((\lambda - w_s)^2 e^{\frac{(w_s - \lambda)H}{2K_v}} - (w_s + \lambda)^2 e^{-\frac{(w_s + \lambda)H}{2K_v}} \right)},$$

$$B_1 = -\frac{B_2(w_s - \lambda)}{w_s + \lambda}.$$

and p_1 and d_1 are coefficients of the Fourier series of the absolute value of the bed shear stress given by Eq. (A.52)

$$\hat{u}^1(x, -H) \frac{\hat{u}^{02}(x, -H)}{|\hat{u}^{02}(x, -H)|} = p_0 + p_1 \cos(\sigma t) + d_1 \sin(\sigma t) + p_2 \cos(2\sigma t) + d_2 \sin(2\sigma t) + \dots$$

A4.3 Morphodynamic equilibrium condition

From the scaled morphodynamic equilibrium condition (A.22) and the fact that in leading order the concentration consists of a residual component and a component with a frequency that is multiple of M_4 (A.30) and velocity only of an M_2 , it is evident that there is no residual sediment transport in order ε . Only in order ε^2 a residual sediment transport is found, due to the interaction of the residual and M_4 $\mathcal{O}(1)$ sediment concentration with the residual and M_4 $\mathcal{O}(\varepsilon)$ velocity components, and the M_2 $\mathcal{O}(\varepsilon)$ sediment concentration with the M_2 $\mathcal{O}(1)$ velocity component. The morphodynamic equilibrium condition reads

$$\int_{-H}^0 (u^{10} c^{00} + \langle u^{02} c^{12} \rangle + \langle u^{14} c^{04} \rangle - K_h \langle c_x^{00} \rangle) dz + \underbrace{\langle \zeta^0 [u^0 c^0]_{z=0} \rangle}_E = 0. \quad (\text{A.58})$$

Note that in Eq. (A.58) the last contribution (E) is a result of Taylor expansion the upper integration boundary in Eq. (A.22) around $z = 0$.

The spatial and temporal structure of the width-averaged sediment concentration c is known but it still depends on the unknown erosion coefficient $a(x)$, i.e. $c^{00} = a(x)c^{00a}$, $c^{04} = a(x)c^{04a}$ and $c^{12} = a(x)c^{12a}$. Here, c^{00a} , c^{04a} and c^{12a} are independent of $a(x)$. The spatial and temporal structure of the width-averaged velocity fields is known. Substituting these expressions in the morphodynamic equilibrium condition (A.58) results in a linear first order ODE with respect to the unknown erosion coefficient $a(x)$

$$F \frac{da}{dx} + Ta = 0, \quad (\text{A.59})$$

where

$$F = \left\langle \int_{-H}^0 -K_h c^{00a} dz \right\rangle,$$

$$T = \int_{-H}^0 \left(u^{10} c^{00a} + \langle u^{02} c^{12a} \rangle + \langle u^{14} c^{04a} \rangle - K_h \langle c_x^{00a} \rangle \right) dz + \left\langle \zeta^0 [u^{02} c^{0a}]_{z=0} \right\rangle.$$

Eq. (A.59) is solved by the method of separation of variables and the solution reads

$$a(x) = a_0 \exp \left(\int -T/F dx \right) \equiv a_0 I(x). \quad (\text{A.60})$$

The integration constant, denoted by a_0 , is determined from condition the boundary condition as

$$a_0 = \frac{a_* \int_0^L B(x) dx}{\int_0^L B(x) I(x) dx}. \quad (\text{A.61})$$

A5 Confidence Intervals for the Best Fit

The vertical eddy viscosity function A_v and stress parameter s are difficult to get from measurements. Therefore we obtain these parameters by calibrating the

model to observations. This is done by minimizing the difference between the observed and modeled semi-diurnal tidal amplitude (ζ_{M_2}), and phase difference between the semi-diurnal free surface elevation and velocity tide ($\phi_{\zeta_{M_2}} - \phi_{u_{M_2}}$) in a least square sense. The other observations, such as the residual and M_4 tidal amplitude and velocity at the surface, are then used to validate the model. The resulting vertical eddy viscosity coefficient A_{v0} for 1980 is $0.019 \text{ m}^2\text{s}^{-1}$ and $0.012 \text{ m}^2\text{s}^{-1}$ in 2005. For the stress coefficient we found 0.098 ms^{-1} in 1980 and 0.049 ms^{-1} in 2005. We also introduce a so-called reasonable fit, which we define as a 1% deviation from the best fit in the least square error. This deviation gives us confidence intervals for the vertical eddy viscosity coefficient and stress parameter, so that any value in this interval provides a reasonable comparison between the model predictions and the observations. The confidence intervals are outlined in Fig. (A.2) by the black solid line. The minimal error value is shown with the red square.

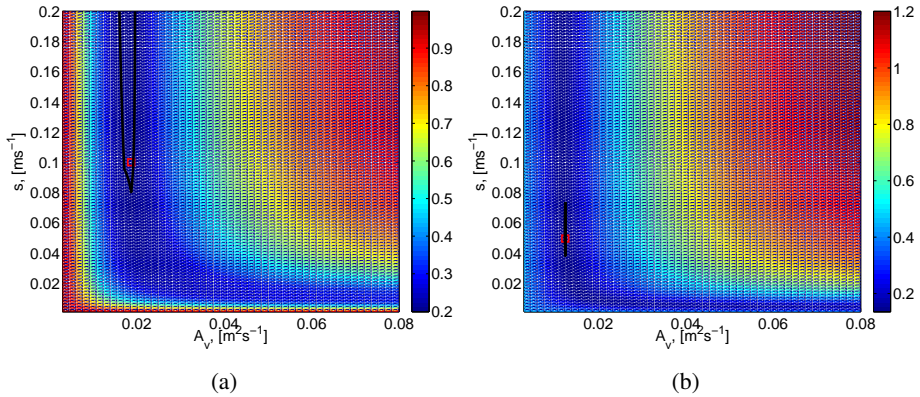


Figure A.2: *Least square error. The left panel represents 1980 and the right one depicts 2005. The black line outlines the reasonable fit. The red square is the minimal error.*

The confidence interval for the vertical eddy viscosity coefficient is $0.016 - 0.0196 \text{ m}^2\text{s}^{-1}$ in 1980 and $0.0123 - 0.0125 \text{ m}^2\text{s}^{-1}$ in 2005. The lower (upper) boundary of the s_0 confidence interval for 1980 is 0.08 (no upper boundary) ms^{-1} and 0.038 (0.074) ms^{-1} for 2005.

A6 Parameter Sensitivity

In this supplement, we investigate the physical mechanisms which are responsible for the amplification of the semi-diurnal tidal amplitude between 1980 and 2005. The M_2 tidal amplitude and relative phase between the horizontal velocity and water level are shown in Fig. A.3 by the solid blue and green lines, respectively. Comparison of these lines suggests that the tidal motion is more resonant in 2005 than 1980: in 1980 the dimensionless M_2 sea surface elevation amplitude at the weir (the ratio of the M_2 sea surface elevation amplitude over its value at the entrance) was approximately 0.74, in 2005 1.12. Moreover, the relative phase (see Fig. A.3(b)) suggests more of a standing wave character in 2005 than in 1980.

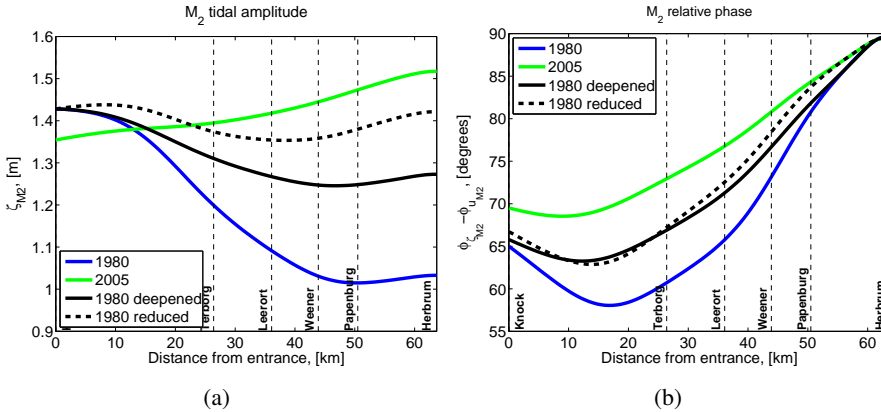


Figure A.3: *The semi-diurnal tidal amplitude and phase difference between the semi-diurnal horizontal velocity and water level. The left panels represent tidal amplitude along the estuary and the right ones depict relative phase shift between the free surface elevation and along-channel velocity component*

The two main differences in the model input between 1980 and 2005 are the depth of the embayment and the change of the vertical eddy viscosity parameter A_v and stress parameter s . As a first step, we want to understand whether these changes result from a combination of those two factors or are primarily caused by one of the factors, for example, deepening. Therefore, we consider deepening and change of parameters A_v and s separately and compare these results with those which are obtained for the 1980 and 2005 experiments. As a first experiment, we take the model setup for 1980 with a deepened bathymetry, but keeping the

parameters of A_v and s unchanged. The resulting M_2 amplitude is shown by the black solid line in Fig. A.3(a), in Fig. A.3(b) the relative phase is shown. It is clear that the system has become more resonant as both the amplitude increases towards the end of the embayment and the relative phase has become closer to 90° . Next, we use the 1980 model setup with reduced values of A_v and s , but keeping the 1980 bathymetry. The M_2 amplitude is depicted by the black dashed line in Fig. A.3(a) and the relative phase is shown in Fig. A.3(b). This model input makes the M_2 amplitude increase even faster and gives higher value of the relative phase, compared to the previous model setup. Hence makes the system more resonant than by only deepening itself. However, we can conclude that it is the combination of deepening and reduced vertical eddy viscosity and stress parameter that makes the M_2 tide amplify towards the end of the estuary.

The M_4 tidal amplitude significantly amplifies towards the end of the embayment in 2005, the dimensionless M_2 sea surface elevation amplitude at the weir is 2.39, whereas in 1980 it is only 0.98 (the green and blue solid lines in Fig. A.4(a), respectively). The relative phase, shown in Fig. A.4(b), suggests more of a standing wave character in 2005. Repeating the above experiments, it turns out that for the M_4 tidal motion, it is mainly the reduction of the vertical viscosity and stress parameter (by the black dashed line in Fig. A.4(a)) that results in the amplification of the M_4 tidal amplitude. For the M_4 relative phase both the deepening and the reduction of the vertical viscosity and stress parameter are essential to reproduce the 2005 model results.

Because we use an analytical approach, we can split the M_4 tidal signal into a part generated due to nonlinear interactions in the model and a contribution due to the external overtide forcing. The amplitude and relative phase of the internally generated M_4 tide is shown in Fig. A.5 and for the externally forced M_4 tide in Fig. A.6. Based on Fig. A.5(a), we observe that the amplification of the internally generated M_4 tide is mainly achieved by a reduction of the bottom friction and vertical eddy viscosity parameters. The externally forced M_4 tide exhibits similar behavior as the M_2 tide.

To get more insight in the effect of the bottom friction and deepening on the resonance characteristics of the tidal embayment, we develop a simple analytical model of an estuary with a flat bed constrained by a weir. To this end we choose a representative water depth (7.7 m, 8.7 m) for 1980 and 2005, respectively, such that the tidal character for the M_2 water motion is well-reproduced in the simplified model (compare Figs. A.3(a) and A.7(a)). We see that in both cases the M_2 tide shows similar behavior. Therefore, we can assume that the flat bed resonance characteristics are similar to model with varying bathymetry.

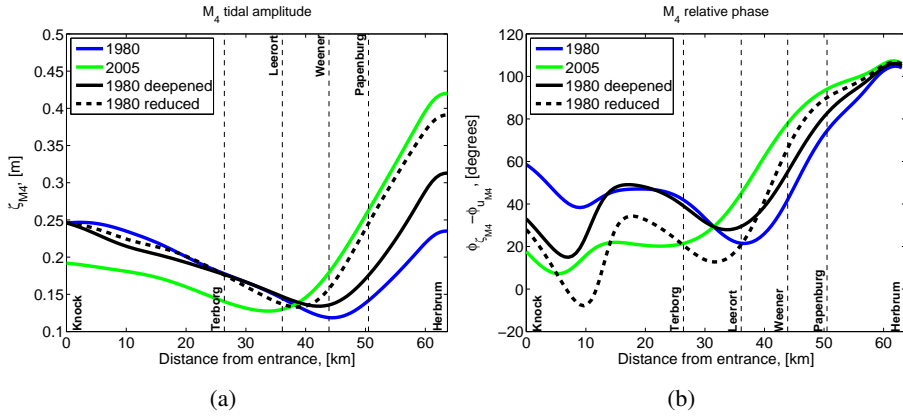


Figure A.4: The M_4 tidal amplitude and phase difference between the M_4 horizontal and vertical tide. The left panels represent tidal amplitude along the estuary and the right ones depict relative phase shift between the free surface elevation and along-channel velocity component.

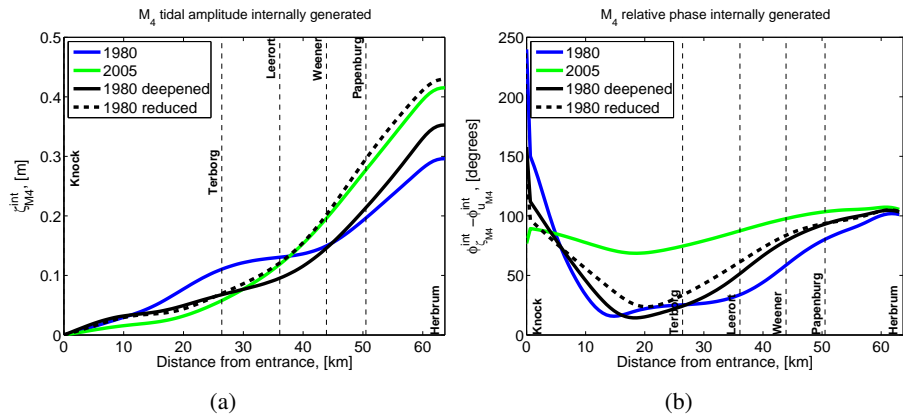


Figure A.5: The M_4 internally generated tidal amplitude and phase difference between the M_4 horizontal and vertical tide internally generated. The left panels represent tidal amplitude along the estuary and the right ones depict relative phase shift between the free surface elevation and along-channel velocity component.

The dimensionless M_2 tidal amplitude at the weir is plotted as a function of the embayment length scaled with a quarter wavelength of the frictionless tidal wave $L_g = \sqrt{gH/\sigma}$ in Fig. A.7(b). The vertical red dashed line represents the length of

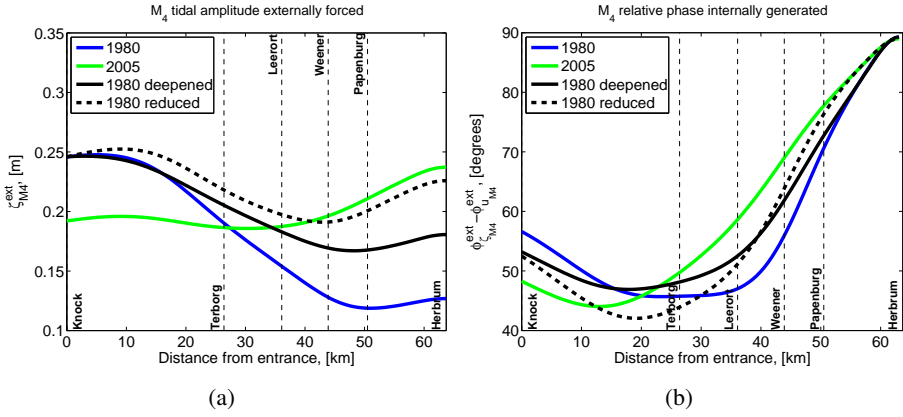


Figure A.6: The M_4 externally forced tidal amplitude and phase difference between the M_4 horizontal and vertical tide externally forced. The left panels represent tidal amplitude along the estuary and the right ones depict relative phase shift between the free surface elevation and along-channel velocity component.

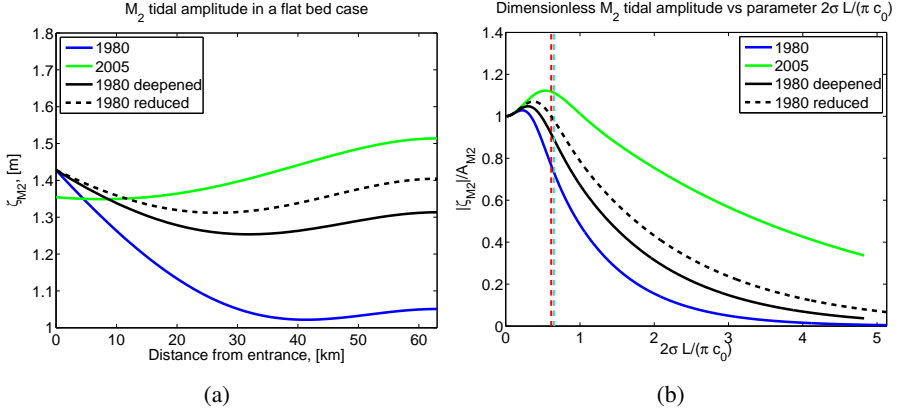


Figure A.7: Flat bed model output. The left panel represent the M_2 tidal amplitude along the estuary and the right one depict the effect of bottom friction and deepening on the resonance characteristics.

the embayment of $L = 63.7$ km, which is the length of the Ems estuary, with depth 8.7 m and the cyan dashed line 7.7 m. In 1980 the estuary is far from resonance, by either deepening or reducing the bottom friction and vertical eddy viscosity the

embayment becomes more resonant. Decreasing the vertical eddy viscosity and friction parameter is slightly more efficient in pushing the embayment towards resonance than deepening. But, as it was already shown above, both deepening and decrease of the vertical eddy viscosity and stress parameter are necessary to reproduce the 2005 amplification. Hence, the combination of these factors enhances the resonance so that the M_2 tide, as well as M_4 , amplifies even further towards the end of the estuary.

A7 Water Motion Components

In this appendix, any left panel of each figure represent 1980 and the right one 2005. In Figs. A.8 - A.10 phase of the M_2 sea surface elevation, the M_2 velocity amplitude and phase at the surface are plotted, respectively. The squares show measurements and the solid lines represent model predictions.

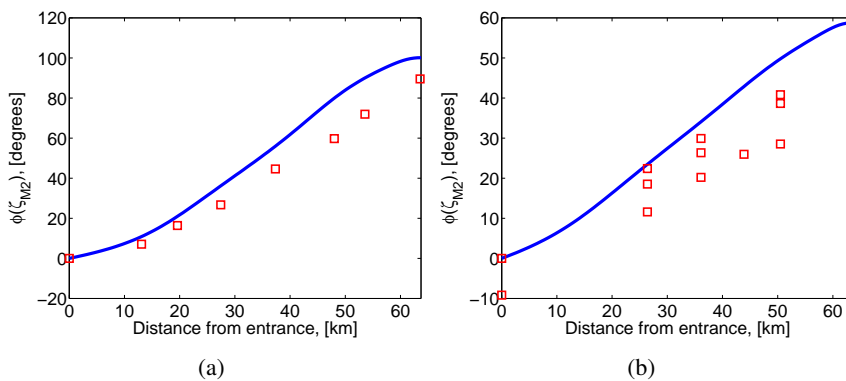


Figure A.8: The M_2 sea surface elevation phase. The left panels represent 1980 and the right ones 2005.

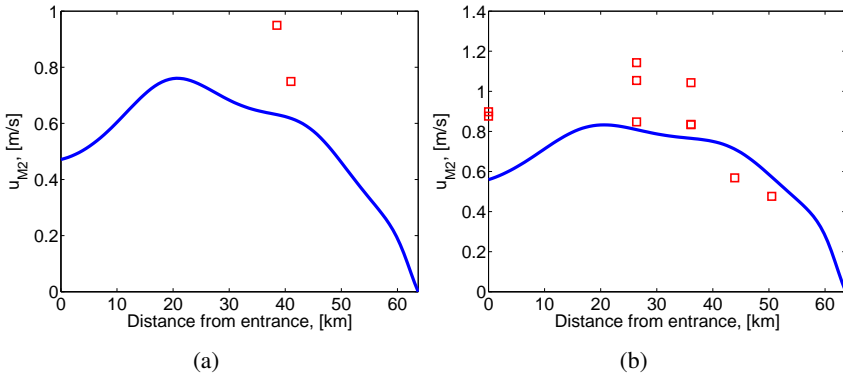


Figure A.9: The M_2 velocity amplitude at the surface. The left panels represent 1980 and the right ones 2005.

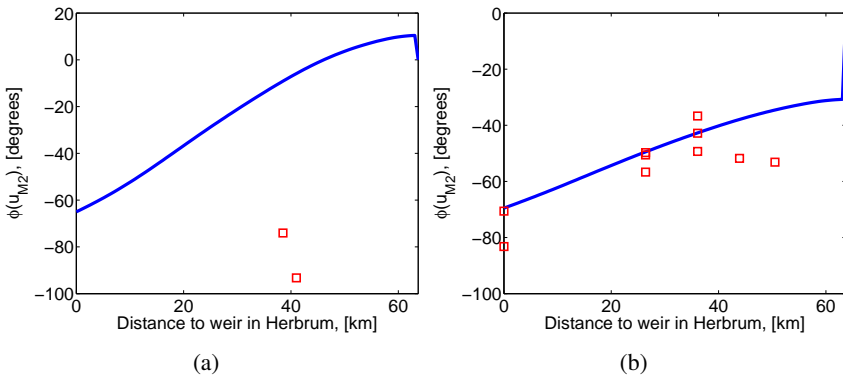


Figure A.10: The M_2 velocity phase at the surface. The left panels represent 1980 and the right ones 2005.

A8 Transport components

In the following paragraphs we provide a detailed analysis of the transport function components T_{res} , T_{M_2} and T_{M_4} .

T_{M_2} transport function. The T_{M_2} contribution plays an important role in the changes of the sediment trapping location in the Ems estuary between 1980 and 2005. To understand which mechanism is responsible for this significant change of T_{M_2} , T_{M_2} will be decomposed into different components. The M_2 concentration

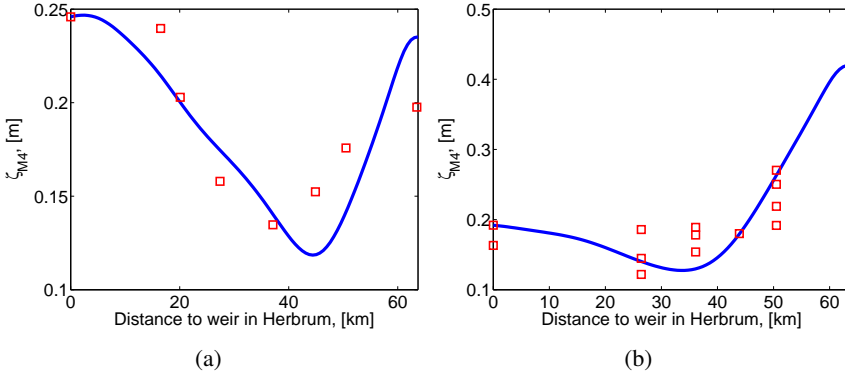


Figure A.11: The M_4 sea surface elevation amplitude. The left panels represent 1980 and the right ones 2005.

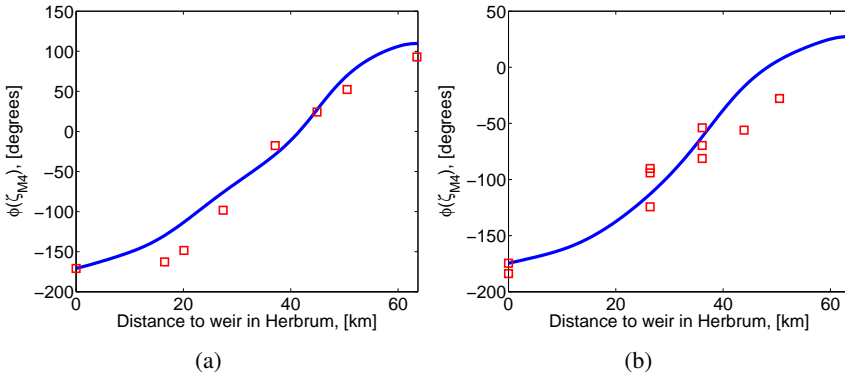


Figure A.12: The M_4 sea surface elevation phase. The left panels represent 1980 and the right ones 2005.

(see Section 2.3.2.2), is forced by the M_2 component of the bed shear stress. From Eq. (2.39) it follows that the M_2 component of the bed shear stress is a result of the interaction of both the residual and the M_4 velocities with the M_2 velocity. Using Section 2.3.2.1, we can distinguish 5 contributions to the M_2 concentration due to the residual flow (see Eq. (2.33)) and 4 due to the M_4 flow (see Eq. (2.38)), each resulting in a contribution to T_{M_2} , that can be studied separately.

The residual contribution to T_{M_2} driven by the gravitational circulation is denoted by $T_{M_2}^{\text{GC}}$, for river discharge by $T_{M_2}^{\text{RI}}$, $T_{M_2}^{\text{SD}}$ denotes the contribution due to

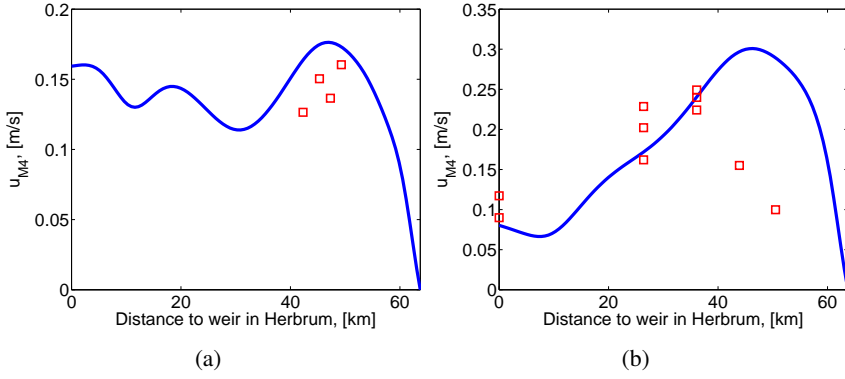


Figure A.13: The M_4 velocity amplitude at the surface. The left panels represent 1980 and the right ones 2005.

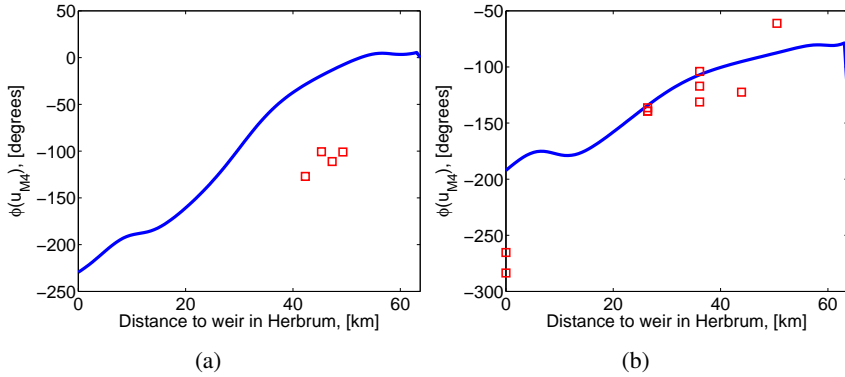


Figure A.14: The M_4 velocity phase at the surface. The left panels represent 1980 and the right ones 2005.

tidal (Stokes) return flow, $T_{M_2}^{SC}$ due to surface contribution and $T_{M_2}^{TS}$ due to tidal stresses. The M_4 velocity components that contribute to T_{M_2} are advective contributions, denoted by $T_{M_2}^{AC}$, free surface contribution, denoted by $T_{M_2}^{FS}$, no-stress contribution, denoted by $T_{M_2}^{NS}$, and the M_4 external forcing, denoted by $T_{M_2}^{EF}$ (see Section 2.3.2.2). The sum of the residual and M_4 contributions is denoted by $T_{M_2}^{res}$

and $T_{M_2}^{M_4}$, respectively. Hence,

$$T_{M_2} = \underbrace{T_{M_2}^{\text{GC}} + T_{M_2}^{\text{RI}} + T_{M_2}^{\text{SD}} + T_{M_2}^{\text{SC}} + T_{M_2}^{\text{TS}}}_{T_{M_2}^{\text{res}}} + \underbrace{T_{M_2}^{\text{AC}} + T_{M_2}^{\text{FS}} + T_{M_2}^{\text{NS}} + T_{M_2}^{\text{EF}}}_{T_{M_2}^{M_4}}.$$

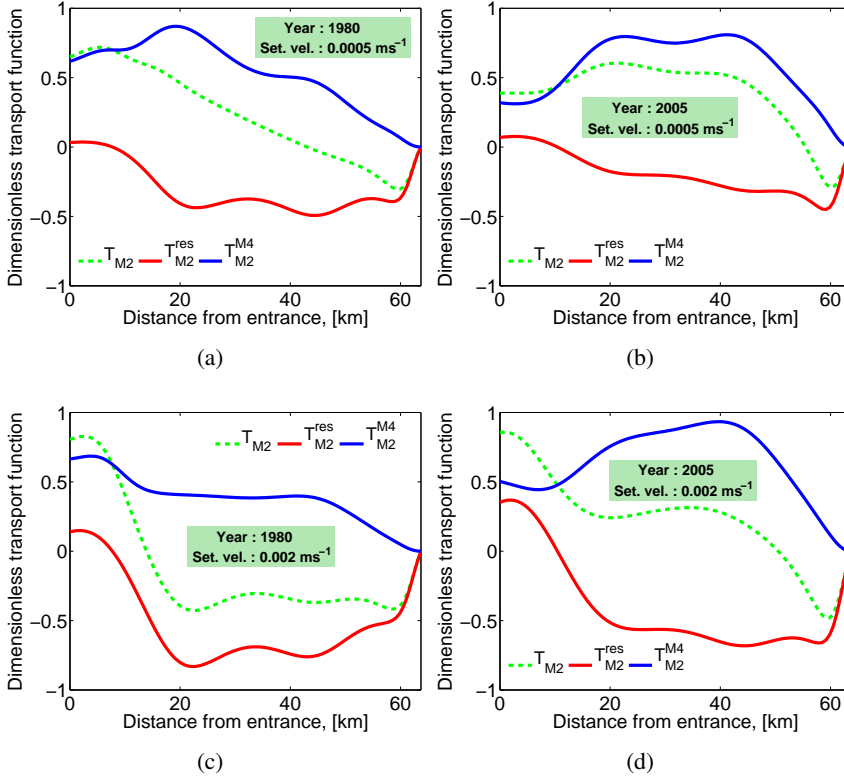


Figure A.15: Dimensionless transport function T_{M_2} and its components.

In Fig. A.15 T_{M_2} and its components $T_{M_2}^{\text{res}}$, $T_{M_2}^{M_4}$ are shown by the dashed green, solid red and solid blue lines, respectively. For fine silt we can observe no significant change of the $T_{M_2}^{\text{res}}$ contribution between 1980 and 2005. Therefore, the change in T_{M_2} is determined by the $T_{M_2}^{M_4}$ contribution. The $T_{M_2}^{M_4}$ transport starts to decrease at approximately km 20 in 1980, whereas in 2005 it stays constant up to approximately km 50 and only then starts to decrease. For coarse silt we observe a similar behavior of the $T_{M_2}^{M_4}$ transport: a smooth decrease from the entrance in

1980 and in 2005 the decrease starts at 50 km. For coarse silt, the magnitude of the $T_{M_2}^{\text{res}}$ transport has decreased between 1980 and 2005. However, the general behavior did not change. Hence, the change of T_{M_2} is again mainly caused by the change of its M_4 contribution. Therefore, further decomposition is needed to find the dominant difference between 1980 and 2005.

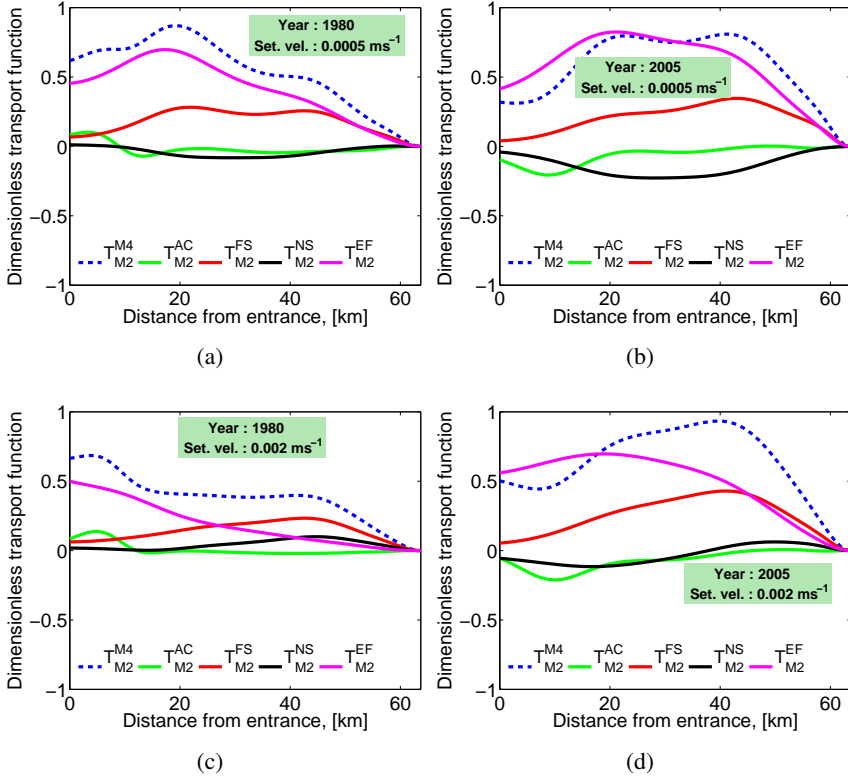


Figure A.16: Dimensionless transport function $T_{M_2}^{M_4}$ and its components.

The M_4 components of the transport function T_{M_2} are shown in Fig. A.16. For both fine silt (Figs. A.16(a) and A.16(b)) and coarse silt (Figs. A.16(c) and A.16(d)), we see that the behavior of $T_{M_2}^{M_4}$ (the dashed blue line) is primarily determined by the contribution which results from the externally forced M_4 tide (the solid magenta line). The other three contributions are much smaller. It follows that for both years and grain sizes the main contribution to $T_{M_2}^{M_4}$ is the externally prescribed M_4 overtide. In 1980 this contribution decreases from the entrance,

whereas in 2005 an abrupt decrease starts only at approximately km 40. Hence the main change between 1980 and 2005 is due to the difference in residual sediment transport by tidal asymmetry: there was less import of sediment in 1980 compared to 2005. This is true for both fine and coarser silt.

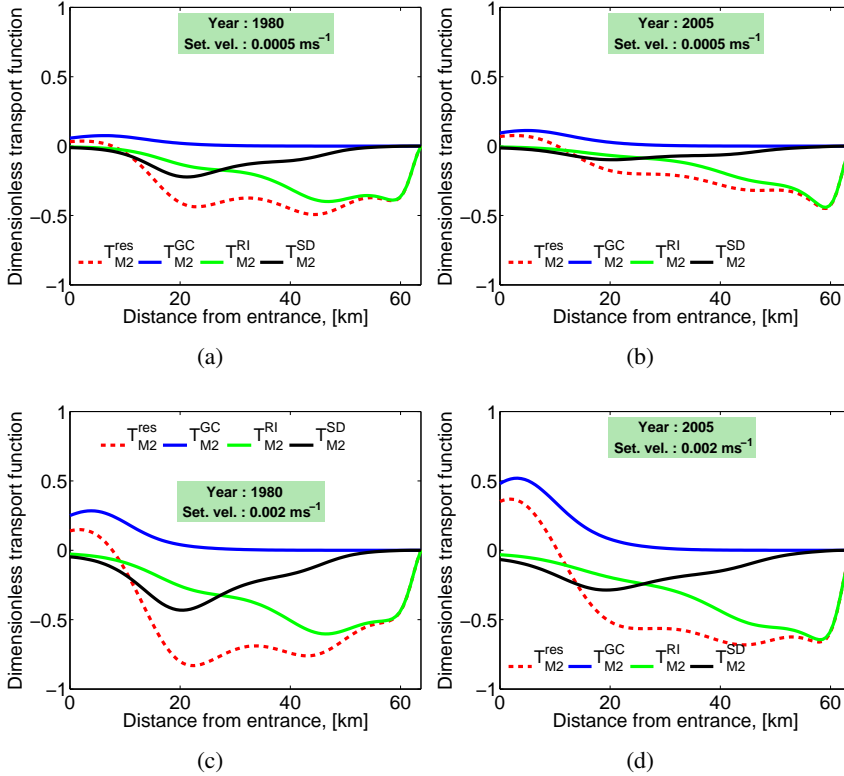


Figure A.17: Dimensionless transport function $T_{M_2}^{res}$ and its components.

In Fig. A.17 a decomposition of $T_{M_2}^{res}$ (the dashed red line) is shown. Three residual constituents ($T_{M_2}^{GC}$, the solid blue line, $T_{M_2}^{RI}$, the solid green line and $T_{M_2}^{SD}$, the solid black line, respectively) are shown. The two remaining contributions ($T_{M_2}^{SC}$, $T_{M_2}^{TS}$) are insignificant and therefore not shown. For fine silt (Figs. A.17(a) and A.17(b)) we observe that a decrease of the $T_{M_2}^{SD}$ contribution between 1980 and 2005. Close inspection of Figs. A.17(c) and A.17(d) shows that, for coarse silt, the $T_{M_2}^{res}$ flux has changed due to the increase of the $T_{M_2}^{GC}$ contribution and the decrease of the $T_{M_2}^{SD}$ contribution between 1980 and 2005. This is caused by an

increase of the gravitational circulation and weakening of the tidal return flow in 2005 (see discussion in Section 2.5.1).

T_{M_4} transport function. The T_{M_4} flux is the result of the M_4 velocity and M_4 concentration interaction. The M_4 velocity consists of four constituents (see Eq. (2.38)) and hence, the T_{M_4} flux has four different contributions, i.e.,

$$T_{M_4} = T_{M_4}^{AC} + T_{M_4}^{FS} + T_{M_4}^{NS} + T_{M_4}^{EF}.$$

The T_{M_4} flux (the dashed black line) and its components are shown in Fig. A.18. For fine and coarse silt (Figs. A.18(a), A.18(b) and Figs. A.18(c), A.18(d), respectively) the main balance is between the $T_{M_4}^{NS}$ contribution (the solid blue line) and the $T_{M_4}^{EF}$ transport (the solid magenta line). For fine silt, none of the components shows more than a 5 % change of behavior between 1980 and 2005. For coarse silt we see that changes of the T_{M_4} transport are primarily caused by changes in the advective contribution $T_{M_4}^{AC}$ (the solid green line) and the $T_{M_4}^{EF}$ transport functions.

T_{res} transport function. The T_{res} flux is a result of interactions of the residual velocity and residual concentration. The residual velocity consists of 5 constituents (see Eq. (32)). Hence, similar to the T_{M_2} transport, the T_{res} transport can be decomposed in contributions forced by: the gravitational circulation T_{res}^{GC} , river inflow T_{res}^{RI} , tidal return flow T_{res}^{SD} , surface contribution T_{res}^{SC} , tidal stresses T_{res}^{TS} and contribution $T_{res}^{\zeta uc}$ resulting from a correlation between the tidal return flow and concentration:

$$T_{res} = T_{res}^{GC} + T_{res}^{RI} + T_{res}^{SD} + T_{res}^{SC} + T_{res}^{TS} + T_{res}^{\zeta uc}.$$

Fig. A.19 shows the T_{res} flux (the dashed red line) and its 4 components: T_{res}^{GC} (the solid blue line), T_{res}^{RI} (the solid green line), T_{res}^{SD} (the solid black line), $T_{res}^{\zeta uc}$ (the solid magenta line). The other two contributions are not shown as they are negligible.

We can see that for both fine (Figs. A.19(a) and A.19(b)) and coarse silt (Figs. A.19(c) and A.19(d)) tidal (Stokes) return flow T_{res}^{SD} is approximately balanced by the $T_{res}^{\zeta uc}$ transport. Therefore, the behavior of the T_{res} transport is mainly determined by the river inflow transport T_{res}^{RI} everywhere in the estuary, except in a region at the entrance. In this region we see the influence of the gravitation circulation transport T_{res}^{GC} .

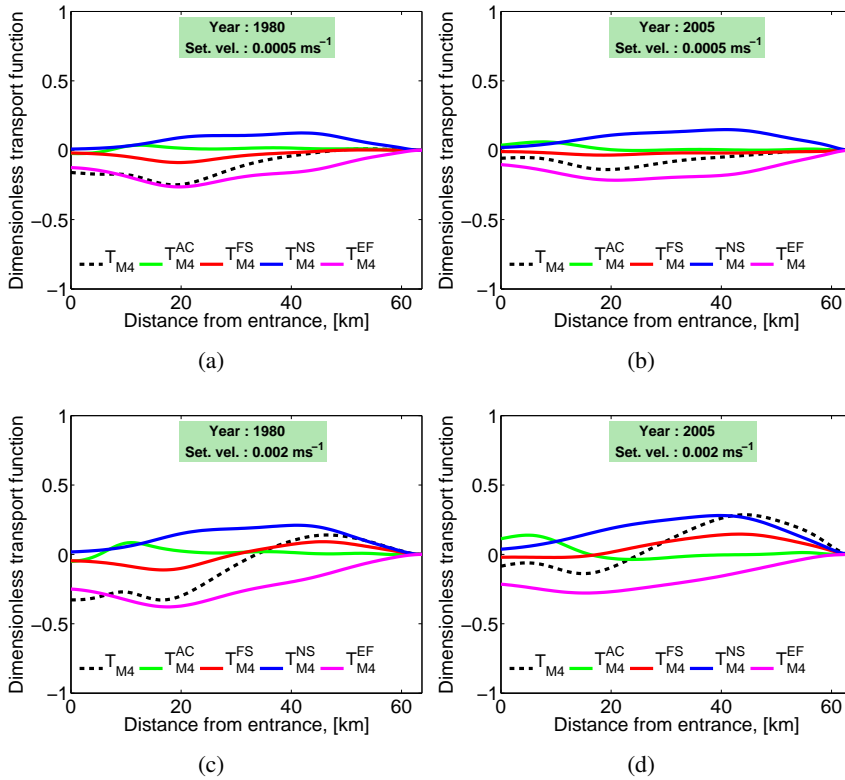


Figure A.18: Dimensionless M_4 transport function in components.

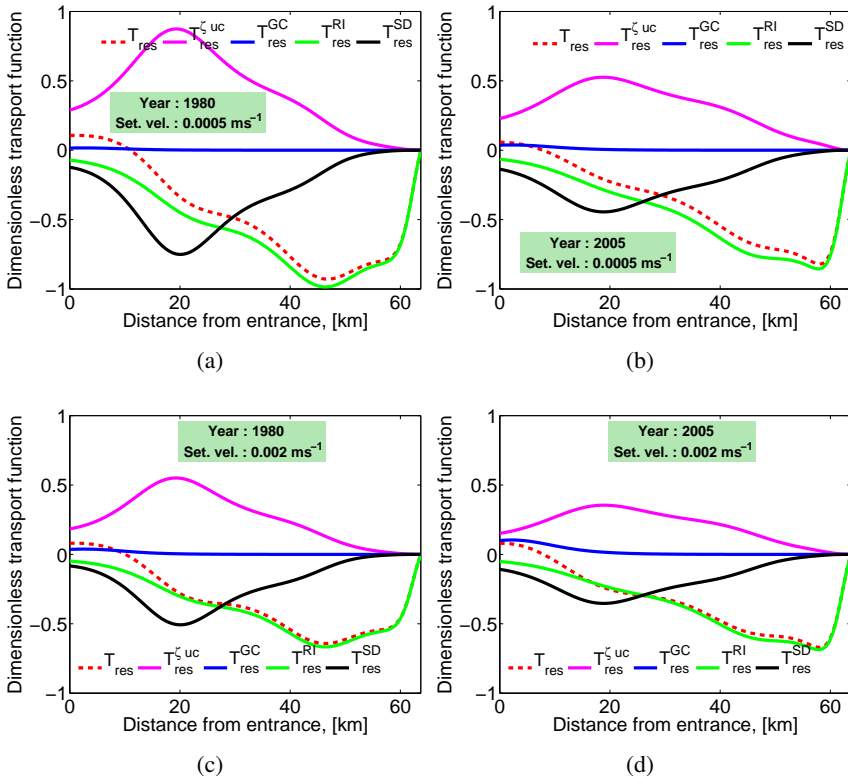


Figure A.19: Dimensionless T_{res} transport function and its components.

Bibliography

- Allen GP, Salomon JC, Bassoullet P, Du Penhoat Y, De Grandpre C (1980) Effects of tides on mixing and suspended sediment transport in macrotidal estuaries. *Sediment Geol* 26:69–90, doi: [10.1016/0037-0738\(80\)90006-8](https://doi.org/10.1016/0037-0738(80)90006-8)
- Aubrey DG, Speer PE (1985) A study of nonlinear tidal propagation in shallow inlet/estuarine systems. Part 1: Observations. *Est Coastal Shelf Sci* 21:185–205, doi: [10.1016/0272-7714\(85\)90096-4](https://doi.org/10.1016/0272-7714(85)90096-4)
- Bowden KF (1965) Horizontal mixing in the sea due to a shearing current. *J Fluid Mech* 21:83–95, doi: [10.1017/S0022112065000058](https://doi.org/10.1017/S0022112065000058)
- Burchard H, Baumert H (1998) The formation of estuarine turbidity maxima due to density effects in the salt wedge. A hydrodynamic process study. *J Phys Oceanogr* 28:309–321, doi: [10.1175/1520-0485\(1998\)028<0309:TFOETM>2.0.CO;2](https://doi.org/10.1175/1520-0485(1998)028<0309:TFOETM>2.0.CO;2)
- Burchard H, Hetland RD (2010) Quantifying the contributions of tidal straining and gravitational circulation to residual circulation in periodically stratified tidal estuaries. *J Phys Oceanogr* 40:1243–1262, doi: [10.1175/2010JPO4270.1](https://doi.org/10.1175/2010JPO4270.1)
- Cáceres M, Valle-Levinson A, Sepúlveda HH, Holderied K (2002) Transverse variability of flow and density in a Chilean fjord. *Cont Shelf Res* 22:1638–1698, doi: [10.1016/S0278-4343\(02\)00032-8](https://doi.org/10.1016/S0278-4343(02)00032-8)
- Cameron WM, Pritchard D (1963) Estuaries. In: Hill MN (ed) *The Sea*, John Wiley & Sons, New York, vol 2, pp 306–324
- Cheng P, Valle-Levinson A, De Swart HE (2010) Residual currents induced by asymmetric tidal mixing in weakly stratified narrow estuaries. *J Phys Oceanogr* 40:2135–2147, doi: [10.1175/2010JPO4314.1](https://doi.org/10.1175/2010JPO4314.1)

- Cheng P, Valle-Levinson A, De Swart HE (2011) A numerical study of residual circulation induced by asymmetric tidal mixing in tidally dominated estuaries. *J Geophys Res* 116, doi: [10.1029/2010JC006137](https://doi.org/10.1029/2010JC006137)
- Chernetsky AS, Schuttelaars HM (2010) The effect of high sediment concentration on sediment trapping in tidal estuaries. In: Pattiaratchi C (ed) *Proceedings of the 15th Physics of Estuaries and Coastal Seas (PECS) Conference 2010: Coastal and estuarine observations and modelling*, pp 48–51
- Chernetsky AS, Schuttelaars HM (2012) Influence of high sediment concentration and geometrical characteristics on the position of estuarine turbidity maxima in tidal estuaries. *J Geophys Res* Submitted
- Chernetsky AS, Schuttelaars HM, Talke SA (2008) The effect of deepening the Ems estuary on tidal dynamics and residual circulation patterns. In: Souza A (ed) *Proceedings of PECS 2008: Physics of estuaries and coastal seas*. Ocean dynamics, Springer, Berlin/Heidelberg, pp 269–272
- Chernetsky AS, Schuttelaars HM, Talke SA (2010) The effect of tidal asymmetry and temporal settling lag on sediment trapping in tidal estuaries. *Ocean Dynamics* 60:1219–1241, doi: [10.1007/s10236-010-0329-8](https://doi.org/10.1007/s10236-010-0329-8)
- Csanady GT (1982) *Circulations in the coastal ocean*. Reidel, Dordrecht, ISBN: [90-277-1400-2](https://doi.org/10.1007/978-94-009-1400-2)
- De Jonge VN (1983) Relations between annual dredging activities, suspended matter concentrations and the development of the tidal regime in the Ems estuary. *Can J Fish Aquat Sci* 40:289–300, doi: [10.1139/f83-290](https://doi.org/10.1139/f83-290)
- De Jonge VN (1992) Tidal flow and residual flow in the Ems estuary. *Est Coast Shelf Sci* 34:1–22, doi: [10.1016/S0272-7714\(05\)80123-4](https://doi.org/10.1016/S0272-7714(05)80123-4)
- De Jonge VN (2000) Importance of temporal and spatial scales in applying biological and physical process knowledge in coastal management, an example for the Ems estuary. *Cont Shelf Res* 20:1655–1686, doi: [10.1016/S0278-4343\(00\)00042-X](https://doi.org/10.1016/S0278-4343(00)00042-X)
- De Swart HE, Zimmerman JTF (2009) Morphodynamics of tidal inlet systems. *Annual review of fluid mechanics* 41:203–229, doi: [10.1146/annurev.fluid.010908.165159](https://doi.org/10.1146/annurev.fluid.010908.165159)

- Dyer KR (1977) Lateral circulation effects in estuaries. In: *Estuaries, Geophysics and the Environment*, National Academy of Science, Washington D.C., ISBN: [0-309-02629-6](#)
- Dyer KR (1986) *Coastal and estuarine sediment dynamics*. John Wiley & Sons, Chichester, ISBN: [0-471-90876-2](#)
- Dyer KR (1997) *Estuaries: A Physical Introduction*, 2nd edn. John Wiley & Sons, Chichester, ISBN: [0-471-97471-4](#)
- Festa JF, Hansen DV (1978) Turbidity maxima in partially mixed estuaries: A two-dimensional numerical model. *Est Coast Mar Sci* 7:347–359, doi: [10.1016/0302-3524\(78\)90087-7](#)
- Friedrichs CT, Aubrey DG (1996) Uniform bottom shear stress and equilibrium hypsometry of intertidal flats. In: Pattiaratchi C (ed) *Mixing in estuaries and coastal seas*, Amer. Geophys. Union, Washington D.C., pp 405–429
- Friedrichs CT, Hamrick JH (1996) Effects of channel geometry on cross sectional variation in along channel velocity in partially stratified estuaries. In: Aubrey DG, Friedrichs CT (eds) *Buoyancy effects on coastal and estuarine dynamics*, AGU, Washington D.C., pp 283–300
- Friedrichs CT, Armbrust BD, De Swart HE (1998) Hydrodynamics and equilibrium sediment dynamics of shallow, funnel-shaped tidal estuaries. In: Dronkers J, Scheffers MBAM (eds) *Physics of Estuaries and Coastal Seas*, PECS 1996, Balkema, Rotterdam, pp 315–327
- Garrett C (1974) Normal modes of the Bay of Fundy and Gulf of Maine. *Can J Earth Sci* 11:549–556, doi: [10.1139/e74-049](#)
- Geyer WR (1993) The importance of suppression of turbulence by stratification on the estuarine turbidity maximum. *Estuaries* 16:113–125, doi: [10.2307/1352769](#)
- Greenberg DA (1975) *Mathematical studies of tidal behaviour in the Bay of Fundy*. PhD thesis, University of Liverpool
- Groen P (1967) On the residual transport of suspended matter by an alternating tidal current. *Neth J Sea Res* 3:564–574, doi: [10.1016/0077-7579\(67\)90004-X](#)
- Hansen DV, Rattray M (1965) Gravitational circulation in straits and estuaries. *J Marine Res* 23:104–122

- Hinrich H (1974) Schwebstoffgehalt, Gebietsniederschlag, Abflu und Schwebstofffracht der Ems bei Rheine und Versen in den Jahren 1965 bis 1971. Dtsch Gewsserk Mitt 18:85–95
- Huijts KMH, Schuttelaars HM, de Swart HE, Valle-Levinson A (2006) Lateral trapping of sediment in tidal estuaries: an idealized model study. J Geophys Res 111, doi: [10.1029/2006JC003615](https://doi.org/10.1029/2006JC003615)
- Huijts KMH, Schuttelaars HM, de Swart HE, Friedrichs CT (2009) Analytical study of the transverse distribution of along-channel and transverse residual flows in tidal estuaries. Cont Shelf Res 29:89–100, doi: [10.1016/j.csr.2007.09.007](https://doi.org/10.1016/j.csr.2007.09.007)
- Huijts KMH, de Swart HE, Schramkowski JP, Schuttelaars HM (2011) Transverse structure of tidal and residual flow and sediment concentration in estuaries. Ocean Dynamics 61:1067–1091, doi: [10.1007/s10236-011-0414-7](https://doi.org/10.1007/s10236-011-0414-7)
- Ianniello JP (1977) Tidally induced residual currents in estuaries of constant breadth and depth. J Marine Res 35:755–786
- Ianniello JP (1979) Tidally-induced residual circulation in estuaries of variable width and depth. J Phys Oceanogr 9:962–974, doi:[10.1175/1520-0485\(1979\)009<0962:TIRCIEj2.0.CO;2](https://doi.org/10.1175/1520-0485(1979)009<0962:TIRCIEj2.0.CO;2)
- Jay DA, Musiak JD (1994) Particle trapping in estuarine tidal flows. J Geophys Res 99:20,445–20,461, doi: [10.1029/94JC00971](https://doi.org/10.1029/94JC00971)
- Jay DA, Musiak JD (1996) Internal tidal asymmetry in channel flows: Origins and Consequences. In: Pattiaratchi C (ed) Mixing Processes in Estuaries and Coastal Seas, American Geophysical Union Coastal and Estuarine Sciences Monograph, pp 219–258
- Jay DA, Smith JD (1990) Circulation, density distribution and neap-spring transitions in the Columbia River Estuary. Prog Oceanogr 25:81–112, doi: [10.1016/0079-6611\(90\)90004-L](https://doi.org/10.1016/0079-6611(90)90004-L)
- Kim YH, Voulgaris G (2008) Lateral circulation and suspended sediment transport in a curved estuarine channel: Winyah Bay, SC, USA. J Geophys Res 113:C09,006, doi: [10.1029/2007JC004509](https://doi.org/10.1029/2007JC004509)
- Krebs M, Weilbeer H (2008) Ems-dollart estuary. Die Kueste 74:252–262

- Lang G, Schubert R, Markofsky M, Fanger HU, Grabemann I, Krasemann HL, Newmann LJR, Riethmüller R (1989) Data interpretation and numerical modeling of the mud and suspended sediment experiment 1985. *J Geophys Res* 94:14,381–14,393, doi: [10.1029/JC094iC10p14381](https://doi.org/10.1029/JC094iC10p14381)
- Lin J, Kuo AY (2001) Secondary turbidity maximum in a partially mixed microtidal estuary. *Estuaries* 24:707–720, doi: [10.2307/1352879](https://doi.org/10.2307/1352879)
- MacCready P (1999) Estuarine adjustment to changes in river flow and tidal mixing. *J Phys Oceanogr* 29:708–726, doi: [10.1175/1520-0485\(1999\)029<0708:EATCIR>2.0.CO;2](https://doi.org/10.1175/1520-0485(1999)029<0708:EATCIR>2.0.CO;2)
- Meadows PS, Tait J (1989) Modification of sediment permeability and shear strength by two burrowing invertebrates. *Mar Biol* 101:75–82, doi: [10.1007/BF00393480](https://doi.org/10.1007/BF00393480)
- Nunes RA, Simpson JH (1985) Axial convergence in a well-mixed estuary. *Est Coastal Shelf Sci* 20:637–649, doi: [10.1016/0272-7714\(85\)90112-X](https://doi.org/10.1016/0272-7714(85)90112-X)
- Officer CB (1976) *Physical oceanography of estuaries (and associated coastal waters)*. John Wiley & Sons, New York, ISBN: [0-471-65278-4](https://www.wiley.com/9780471652784)
- Pedlodysky J (1987) *Geophysical fluid dynamics*. Springer-Verlag, New York, ISBN: [0-387-96387-1](https://www.springer.com/9780387963871)
- Perillo GME (1995) *Geomorphology and Sedimentology of Estuaries*. Elsevier, Amsterdam, ISBN: [0-444-88170-0](https://www.elsevier.com/9780444881700)
- Peters H (1997) Observations of stratified turbulent mixing in an estuary: Neap-to-spring variations during high river flow. *Est Coastal Shelf Sci* 45:69–88, doi: [10.1006/ecss.1996.0180](https://doi.org/10.1006/ecss.1996.0180)
- Postma H (1954) Hydrography of the Dutch Wadden Sea. *Arch Neerl Zool* 10:405–511, doi: [10.1163/036551654X00087](https://doi.org/10.1163/036551654X00087)
- Pritchard DW (1955) Estuarine circulation patterns. In: *Proceedings of the American Society of Civil Engineers*, vol 81, pp 1–11
- Ralston DK, Stacey MT (2005) Stratification and turbulence in subtidal channels through intertidal mudflats. *J Geophys Res* 110:C08,009, doi: [10.1029/2004JC002650](https://doi.org/10.1029/2004JC002650)

- Schramkowski GP, Schuttelaars HM, de Swart HE (2002) The effect of geometry and bottom friction on local bed forms in a tidal embayment. *Cont Shelf Res* 22:1821–1833, doi: [10.1016/S0278-4343\(02\)00040-7](https://doi.org/10.1016/S0278-4343(02)00040-7)
- Schuttelaars HM, De Jonge VN, Chernetsky AS (2012) How to improve the predictive power when modelling the physical effects of human interventions in estuarine systems? *Ocean and Coastal Management* Submitted
- Scully ME, Friedrichs CT (2003) The influence of asymmetries in overlying stratification on near bed turbulence and sediment suspension in a partially mixed estuary. *Ocean Dynamics* 53:208–219, doi: [10.1007/s10236-003-0034-y](https://doi.org/10.1007/s10236-003-0034-y)
- Scully ME, Geyer WR, Lerczak JA (2009) The influence of lateral advection on the residual estuarine circulation: a numerical modeling study of the Hudson River Estuary. *J Phys Oceanogr* 39:107–124, doi: [10.1175/2008JPO3952.1](https://doi.org/10.1175/2008JPO3952.1)
- Sharples J, Simpson JH (1995) Semi-diurnal and longer period stability cycles in the Liverpool Bay region of fresh-water influence. *Cont Shelf Res* 15:295–313, doi: [10.1016/0278-4343\(94\)E0003-5](https://doi.org/10.1016/0278-4343(94)E0003-5)
- Shaw J, Amos CL, Greenberg DA, O'Reilly CT, Parrott DR, Pattona E (2010) Catastrophic tidal expansion in the Bay of Fundy, Canada. *Can J Earth Sci* 47:1079–1091, doi: [10.1139/E10-046](https://doi.org/10.1139/E10-046)
- Simpson JH, Brown J, Matthews J, Allen G (1990) Tidal straining, density currents, and stirring in the control of estuarine stratification. *Estuaries* 13:125–132, doi: [10.2307/1351581](https://doi.org/10.2307/1351581)
- Sleath JFA (1984) *Sea bed mechanics*. John Wiley & Sons, New York, ISBN: [047189091X](https://doi.org/10.1002/978111890911X)
- Stacey MT, Burau JR, Monismith SG (2001) Creation of residual flows in a partially stratified estuaries. *J Geophys Res* 106:17,013–17,037, doi: [10.1029/2000JC000576](https://doi.org/10.1029/2000JC000576)
- Stacey MT, Fram JP, Chow FK (2008) Role of tidally periodic density stratification in the creation of estuarine subtidal circulation. *J Geophys Res* 113:C08,016, doi: [10.1029/2007JC004581](https://doi.org/10.1029/2007JC004581)
- Sutherland TF, Amos CL, Grant J (1998) The effect of buoyant biofilms on the erodibility of sublittoral sediments of a temperate microtidal estuary. *Limnol Oceanogr* 43:225–235, doi: [10.4319/lo.1998.43.2.0225](https://doi.org/10.4319/lo.1998.43.2.0225)

- Talke SA, de Swart HE, de Jonge VN (2009a) An idealized model and systematic process study of oxygen depletion in highly turbid estuaries. *Estuaries and Coasts* 32:602–620, doi: [10.1007/s12237-009-9171-y](https://doi.org/10.1007/s12237-009-9171-y)
- Talke SA, de Swart HE, Schuttelaars HM (2009b) Feedback between residual circulations and sediment distribution in highly turbid estuaries: An analytical model. *Cont Shelf Res* 29:119–135, doi: [10.1016/j.csr.2007.09.002](https://doi.org/10.1016/j.csr.2007.09.002)
- Uncles RJ, Smith RE (2005) A note on the comparative turbidity of some estuaries of the Americas. *J Coast Res* 21:845–852, doi: [10.2112/016-NIS.1](https://doi.org/10.2112/016-NIS.1)
- Uncles RJ, Stephens JA, Smith RE (2002) The dependence of estuarine turbidity on tidal intrusion length, tidal range and residence time. *Cont Shelf Res* 22:1835–1856, doi: [10.1016/S0278-4343\(02\)00041-9](https://doi.org/10.1016/S0278-4343(02)00041-9)
- Valle-Levinson A (ed) (2010) *Contemporary Issues in Estuarine Physics*. Cambridge University Press, Cambridge, ISBN: [978-0-521-89967-3](https://doi.org/10.1017/9780521899673)
- Van de Kreeke J, Dunsbergen DW (2000) Tidal asymmetry and sediment transport in the Frisian Inlet. In: Yanagi T (ed) *Interactions between Estuaries, Coastal Seas and Shelf Seas*, Terra Scientific Publishing Company, Tokyo, pp 139–159
- Van der Lee WTB (2000) Temporal variation of flocculation size and settling velocity in the Dollard estuary. *Cont Shelf Res* 20:1495–1511, doi: [10.1016/S0278-4343\(00\)00034-0](https://doi.org/10.1016/S0278-4343(00)00034-0)
- Van Leussen W (1988) Aggregation of particles, settling velocity of mud flocs: A review. In: Dronkers J, Van Leussen W (eds) *Physical processes in estuaries*, Springer-Verlag, New York, pp 347–403
- Van Leussen W, Cornelisse JM (1993) The determination of the sizes and settling velocities of estuarine flocs by an underwater video system. *Neth J Sea Res* 31:231–241, doi: [10.1016/0077-7579\(93\)90024-M](https://doi.org/10.1016/0077-7579(93)90024-M)
- Van Leussen W, Cornelisse JM (1996) The underwater video system VIS. *J Sea Res* 36:77–81, doi: [10.1016/S1385-1101\(96\)90774-1](https://doi.org/10.1016/S1385-1101(96)90774-1)
- Van Rijn LC (1993) *Principles of sediment transport in rivers, estuaries and coastal seas*. Aqua Publ., Amsterdam, ISBN: [90-800356-2-9](https://doi.org/10.1017/9080035629)
- Weilbeer H (2008) Numerical simulation and analyses of sediment transport processes in the Ems-Dollard estuary with a three-dimensional model. In: Kusuda

- T, Yamanishi H, Spearman J, Gailani JZ (eds) Sediment and Ecohydraulics - INTERCOH 2005, Elsevier, Proceedings in Marine Science, vol 9, pp 447–462, doi: [10.1016/S1568-2692\(08\)80032-0](https://doi.org/10.1016/S1568-2692(08)80032-0)
- Weir DJ, McManus J (1987) The role of wind in generating turbidity maxima in the Tay Estuary. *Cont Shelf Res* 7:1315–1318
- Widdows J, Brinsley MD, Elliott M (1998a) Use of in situ flume to quantify particle flux (deposition rates and sediment erosion) for an intertidal mudflat in relation to changes in current velocity and benthic macrofauna. In: Black KS, Paterson DM, Cramp A (eds) *Sedimentary Processes in the Intertidal Zone*. Special Publications, Geological Society, London, vol 139, pp 85–97
- Widdows J, Brinsley MD, Salkeld PN, Elliott M (1998b) Use of annular flumes to determine the influence of current velocity and biota on material flux at the sediment-water interface. *Estuaries* 21:552–559
- Winterwerp JC (2011) Fine sediment transport by tidal asymmetry in the high-concentrated Ems River: indications for a regime shift in response to channel deepening. *Ocean Dynamics* 61:203–215, doi: [10.1007/s10236-010-0332-0](https://doi.org/10.1007/s10236-010-0332-0)
- Winterwerp JC, Lely M, He Q (2009) Sediment-induced buoyancy destruction and drag reduction in estuaries. *Ocean Dynamics* 61:781–791, doi: [10.1007/s10236-009-0237-y](https://doi.org/10.1007/s10236-009-0237-y)
- Wurpts R, Torn P (2005) 15 years experience with fluid mud: definition of the nautical bottom with rheological parameters. *Terra et Aqua* 99:22–32
- Zimmerman JTF (1992) On the Lorentz linearization of a nonlinearly damped tidal Helmholtz oscillator. *Proc Kon Ned Akad v Wetensch* 95:127–145

Summary

The fast industrial development and the subsequent growth of cities and trade have led to large-scale anthropogenic alterations of estuarine systems. Estuaries are streamlined and deepened to ensure a safe navigation for larger ships. Dams are constructed to protect the farmland, households and industrial buildings from floods. Moreover, land reclamation, deforestation and various agricultural activities result in higher sediment and freshwater input into estuaries. All these activities lead to fundamental alterations of the hydro- and sediment dynamics, mixing and circulation processes within estuarine systems.

An estuarine system, taken out of its natural balance, is always trying to restore this equilibrium or reach a new balance. This can result in, for example, an increased siltation such that the estuarine depth has to be constantly maintained via annual dredging activities. Engineering interventions are expensive and they create a substantial load on the local ecosystem, because a biological system cannot readjust to new conditions within a short period of time. Hence, these activities pose many problems from both the ecological and economic point of view. A proper understanding of estuarine processes is essential to minimize the negative consequences of human influence and to develop a long-term restoration and development plan for many problematic estuaries.

The main objective of this thesis is to investigate physical mechanisms in the along-estuary direction that result in the trapping of suspended sediment in partially and well mixed tidal estuaries and to analyze the influence of individual mechanisms on the trapping location. The investigation is conducted using an idealized model approach. A width-averaged analytical model of a tidal estuary is developed, which allows to model the velocity distribution, the suspended sediment dynamics and analyze the occurrence of suspended sediment trapping in morphodynamic equilibrium, i.e., a situation in which there is no tidally averaged sediment transport. The model allows to reproduce hydro- and sediment dynamic conditions in tidal estuaries via a calibration of model parameters using field observations. Once the model is properly calibrated and results are validated, the

importance of various trapping mechanisms and their sensitivity can be studied.

As a case study, the formation of ETMs in the Ems estuary was investigated. It was shown that the occurrence of an estuarine turbidity maximum and its location are determined by a complex interaction between various components of exporting and importing (upstream and downstream) suspended sediment transports. It was shown that the main import of sediment into the estuary is due to the correlation of the M_2 tidal velocity and M_2 suspended sediment concentration (' M_2 transport'), and the major export is caused by the residual transport. There is no single dominant physical mechanism that controls the formation of a turbidity region in an estuary.

Multiple ETMs are observed when constituents of exporting and importing transport balance each other at several locations in the estuary. We have observed (modeled) the formation of either one or two ETMs in the Ems estuary. The first turbidity region was located at the entrance of the estuary and the second one near the tidal weir. It was shown that an ETM at the entrance results from an interaction of various contributions of the residual and ' M_2 transport', and an ETM near the end of the estuary results from the import of sediment by a specific component of the ' M_2 transport', the so-called tidal asymmetry, and export due to river outflow. The sensitivity analysis reveals that there is a competition between these trapping mechanisms. The dominant mechanism determines the position of the ETM. Two ETMs are observed when both mechanisms are of equal strength. The dominance of both mechanisms can change when either geometrical characteristics of the estuary or external forcing is altered. This means that any change of the geometrical characteristics or/and the external forcing will influence either the position or the occurrence of an ETM in the estuary.

Furthermore, it was shown that the time-dependency of the vertical eddy viscosity produces an important contribution that can result in a strong importing sediment transport into the estuary upstream. The effect of this mechanism on the location(s) of the turbidity zone is of the order or can exceed the influence of the gravitational circulation.

Samenvatting

Snelle industriële ontwikkeling en de daaruit voortvloeiende groei van steden en handel hebben geleid tot grootschalige antropogene ingrepen in estuariene systemen. Estuaria zijn gestroomlijnd en verdiept om een veilige navigatie voor schepen te garanderen. Er zijn dammen gebouwd om landbouwgronden, huishoudens en industrie te beschermen tegen overstromingen. Landaanwinning, ontbossing en diverse agrarische activiteiten hebben geresulteerd in hogere sediment en zoetwater toevoer. Al deze activiteiten leiden tot fundamentele veranderingen in de hydro- en sediment dynamiek, menging en circulatie processen binnen estuariene systemen.

Als het natuurlijk evenwicht van een estuarien systeem verstoord is, zal zo'n systeem in het algemeen proberen om dit evenwicht te herstellen of een nieuw evenwicht te bereiken. Dit kan leiden tot bijvoorbeeld een verhoogde aanslibbing, waardoor het estuarium constant moet worden verdiept door baggerwerkzaamheden om de gewenste diepte te behouden. Antropogene interventies (zoals bijvoorbeeld het verdiepen van de vaargeul) en de daaruit voortvloeiende maatregelen (onderhoudsbaggerwerk) zijn in het algemeen duur. Verder vormen ze een aanzienlijke belasting van het ecosysteem, een biologisch systeem kan zich immers niet op korte termijn aanpassen aan deze nieuwe omstandigheden. Dit soort activiteiten resulteert dus in veel problemen vanuit zowel ecologisch als economisch oogpunt. Een goed begrip van estuariene processen is dus essentieel om de negatieve gevolgen van menselijke invloed te minimaliseren en om een lange termijn herstel- en ontwikkelingsplan voor estuaria te ontwikkelen.

Het belangrijkste doel van dit proefschrift is om systematisch de fysische mechanismen in de langsrichting te onderzoeken die resulteren in het invangen van gesuspendeerd sediment in gedeeltelijk en goed gemengde estuaria. De invloed van de afzonderlijke mechanismen op het invangen van gesuspendeerd sediment en de resulterende plaats waar de sedimentconcentratie het hoogst is worden geanalyseerd. Hiertoe wordt een geïdealiseerd model ontwikkeld, dat de breedte-gemiddelde waterbeweging en dynamica van gesuspendeerd sediment beschrijft.

Hiermee wordt de ruimtelijke verdeling van de concentratie van opgelost sediment in morfodynamisch evenwicht bestudeerd, dat wil zeggen een situatie waarin er geen getij-gemiddeld sedimenttransport is. Het model maakt het mogelijk om hydro- en sediment dynamica in estuaria te reproduceren na kalibratie van modelparameters met behulp van veldwaarnemingen. Als het model correct is gekalibreerd, kan het relatieve belang van de verschillende mechanismen die leiden tot het invangen van gesuspendeerd sediment en hun gevoeligheid voor parameterwaarden worden bestudeerd.

Als case study is de vorming van estuariene troebelheidsmaxima (ETM's) in het Eems estuarium onderzocht. Het optreden van een ETM en de locatie ervan worden bepaald door een complexe interactie tussen de diverse componenten van de exporterende en importerende sedimenttransport. De belangrijkste bijdrage aan de import van sediment in het estuarium is het gevolg van het residueel transport ten gevolge van correlaties tussen M_2 getijde-snelheden en M_2 zwevende sediment concentraties (' M_2 transport'), de grootste exportbijdrage is het gevolg van getijgemiddelde concentraties die door residuele snelheden worden getransporteerd ('residueel transport'). Meerdere ETM's worden waargenomen wanneer verschillende exporterende en importerende sedimentfluxen met elkaar balanceren op verschillende locaties in het estuarium. We hebben de vorming van zowel één als twee ETM's in het Eems-estuarium gemodelleerd. Het eerste troebelheidsmaximum wordt aan de zeewaartse kant van het estuarium gevonden, de tweede aan de landwaartse kant (bij de stuw). Het ETM aan de zeewaartse kant is het resultaat de interactie tussen verschillende bijdragen van de residuele en M_2 transport, het ETM aan de landwaartse zijde wordt gevormd door een balans tussen import ten gevolge van de zogenaamde getijde-asymmetrie, en export als gevolg van de rivier uitstroom. Op welke plek een ETM wordt waargenomen hangt af van de efficiëntie van de verschillende mechanismen, wat weer afhangt van de parameterwaarden gebruikt in het model. Twee ETM's worden gevormd wanneer beide mechanismen van gelijke sterkte zijn. De dominantie van beide mechanismen kan veranderen als geometrische kenmerken van het estuarium of externe forceringen worden gewijzigd. Dit betekent dat elke wijziging van de geometrische kenmerken en/of de externe forcering de positie en het aantal ETM's in een estuarium kan beïnvloeden.

Acknowledgements

I spent five unforgettable years in the Netherlands at the Department of Mathematical Physics. During this time, I had an incredible opportunity to meet diverse people, each having his unique character. This was an incredible life experience and it allowed me to learn a lot. In this final, but most frequently read ;), section of thesis, I would like to express my gratitude to these people.

First of all, I would like to express my sincere gratitude to my supervisor, Dr. Henk Schuttelaars, for his help, guidance and inspiration. His support and neverending enthusiasm was an important contribution for the successful completion of this thesis. Henk, thanks a lot for your support, patience, encouragement and that you were always there for me for the past five years. It has been a great pleasure doing the research with you.

I am very grateful to my promotor, Prof. Arnold Heemink, for his enthusiasm and help with the preparation of this thesis. I would also like to say a big thank you to Prof. Huib de Swart for his support, excellent ideas and an authentic interest in my research during my Ph.D. study. Thanks a lot for your thorough feedback. Your opinion and positive perception of the thesis means a lot to me.

There are many people, who made me study at TU Delft possible. I would like to take the opportunity and say thank you to Prof. Igor Andrianov for introducing me to Delft University of Technology and encouraging me to continue my study in Delft. Moreover, I am very grateful to Dr. Wim van Horssen for offering me a position at the department of Mathematical Physics as well as helping me with many organizational and administrative matters.

I am grateful to my colleagues who helped me a lot with my daily life. I am very grateful to Kees Lemmens for his help and support with computer and programing related issues, advises and occasional chit chats. I would like to thank Evelyn Sharabi and Dorothee Engering for helping me to sort out many matters and answering a lot of my questions.

During the past five years, I was the lucky one to share my office with the only two dutch students of our department. They did the best to create the dutch

atmosphere for me and integrate me more into the culture. I am very grateful Jelle and Miriam for that. I also want to say many thanks to Miriam for having wonderful talks just about everything and keeping me a great company during many workshops and conferences we attended together. I have never been board when you were around. I would like to say thank you to Asia, Edwin and Michele for a nice atmosphere, jokes and talks we had.

My life in Delft would not have been so full without my other friends and colleagues who helped me to adapt to a life in a new country. I would like to say a big thank you to Alexey, Daria, Maria and Andrey, who were the first ones to greet me in the Netherlands. I am grateful for the good time we had, for parties, laughs and many activities we did together. I am also grateful to Svetlana Ponomareva for her cheerfulness, nice mood and constant encouragements and Maria Krymskaya for the help, interesting talks and exchange of ideas. Many thanks go also to Dima and Oksana for their hospitality and kindness.

This acknowledgments would be simply incomplete without expressing my gratitude to my best friend Alex Kirichuk. Thanks a lot for all the time we spent together, for keeping me a great company, for neverending laughs, support and encouragement I received from you during all this time. We visited together over 20 different countries and our last trip to Ireland is still vivid in my mind. We only have over 150 to go :)

The final words of gratitude go to my parents Nina and Sergey. I am deeply grateful for their love, kindness, cheerfulness, inspiration, understanding and support. It is an inspiring feeling to know that there are people who believe in you and are proud of all your achievements. I am truly grateful for everything you did, do, and will do for me. I love you very much!

March 2012
Alexander Chernetsky

Curriculum Vitae

Alexander Chernetsky was born on June 3, 1983 in Dnepropetrovsk, Soviet Union (nowadays Ukraine). From 1990 until 1998, he attended primary and secondary school No 83 in Dnepropetrovsk and from 1998, he studied at Dnepropetrovsk Regional Physics and Mathematics Lyceum. He graduated from the Lyceum in 2000.

The same year, he entered a Bachelor of Science and subsequently Master of Science program at the Department of Theoretical and Applied Mechanics of the Mechanics and Mathematics Faculty, Dnepropetrovsk National University. In June 2005, Alexander Chernetsky defended his Master thesis "Analysis of the behavior of yield surfaces" under supervision of Prof. dr. U.A. Chernyakov and obtained his M.Sc. degree (with honors). After graduation, he continued the research work in the field of elastic-plastic deformation of solids in Dnepropetrovsk National University until August 2006.

From September 2006, Alexander Chernetsky started a Ph.D. research at Delft Institute of Applied Mathematics (DIAM), Delft University of Technology, The Netherlands. He worked on the project "Trapping of Sediment in Tidal Estuaries" under supervision of Prof. dr. ir. A.W. Heemink and Dr. ir. H.M. Schuttelaars. The research was related to understanding of individual physical processes and their interaction, which result in transport and accumulation of suspended sediment in tidal estuaries. The work that has been conducted during his Ph.D. research resulted in this thesis.

Since August 2011, Alexander Chernetsky works as a Petroleum Engineer at Royal Dutch Shell in The Netherlands.